NOTICE

The quality of this microform is heavily dependent upon the quality of the original thesis submitted for microfilming. Every effort has been made to ensure the highest quality of reproduction possible.

If pages are missing, contact the university which granted the degree.

Some pages may have indistinct print especially if the original pages were typed with a poor typewriter ribbon or if the university sent us an inferior photocopy.

Previously copyrighted materials (journal articles, published tests, etc.) are not filmed.

AVIS

La qualité de cette microforme dépend grandement de la qualité de la thèse soumise au microfilmage. Nous avons tout fait pour assurer une qualité supérieure de reproduction.

S'il manque des pages, veuillez communiquer avec l'université qui a conféré le grade

La qualité d'impression de certaines pages peut laisser à désirer, surtout si les pages originales ont été dactylographiées à l'aide d'un ruban usé ou si l'université nous a fait parvenir une photocopie de qualité inférieure.

Les documents qui font déjà l'objet d'un droit d'auteur (articles de revue, tests publiés, etc.) ne sont pas microfilmés.

The Torque-Thrust Coupling Effect in Twist Drills and its Influence on Drill Characteristics and Drilling Forces

Narasimha Kramadhati

A Thesis
in
the Department
of
Mechanical Engineering

Presented in Partial Fulfillment of the Requirements
for the Degree of Master of Engineering at
Concordia University
Montréal, Québec, Canada

March 1988

ISBN 0-315-41590-8

ABSTRACT

The Torque-Thrust Coupling Effect in Twist Drills and its Influence on Drill Characteristics and Drilling Forces

Narasimha Kramadhati

Concordia University, 1988

The torque-thrust coupling effect in twist drills is investigated experimentally, and is found to be a highly prominent phenomenon. A set of direct and cross-coupling stiffness coefficients are defined and determined experimentally. Coupling interaction increases steeply with helix angle, has a distinct maximum around 28 degrees, and decreases drastically at higher values. For drills of a given helix angle, the interaction increases parabolically with diameter. When tested under axial restraint, a clear increase in torsional stiffness is observed, owing to the coupling interaction - The higher the interaction, higher will be the torsional stiffening effect.

Examination of the coupling from a forces point of view indicates that significant torque and thrust forces are mutually induced during drilling, which add up with the cutting forces. Therefore it is erroneous to attribute the entire measured torque and thrust forces to metal-cutting. So-called 'separation equations' are derived for drills, which enable the

separation of the true cutting and the induced components from the measured torque and thrust values. Thrust inducement is inversely proportional to drill diameter, whereas torque inducement is directly proportional.

The decaying trends in the torque and thrust signals of pilot hole drilling, are actually considered to be the gradual 'release' of the induced forces. It is shown that the decay magnitudes are predictable using the results of coupling experimentation. By inference, the force-inducement hypothesis is also verified. The coupling effect and the force-inducement have significant implications to the static and dynamic characteristics of drills.

A new criterion for sizing pilot holes is proposed, based on the cutting mechanics in drilling. It is shown by drilling tests that sizing pilot holes by this criterion improves the roundness of the final holes significantly. Accordingly, a set of recommended pilot hole diameters is presented for common drill sizes.

DEDICATED

TO

LORD ANJANEYA

ACKNOWLEDGEMENT

The author expresses his sincere gratitude to Dr. M.O.M. Osman for his encouragement and guidance throughout this investigation. The support given by the Natural Sciences and Engineering Research Council (grant A5181) and the Formation de Chercheurs et d'action Concerteé of the Government of Quebec (grant G12) is appreciated.

Thanks are also due, to the personnel of the Engineering Machine Shop and the various Mechanical Engineering Laboratories, for their technical and material help. Special thanks are due to Dr. A.S. Ramamurthy for the use of his equipment on many occasions, and to Mr. R. Balachander and Mr. Ramesh Rajagopalan for their immense help.

Finally, the author is indebted to his parents for their patience and understanding throughout this investigation.

TABLE OF CONTENTS

LIST OF FIGURES

LIST OF TABLES

NOMENCLATURE

F	Axial thrust force [lb (N)]
F_{cut}	Cutting thrust [lb (N)]
F_{er}	Thrust measurement error
F_i, F_{ind}	Induced thrust [lb (N)]
F_m	Measured thrust [lb (N)]
K_{ff}	Axial stiffness under torsional restraint [lb (N)]
K_{ft}	Thrust-on-torque coupling stiffness coefficient [lb.in (N.m)]
K_{tf}	Torque-on-thrust coupling stiffness coefficient [lb.in/rad (N.m/rad)]
K_{tt}	Torsional stiffness under axial restraint [lb.in^2/rad (N.m^2/rad)]
K_1	Induced thrust coefficient [in^{-1} (m^{-1})]
K_2	Induced torque coefficient [in (m)]
L	Lead of the helix [in (m)]
p	Half-point angle [radian]
r	radius at given point on the cutting edge [in (m)]
T_{er}	Torque measurement error
T_i, T_{ind}	Induced torque [lb.in (N.m)]
T_m	Measured torque [lb.in (N.m)]

W	Half-web thickness [in (m)]
α_f	Reference rake angle [deg (rad)]
α_{ij}	Maxwell's influence coefficients
α_n	Normal rake angle [deg (rad)]
δ	Helix angle [deg (rad)]
ϵ	Shortening of Drill length [in (m)]
θ	Angle of twist [deg (rad)]
ϕ_{ph}	Pilot hole diameter [in (m)]
ϕ_1	'Wrong size' pilot hole [in (m)]
ϕ_2	'Right size' pilot hole [in (m)]

CHAPTER 1

INTRODUCTION

Since pre-historic times man has faced the necessity of forming holes in the materials he used. The earliest known form of the drill consisted of a sharp piece of stone mounted at the tip of a wooden shaft. The tool was spun either by the palms of the hands or by means of a bow string, and forced down into the work material.

Today hole production is the most common of all machining operations, and drilling is the most widely used technique for the purpose. Drilling is itself a family of processes, classified by the type of tool used. The choice of a specific process depends on the requirements such as hole-depth, diameter, tolerances, surface quality etc. Amongst the various methods, drilling with twist drills is the most widely employed hole-machining operation [6]. This investigation concerns exclusively with twist drilling, henceforth referred to as drilling.

1.1 The Twist Drill

Twist drills are unique amongst all metal cutting tools, both in their geometry and their method of operation. Figure 1.1 describes the salient geometrical features of a standard twist drill. The shank portion is for gripping the drill in the machine tool and the 'body' is the working

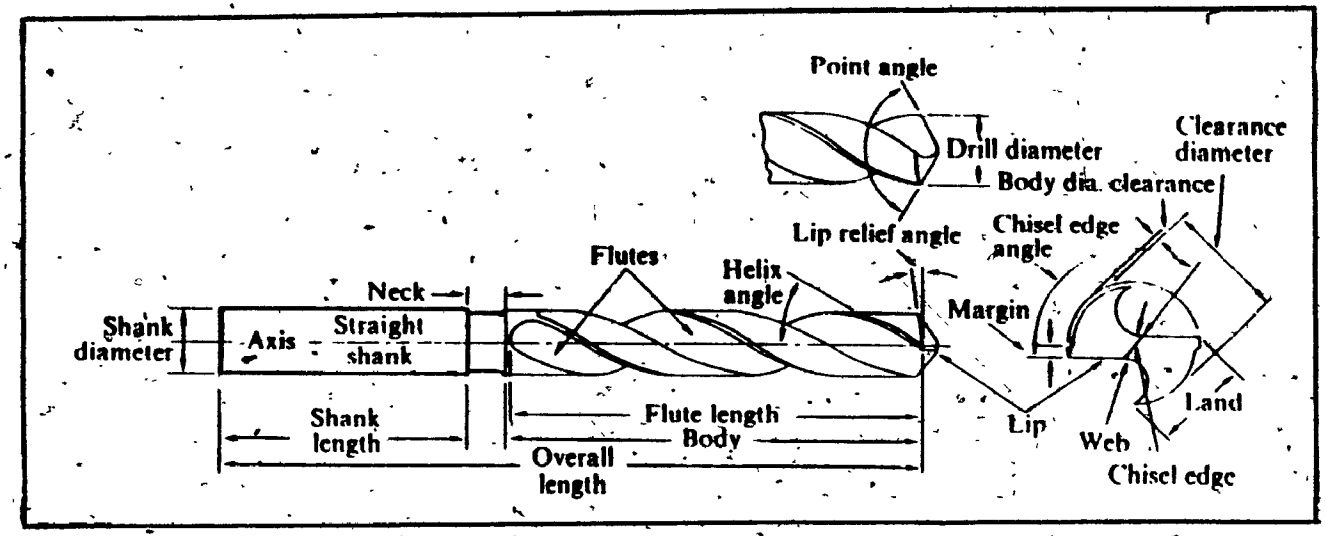

Figure 1.1 Twist drill : Geometrical features.

portion of the drill. The most prominent feature of the drill body is the double helical flutes which allow the formation of the two cutting lips at their intersection with the conical point surfaces. The cutting lips are seen to be straight edges in all drill specifications. Such a condition occurs only for pre-determined combinations of the flute contour, lead of the helix and the point angle. Thus on a given drill, if the point angle is changed, the cutting edges become either concave or convex. The rake angle and clearance angles on the cutting lips vary widely from near the web towards the drill periphery.

The distance between the straight cutting edges, called the web thickness, is necessary to protect the drill point and stiffen the drill. The web thickness increases towards the shank along the body. The 'chisel edge', formed by the intersection of the two conical surfaces at the web, acts as a secondary cutting edge.

In order to reduce the frictional forces between the drill and the hole, the drill diameter is decreased over a portion of its circumference leaving a short 'margin' at the full diameter to support the drill body against the hole surface. The entire drill body is given a slight taper towards the shank, to give a further clearance [18].

Although the outward appearance of the twist drill has not changed for over 60 years, major improvements have come about in the point geometries. Numerous special-purpose drills have also been developed.

This has resulted in improved accuracy and productivity in drilling. A more detailed examination of the cutting angles is presented in chapter 4.

1.2 Drilling Process

The cutting mechanics of a twist drill are unique amongst all metal cutting tools. The cutting velocity developed by the rotation of the tool (with respect to the workpiece) varies widely among the cutting regions, starting with zero at the centre and increasing linearly to a maximum at the periphery. This, and the variation of the cutting angles together produce vastly differing cutting mechanics - From a severe, extrusion type of process at the centre, to normal lathe-tool like cutting, at the periphery.

As the rotating drill is fed into the work material, the chips produced are removed from the cutting region by the pumping action of the helical flutes. The chips traverse the flutes and are ejected at the hole-mouth. The following virtues are attributed to the twist drilling process :

i) It is a remarkably simple process to generate circular holes.

ii) A very simple machine tool is sufficient for the purpose. In the simplest, a hand-drill can be used. In general, almost any machine tool that can give a relative rotation between the drill and the workpiece, can be used for drilling.

iii) A wide range of work materials can be drilled with a standard twist drill. And with modifications to the drill point, tough work materials can also be drilled.

iv) Tool maintenance is relatively simple - a limited amount of skill is sufficient to regrind drills.

However, numerous drawbacks are also associated with drilling, mostly owing to the geometrical characteristics of a twist drill :

i) The cutting takes place in an inaccessible region, preventing proper lubrication. This results in poor cutting conditions, tool over-heating, etc.

ii) Chip removal is inefficient at best, requiring frequent withdrawal of the drill to un-clog the chips along the flutes. This limits the maximum depths reachable, and the productivity of the process.

iii) The tool is inherently slender, and the severe cutting process imposes large forces on the drill-tip, leading to undesirable tool-deflection and vibration, in turn resulting in poor quality of holes. This characteristic, also imposes limits on the maximum metal-removal rate possible.

iv) Tool-life is relatively low (particularly with tough work materials), necessitating frequent tool grinding.

Although relatively accurate holes can be machined with a standard twist drill, the above factors make twist drilling in general, a mere preliminary operation. If holes require higher accuracy and surface finish, further processing such as reaming, boring, etc., is required. The depth of holes is commonly limited to five or six times the diameter of the drill.

In establishing the objectives of the present investigation, a literature survey was carried out and is presented below.

1.3 Literature Survey

A vast amount of literature is available on research related to the twist drilling process and the tool. Most of the earlier research is dedicated to refining the conical point geometry and studying the effects of the various process variables. Much of the knowledge has come about from actual drilling practice and experimental research work. Among the prominent (past and present) research areas are; tool-life of drills, performance study of coated drills, and the development of newer point geometries and their grinding methods. Also, a substantial research interest has been and continues to be directed at developing a theoretical cutting mechanics model and a means of predicting the forces in drilling.

Lorenz [9] reports the findings of a previous investigator that the resistance of a twisted profile to loading is about 85 percent higher than an untwisted bar of the same profile. He also notes that the torque tries

to reduce the twist by unwinding the profile, which is counteracted by an increasing thrust. And it is construed that drills with a large helix angle may not have been used efficiently due to the ineffective thrust provided by the applied feed. From his own experiments, Lorenz concludes that an increase in helix angle (from 25 degrees) increases drill life dramatically, peaks at 40 degrees and then decreases.

De Beer [8] carried out an experimental investigation on the effect of web thickness on the rigidity and drill life. It is shown that a decrease of web thickness does not necessarily weaken a drill (torsionally), nor does an increase result in unconditional increase of rigidity. Rather, the way in which the web thickness is changed, affects rigidity. A localized thinning near the web has minimal effect on drill rigidity, but if web thickness is reduced by moving the two flute boundaries together, rigidity reduces drastically. Similar to the observations of Lorenz [9], it is noted that torsion of the drill affects its length and conversely, axial force causes a twist on the fluted portion. The author reports some previous research which defines the so-called Maxwell's influence coefficients, relating the torsional and axial deformations with loading. It is shown that decreasing the web thickness increases the interaction between the two deformations. The author's experiments indicate that thin webs do not unconditionally impair drill life.

A more detailed study of the influence of cross-section profiles on drill static and dynamic characteristics, was conducted by Spur and Masuha [10]. In general, profile design is a compromise between chip-flow area and torsional rigidity. It is shown that the distribution of the area rather than just its magnitude, has a significant effect on the torsional stiffness. Concentration of the area to be more at the periphery (at a large radius) increases the second moment of area, increasing the torsional stiffness. Conversely, distributing the area more near the centre (thickening the web) can actually result in lower stiffness. In changing the stiffness, the profile design also affects the natural frequency of vibration. Helix angle is also seen to affect the dynamic behaviour of drills - Decreasing the helix angle increases the natural frequency. Another, unique form of vibration is also observed. It consists of high frequency torsional vibrations which give rise to synchronous longitudinal vibrations in phase with the torsional ones. The characteristic form of the drill is suggested as the cause of such vibrations.

Kahng and Ham [20] studied the hole quality after twist drilling, and its effect on subsequent hole-finishing operations. It is noted that the force differences resulting from the asymmetric cutting action on the two lips, cause the drill to bend and in turn cause roundness and parallelism errors of the hole. The authors refer to a previous investigation which demonstrates the relationship between radial forces and oversized hole geometry. It is found that the magnitude of the radial forces is related

to the degree of stability in drilling. Another previous study is quoted, which studies the roundness error of drilled holes. Experiments are conducted with a 12.7 mm diameter drill having a 2 mm chisel-edge ; drilling with a smaller pilot hole results in a pentagonal hole with a maximum roundness error of 120 μm. Whereas a larger pilot hole (6.5 mm) causes the final hole to be nonagonal with a much lower roundness error (60 μm). Centering prior to drilling, produced holes of higher quality, than without it.

Sakuma et al. [22], studied hole-accuracy in view of drill rigidity and point geometry. The positional deviation of the hole (run-out) from the true axis seems mostly to be determined at the beginning of penetration. Feed method has a clear influence on the run-out. Drilling with a 2-step feed method (initiating at a low feed and then increasing to high feed) significantly reduces the run-out of the hole, compared to drilling at high feed throughout. The feed method has a similar effect on roundness error of the hole.

Chahil [5] studied the nature of the dynamic components of torque and thrust forces in drilling. The results of his statistical analysis show that the dynamic fluctuations of torque and thrust forces in drilling are stationary random processes with a Gaussian density function.

Galloway [14] conducted an extensive experimental investigation into various factors that influence drill performance. A detailed discussion of

relevant portions of his results is presented in chapter 3 (section 3.8.1).

Oxford [19] studied the basic cutting mechanics in the various cutting regions of a twist drill, through his experimental investigation. He also attempted a relationship between the cutting geometry and the mechanics of metal removal.

Shaw and Oxford [15] developed empirical equations to predict torque and thrust forces in drilling, based on a dimensional approach. Following extensive experimental measurement of forces, equations have been developed to compute the forces from the tool, materials and process parameters given.

The theoretical modelling of the cutting mechanics in drilling has been and continues to be the focus of numerous investigations. Notable among earlier researchers, Pal et al. [23] modelled the cutting mechanics. Their model avoided the chisel-edge region due to its complexity, and considered only the cutting lips. Relations are developed between the various tool, materials and process variables, to obtain an expression to compute the torque in drilling. The results are compared to the experimental force measurements. Williams [24], and Wiriyacosol and Armarego [25] have attempted a complete model to predict torque as well as thrust, including cutting in the chisel-edge region. The former researcher takes into consideration the feed velocity and the resulting dynamic cutting geometry. More recently, Watson [26] has attempted the

theoretical prediction of torque and thrust forces. A thorough model is developed separately for the chisel-edge region and the lips, and later integrated.

All of the theoretical models mentioned above, give reasonably accurate estimates of the forces in drilling. However, their success is limited to specific work materials. The models are not amenable to parametric studies regarding tool geometry or process parameters other than feed and speed. Above all, they are concerned only with the static components of the forces.

1.4 Objectives of this Investigation

The geometrical features of twist drills are complex and unique as described in previous sections. Its features have been developed and refined over a long period of time. Yet many of these geometrical features which have long been standardized, are designed merely for functionality. Their potential effects on drill performance are barely understood. No clear reasoning is seen for the existence and/or the design of some of the drill features. Most research found on these features are mere parametric studies to obtain certain apparently optimal performance.

The helical flutes of a drill constitute one such design feature which warrants a closer examination. Thus the objectives of this investigation are as follows :

I. An investigation of the torque-thrust coupling effect.

- A thorough understanding of the interactions
- Determine the effect of helix angle on this coupling interaction
- Study the variation of the interaction with such parameters as drill diameter, fluted length in torsion etc.

II. A study of the influence of torque-thrust coupling on drills and drilling

- Investigation of the torsional stiffening due to coupling
- Study of the coupling effect from a forces point of view
- Possible effects of coupling on drilling forces and drill behaviour

III. An investigation of the effect of pilot hole size on hole quality

- Study of the cutting mechanics and its effect on forces
- Proposal of a new criterion for sizing pilot holes

1.5 A Brief Outline of the Thesis

Chapter 2 presents a thorough analysis of the torque-thrust coupling effect in twist drills. The experimentation conducted to determine the various stiffness coefficients is described. The results are analyzed for the effect of helix angle on the coupling effect, and in turn its influence on the torsional stiffness of the drill.

Chapter 3 studies the coupling effect from the forces point of view. The effect of coupling on drilling forces is explored, and a set of equations are derived to separate the true and induced forces in drilling. The possible effects of torque-thrust coupling on drill dynamic behaviour is also investigated.

Chapter 4 presents an analysis of pilot hole drilling. The effect of pilot hole size on the quality of the final hole, is studied from a cutting mechanics point of view. Based on the analysis, a new criterion is proposed for sizing pilot holes.

Chapter 5 describes in detail the instrumentation, the format and design of the drilling experiments conducted for the investigation. The design of the dynamometer to measure drilling forces, and a detailed description of its static and dynamic calibration procedure is also presented.

Chapter 6 contains the data reduction, analysis and detailed discussion of the results from the drilling experiments, in the light of the various objectives of the investigation. Mainly, the static components of torque, and thrust, and the dynamic components of torque, thrust and the radial forces are analyzed. From the analysis, the various static and dynamic effects of coupling, predicted in chapter 3 are verified. Hole quality measurements (in terms of roundness error) are also presented to evaluate the pilot hole sizing criterion proposed in chapter 4.

Chapter 7 presents an overall summary of the conclusions arising from this investigation. With relevance to the findings of this investigation, numerous aspects that warrant further study are suggested for future research work.

CHAPTER 2

THE TORQUE-THRUST COUPLING EFFECT IN TWIST DRILLS

From the twisted appearance of its body, it is apparent to one's intuition that a drill behaves similar to a rubber band which, when twisted several turns, pulls on itself and contracts. In drills this behaviour can be visualized to be bi-directional, as shown in figure 2.1. That is, applying a twist in the direction of cutting torque will tend to 'unwind' the helix, increasing the drill length and an opposite twist will 'wind' the helix to contract the drill. Conversely, applying a compressive axial force winds the drill and tension unwinds it. In comparison, a prismatic bar contracts regardless of the direction of twist applied.

The above intuitive observation has been made by many earlier researchers [8, 9, 10, 11]. Among them, De Beer [8] refers to an earlier researcher and defines the so called Maxwell's influence coefficients, α_{ij} as follows,

$$\begin{bmatrix} \alpha_{11} & -\alpha_{12} \\ -\alpha_{21} & \alpha_{22} \end{bmatrix} \begin{Bmatrix} F \\ T \end{Bmatrix} = \begin{Bmatrix} \epsilon \\ \theta \end{Bmatrix} \tag{2.1}$$

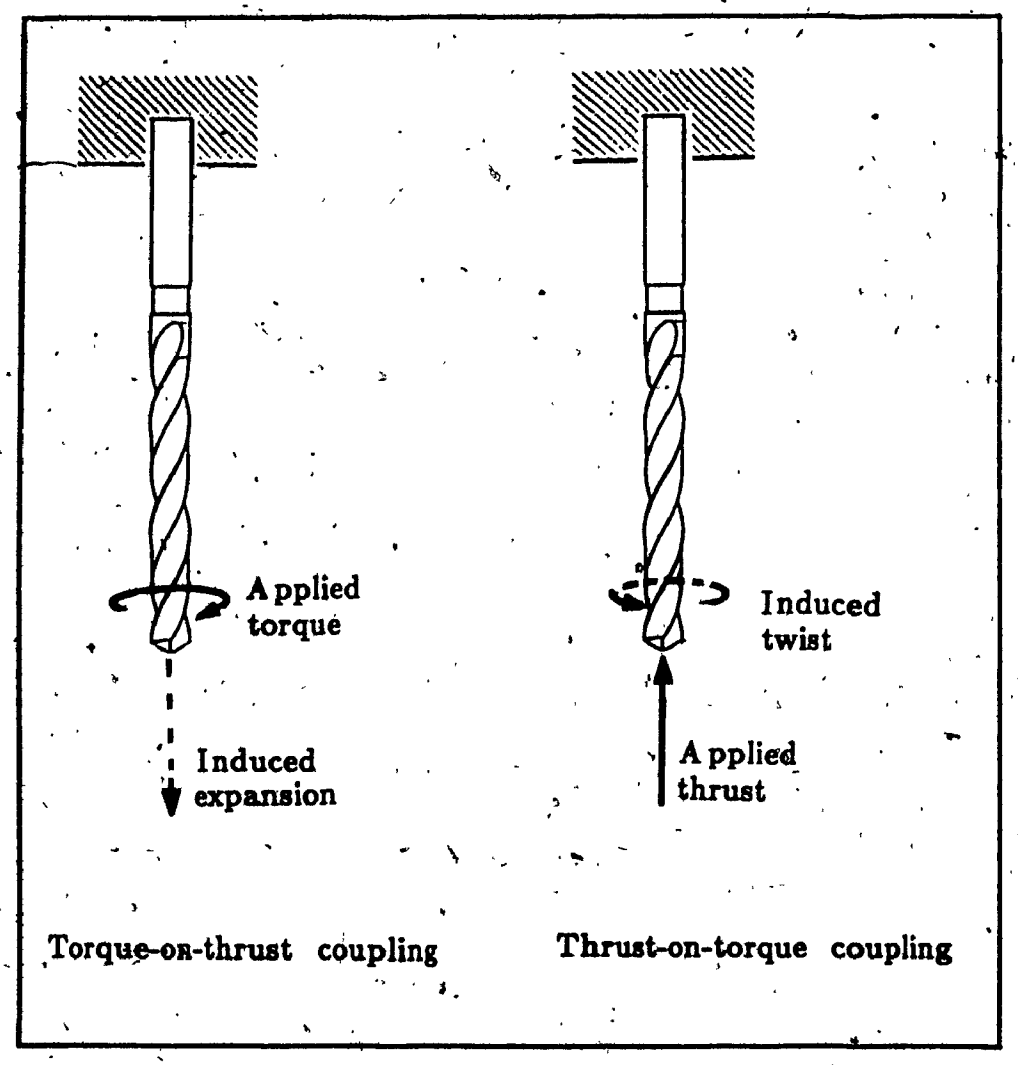

Figure 2.1 Schematic illustration of the coupling effect.

where

ϵ = shortening of the drill

θ = angle of twist

F = axial thrust force

T = torque

α_{ij} = Maxwell's influence coefficients

Figure 2.2 shows the implicit definitions of positive directions of all quantities, consequently the coefficients α_{ij} are all positive. The cross-coupling between torque and thrust (or twist and axial strain) is symmetric and so, α_{12} and α_{21} have the same magnitude. Values of α_{ij} have been determined experimentally for drills of various web thicknesses and it is shown [8] that decreasing the web thickness increases the interaction between twist and axial strain.

Theoretical treatment of the general topic of twisted bars has been attempted by Rosen [12]. A set of equations that describe the nonlinear deformation of initially twisted bars under the simultaneous influence of torque and tension force are derived. The theory is verified for thin metal strips of symmetrical cross sections with a slight initial twist and small applied deformations.

However, the nature of twist drill geometry stifles such an analytical approach. The cross section profile of a standard drill is anti-symmetric,

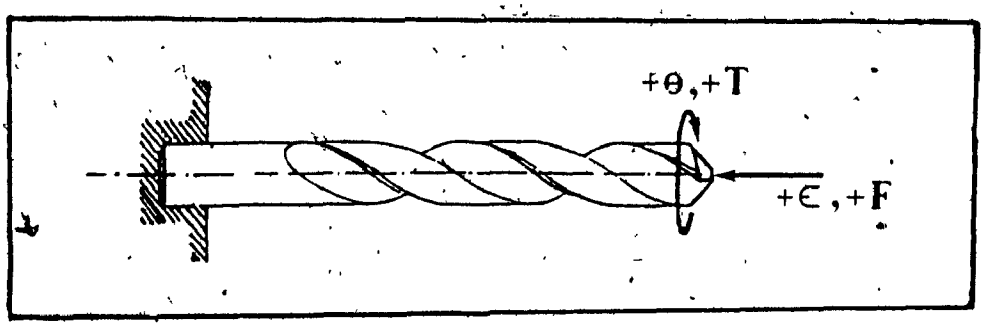

Figure 2.2 The coupling effect : Sign convention.

and it varies significantly due to the increasing web thickness along the fluted portion. The fluted portion is thoroughly non-prismatic due to the large helix angle, and the entire body has a taper towards the shank. An analytical static deformation model obtained in spite of these complexities would not lend itself to a parametric study. Therefore an experimental approach has been resorted to in the present investigation.

2.1 Format and Design of Experimentation

Accurate measurement of the static deformations (twist angle and axial strain) of a drill under loading is impractical. Therefore the converse approach is taken, that is, metered values of twist and axial strain are applied, measuring the torque and thrust reactions produced by the drill. For this purpose, a set of 'coupling stiffness coefficients' are defined as follows

$$\begin{Bmatrix} F \\ T \end{Bmatrix} = \begin{bmatrix} K_{ff} & K_{tf} \\ K_{ft} & K_{tt} \end{bmatrix} \begin{Bmatrix} \epsilon \\ \theta \end{Bmatrix} \qquad (2.2)$$

where

K_{ff} = Axial stiffness under torsional restraint

K_{tf} = Torque-on-thrust coupling stiffness

K_{ft} = Thrust-on-torque coupling stiffness

K_{tt} = Torsional stiffness under axial restraint

It can be easily seen that the matrix of coefficients in equation 2.2 is the exact inverse of that in equation 2.1. The cross-coupling coefficients K_{ft} and K_{tf} are of equal magnitudes.

Three types of experiments are performed to determine the various stiffness coefficients.

Type I. Pure torsion experiments

Type II. Torque-on-thrust coupling experiments to find K_{tf} and K_{tt}

Type III. Thrust-on-torque coupling experiments to find K_{ft} and K_{ff}

The type I experiments are done by applying positive twist (figure 2.2) at the point end and measuring the torque in the drill, allowing free axial expansion. The slope of the torque versus twist graph is the simple torsional stiffness of the drill. The torque-on-thrust coupling experiments (type II) involve applying a positive twist, measuring both torque and the thrust reaction induced by rigidly restraining the axial expansion. The slope of the twist versus thrust graph is the stiffness coefficient K_{tf}, and that of twist versus torque is K_{tt}. For the thrust-on-torque experiments (type III), compressive axial strain is applied, measuring thrust and the torque reaction induced by keeping the drill rotationally restrained.

Table 2.1 shows the various drills used and their specifications. The conical point on the drills are removed and made flat-faced, also flats are ground on either rake-face. These modifications are made to adapt the

Table 2.1 Specifications of drills used and experimental parameters.[21]

Drill Size	Helix type	Web Thickness inch (mm)	Lead inch (mm)	Peripheral helix angle [deg]	Gage Length in loading inch (mm)	Fluted Length in loading inch (mm)
1/2"	Regular (RH)	0.075 (1.905)	2.441 (62)	32.76	5.472 (139)	4.409 (112)
	High (HH)	--do--	1.969 (50)	51.42	5.433 (138)	4.331 (110)
13/32"	Low (LH)	0.061 (1.549)	5.118 (130)	14.0	3.976 (101)	3.228 (82)
	Regular (RH)	--do--	2.047 (52)	31.94	--do--	3.622 (92)
	High (HH)	--do--	1.654 (42)	37.65	--do--	3.268 (83)
3/8"	Low (LH)	0.058 (1.473)	5.118 (130)	12.96	3.740 (95)	3.228 (82)
	Regular (RH)	--do--	1.850 (47)	32.49	3.6[illegible] (93)	3.661 (93)
	High (HH)	--do--	1.575 (40)	36.80	3.622 (92)	3.543 (90)
1/4"	Low (LH)	0.048 (1.219)	3.228 (82)	13.67	2.795 (71)	2.244 (57)
	Regular (RH)	--do--	1.260 (32)	31.94	2.756 (70)	2.677 (68)
	High (HH)	--do--	1.102 (28)	35.48	2.795 (71)	--do--

point ends for the special gripping fixture designed for the experiments.

2.2 Experimental set-up

The experiments are carried out on an Instron model 1125 tension/compression cum torsion testing machine. For torsion tests vertical movement of the cross-head is prevented, whence, the main drive spindle gives rotation to the lower sample-holding fixture. A wide choice of twist and compression rates are available. The present experiments were done at a torsion rate of 3.6 degrees per minute.

For pure torsion experiments (figure 2.3) the gripping fixture is connected to the main spindle through a spring-loaded chuck fixture. This allows the free axial expansion of the sample while applying torsion. The strain gage load cell above the upper chuck reads torsion and drives the plotter attached.

The torque-on-thrust and thrust-on-torque coupling experiments are carried out with the gripping fixture connected to the spindle through a piezoquartz load cell (Kistler 9271A) which measures both torque and thrust (figure 2.4). A Philips X-Y-T chart recorder is used to plot the torque and thrust signals simultaneously with respect to time.

The three types of experiments were carried out on all the drills, keeping a constant gage length for a given drill type. The gage lengths and fluted lengths used are listed in table 2.1. The deformations applied

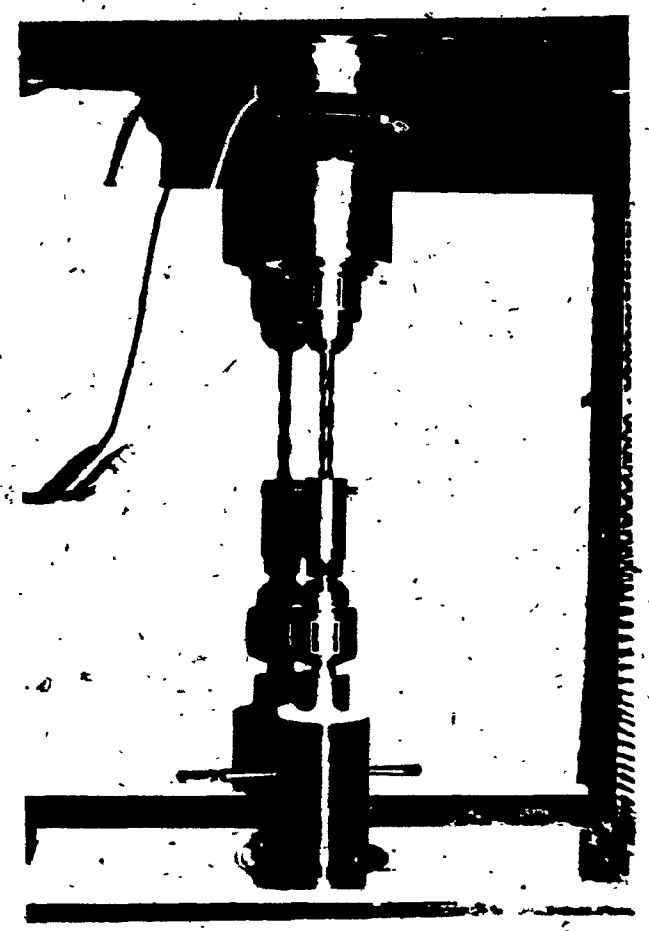

Figure 2.3 Set-up for pure torsion experiments.

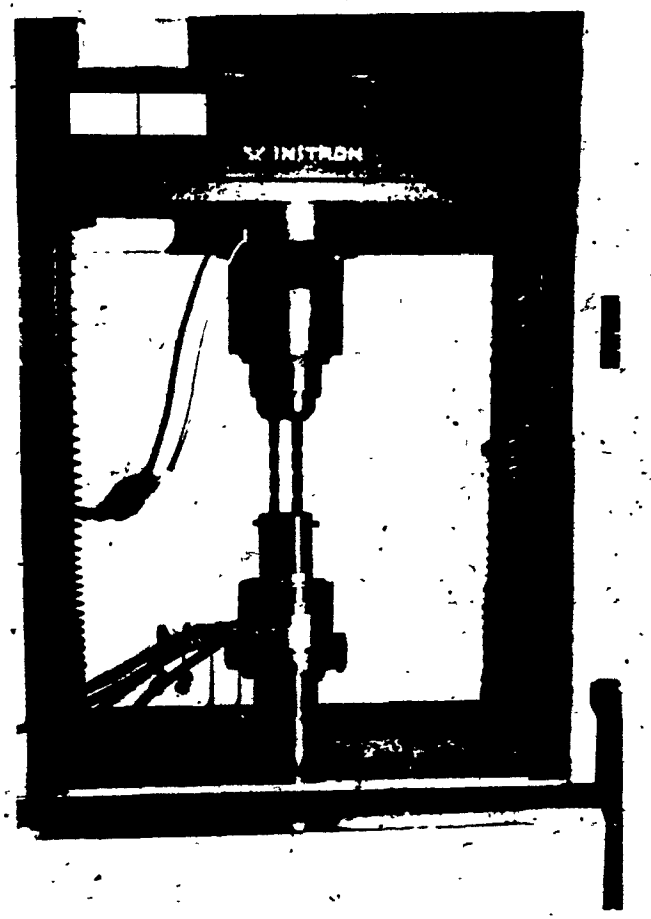

Figure 2.4 Set-up for coupling experiments.

were within their elastic limits for the drill.

2.3 Results and Parametric Analysis

From the raw experimental graphs it is seen that the static behaviour of the drills is highly linear. Some small irregularities resulted at the beginning of these plots due to the clearances at the gripper, voltage residues in the charge amplifier, etc.. For this reason the load-deflection graphs were reconstructed with the data from the original graphs.

Figures 2.5, 2.6, and 2.7 are a few examples of the reconstructed graphs, showing the effect of helix angle on the static characteristics of drills. Notable among these graphs is the induced thrust versus twist behaviour. In figure 2.5b, a 1/4-inch diameter drill twisted through 7 to 8 degrees shows an induced thrust of 200 pounds. This is a significant value considering the drill size. The values are equally dramatic for the other sizes tested. The slopes of these graphs are the corresponding stiffness coefficients. The units used for the stiffness coefficients are meant for an easy comprehension of the results.

2.3.1 Effect of Fluted length/Gage length

On drills of several sizes and types, type I and type II experiments were repeated with an increased shank length under torsion (same fluted length). The stiffness coefficients from the two trials compared better

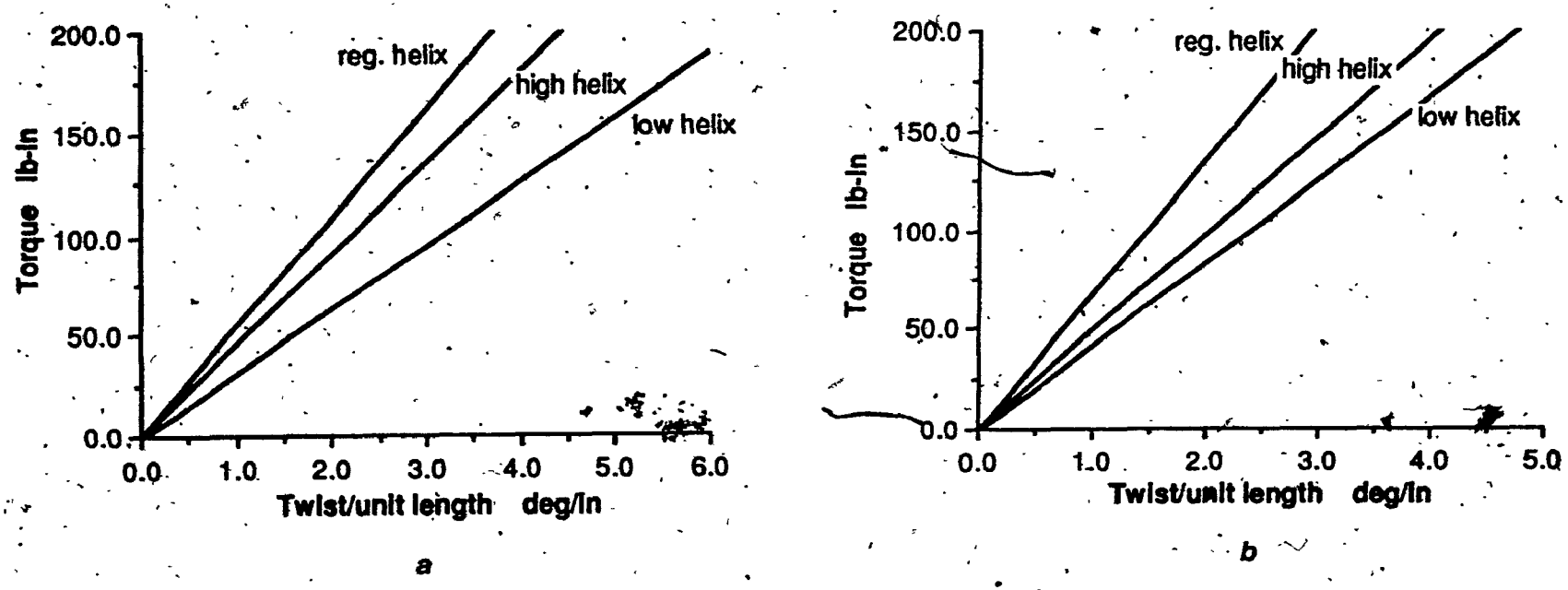

Figure 2.5 Results of pure torsion tests on (a) 3/8" drills and b) 13/32" drills.

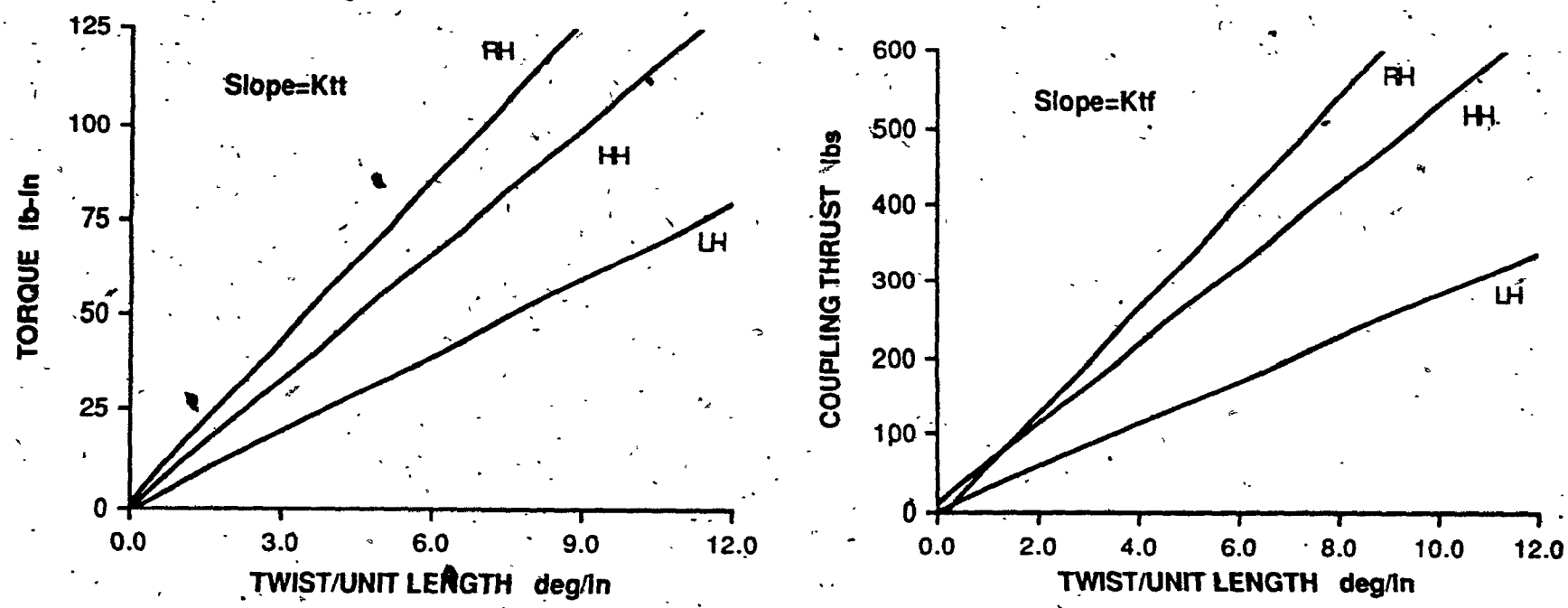

Figure 2.6 Graphs of applied twist versus torque and induced thrust for 1/4" drills.

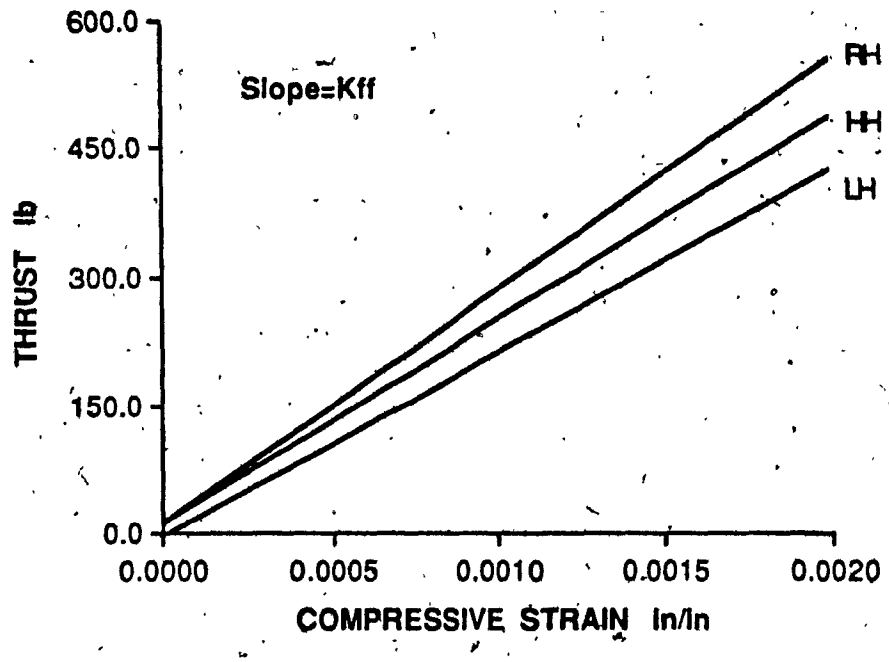

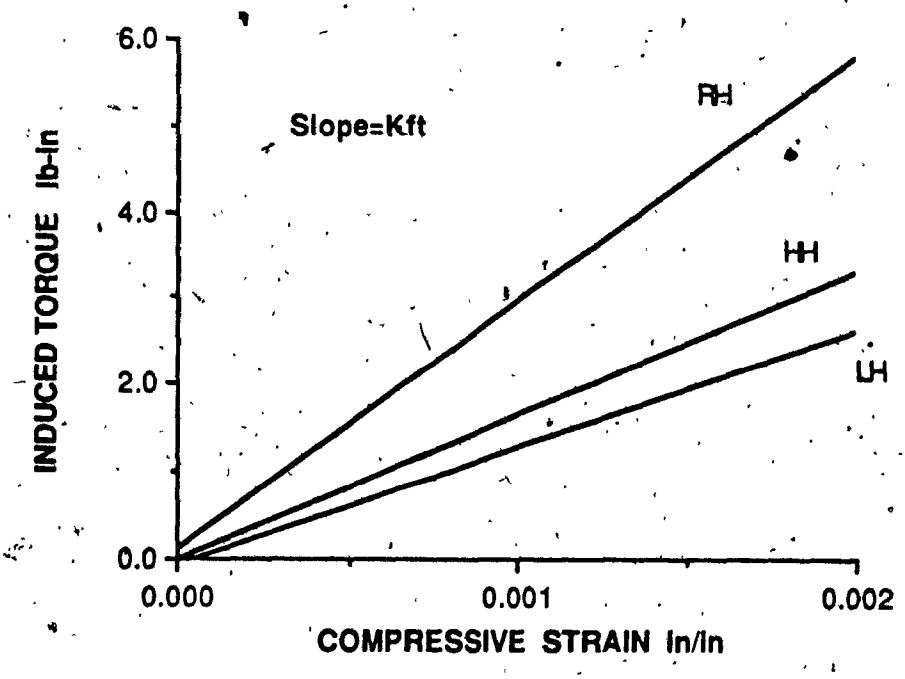

Figure 2.7 Graphs of applied axial strain versus thrust and induced torque for 1/4" drills.

when normalized with respect to the fluted length, than if gage length were used. Therefore throughout these results (including type III experiments) the applied deformations (and thus the stiffness coefficients) have been normalized with respect to the fluted lengths listed in table 2.1.

2.3.2 Effect of pre-load

To test the influence of axial pre-load, some of the type II experiments were repeated with various values of axial pre-load applied before beginning torsion. Similarly, several type III experiments were done with a torsional pre-load. Contrary to one's expectation of a stiffening trend, the coupling stiffness coefficients are unaffected by pre-loading as seen in the numerical examples of Table 2.2. If the coefficients were of an increasing nature with pre-load, the graphs of twist versus thrust and axial strain versus torque would be polynomials with monotonously increasing slopes. Highly linear trends are observed instead (figures 2.6b and 2.7b), leading to the conclusion that pre-load does not affect the static behaviour of drills.

The stiffness coefficients of the various drills tested are listed in table 2.3. As mentioned earlier, the two coefficients K_{tf} and K_{ft} should have the same magnitudes. But as seen in the table of values, they differ significantly in some experiments. These differences may be entirely due to experimental factors, especially in type III experiments. The clearances in the gripping fixture, insufficient torsional restraint, unevenness of the

Table 2.2 Effect of pre-load on K_{tf} and K_{ft}.[21]

Drill Size	Helix type	Axial Preload lbs (N)	K_{tf} $\frac{lb\text{-}in}{rad}$ $(\frac{N\text{-}m}{rad})$	Torsional pre-load lb-in (N-m)	K_{ft} lb-in (N-m)
1/2"	Regular	50 (222.5)	1.72×10^4 (1948.1)	0	1.77×10^4 (2004.7)
		25 (111.3)	1.69×10^4 (1914.1)	18.3 (2.07)	1.90×10^4 (2151.9)
		35 (155.8)	1.71×10^4 (1936.8)		
13/32"	Regular	25 (111.3)	9300 (1053.3)	--	--
		40 (178.0)	1.04×10^4 (1177.9)	--	--
3/8	Low	5 (22.3)	3867 (438.0)	--	--
		15 (66.8)	3641 (412.4)	--	--
	Regular	35 (155.8)	8800 (996.7)	0	1.14×10^4 (1291.2)
		25 (111.3)	9397 (1064.3)	5.5 (0.623)	1.19×10^4 (1347.8)
1/4"	Regular	25 (111.3)	3527 (399.5)	0	2841 (321.8)
		10 (44.5)	3541 (401.1)	4.0 (0.453)	2926 (331.4)
	High	15 (66.8)	2999 (339.7)		
		45 (200.3)	3038 (344.1)		

Table 2.3 Experimental results : Stiffness coefficients.[21]

Drill Size	Helix type	K_{ff} lb(N)	K_{tf} $\frac{lb\text{-}in}{rad}$ $(\frac{N\text{-}m}{rad})$	K_{ft} lb-in (N-m)	K_{tt} $\frac{lb\text{-}in^2}{rad}$ $(\frac{N\text{-}m^2}{rad})$
1/2"	Regular	5.54×10^5 (2.47×10^6)	1.69×10^4 (1.91×10^3)	1.77×10^4 (2.0×10^3)	194.24 (0.559)
	High	4.57×10^5 (2.04×10^6)	1.48×10^4 (1.68×10^3)	1.38×10^4 (1.56×10^3)	150.46 (0.433)
13/32"	Low	4.98×10^5 (2.22×10^6)	4540 (514.2)	5813 (658.4)	45.51 (0.131)
	Regular	5.4×10^5 (2.41×10^6)	1.04×10^4 (1.18×10^3)	1.42×10^4 (1.61×10^3)	79.59 (0.229)
	High	4.2×10^5 (1.88×10^6)	8642 (978.8)	12000 (1359.1)	57.2 (0.165)
3/8"	Low	4.68×10^5 (2.09×10^6)	3867 (437.9)	4724 (535.0)	34.6 (0.100)
	Regular	4.99×10^5 (2.23×10^6)	8474 (959.8)	1.14×10^4 (1.29×10^3)	62.45 (0.180)
	High	4.05×10^5 (1.81×10^6)	6755 (765.1)	7070 (800.8)	50.67 (0.146)
1/4"	Low	2.15×10^5 (0.96×10^6)	1642 (185.9)	1339 (151.7)	6.69 (0.019)
	Regular	2.74×10^5 (1.22×10^6)	3527 (399.5)	2841 (321.8)	13.21 (0.038)
	High	2.39×10^5 (1.07×10^6)	2999 (339.7)	1658 (187.8)	11.04 (0.032)

flat-face on the point end, and eccentricity of loading are some of the possible sources of error. However, the results of type II and type III experiments exhibit qualitative consistency as shown further. For numerical purposes however, the K_{tf} values (obtained by type II experiments) will be taken as the correct cross-coupling coefficients for the drills.

In order to investigate the influence of helix angle, the stiffness coefficients are plotted against the peripheral helix angles of the respective drills, and the results are discussed below.

2.4 Effect of Helix Angle on Cross Coupling Interaction

Figure 2.8 illustrates the profound influence that helix angle has on the torque-thrust coupling interaction as measured by the coupling coefficient K_{tf}. The value of K_{tf} increases between a low helix type and a regular helix type of drill, and then again decreases for a high helix drill. Thus the coupling interaction exhibits a distinctly defined maximum with respect to helix angle. From the graphs this 'optimum' helix angle appears to be around 28 degrees. It is interesting to note that this optimum helix angle is lower than those of the drills most commonly used (regular helix, 32 degrees). However more tests with a larger choice of helix angles are necessary to confirm the exact value of this optimum. Also notable is the drastic decrease of the coupling coefficients away from the optimum helix angle.

The extrapolation of the curves (figure 2.8) to very small helix angles indicates a change of sign for K_{tf} values. This is consistent with the actual behaviour of prismatic members, which contract under torsion, producing tensile reaction forces. The coefficient value reaches zero at a helix angle of about 10 degrees in all drills.

The effect of helix angle on the thrust-on-torque interaction as measured by the coupling coefficient K_{ft} was also investigated. Figure 2.9 is the plot of K_{ft} against helix angle, and it illustrates qualitative consistency with the graph in figure 2.8. That is, the coupling interaction has a distinct maximum around a helix angle of 28 degrees, with a drastic rate of change. The distortion in some of the curves is attributable to the errors in the measurement of K_{ft} values, as described earlier (section 2.3.2).

2.5 Variation of Coupling Interaction with Drill Diameter

As seen in figures 2.8 and 2.9, the coupling interaction curves shift upward for increasing diameter of drills. There is some evidence of the optimum helix angle increasing with drill size, but it is inconclusive due to the limited number of drill sizes tested.

Further, the rate of increase/decrease of the coupling coefficients with helix angle depends on the drill diameter. The larger the drill, the higher is the rate of increase of K_{ft} and K_{tf} with helix angle (figures 2.8 & 2.9).

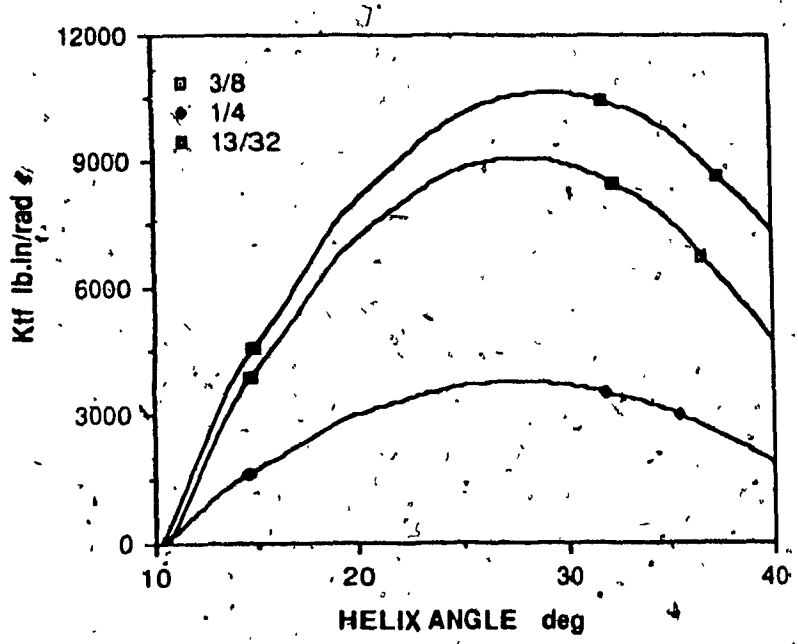

Figure 2.8 Variation of coupling stiffness Ktf, with helix angle.

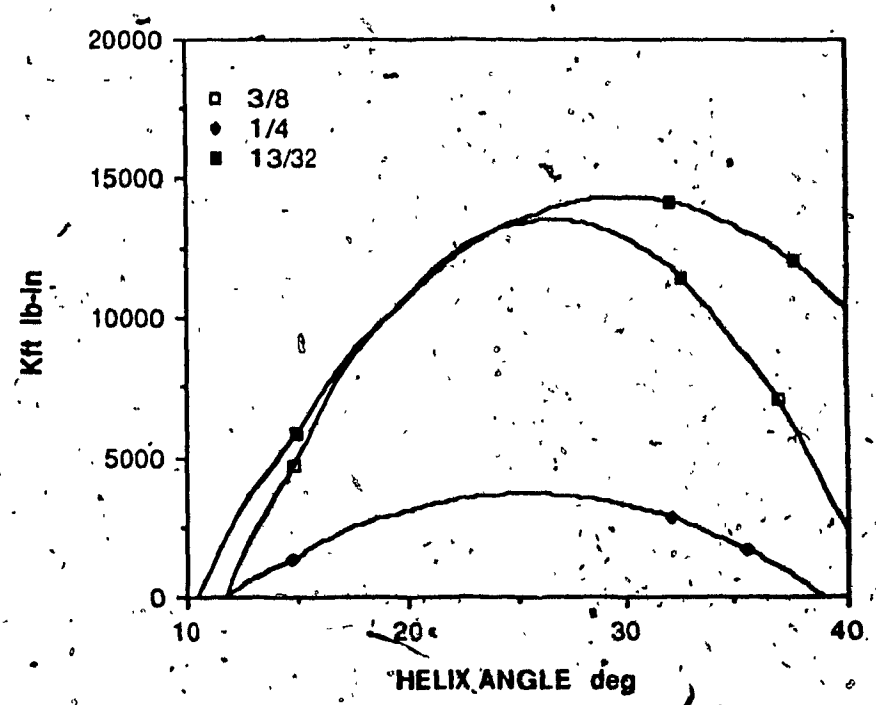

Figure 2.9 Variation of coupling stiffness Kft, with helix angle.

This aspect is better demonstrated in the plot of K_{tf} versus drill diameter (figure 2.10). The coupling interaction is shown to increase parabolically with drill diameter. It follows from the above observations that in the case of small drills, helix angle has a relatively minor influence on the coupling interaction.

2.6 Effect of Helix Angle on Torsional Stiffness

The pure torsional stiffnesses (without axial restraint) of drills show a clear dependence on helix angle (figure 2.11). Interestingly, even without the torque-thrust interaction, the torsional stiffness variation has a distinct maximum around a helix angle of 28 degrees. Similar to the coupling interaction, the torsional stiffness variation with helix angle is more pronounced in larger drills.

Torsional stiffnesses measured under axial restraint (type II experiments) are found to be 10 to 25 percent higher than the corresponding pure torsional stiffnesses. When the stiffnesses are plotted against helix angle (figure 2.12), a trend identical to that of pure torsional stiffness is observed. Amongst drills of a given size, regular helix drills show the highest increase in torsional stiffness. This corresponds to the observation that regular helix drills have the highest level of torque-thrust interaction. High helix drills show slightly lower increases in torsional stiffness, while low helix drills show the least. Thus it is clearly demonstrated that the torque-thrust interaction causes a torsional stiffening

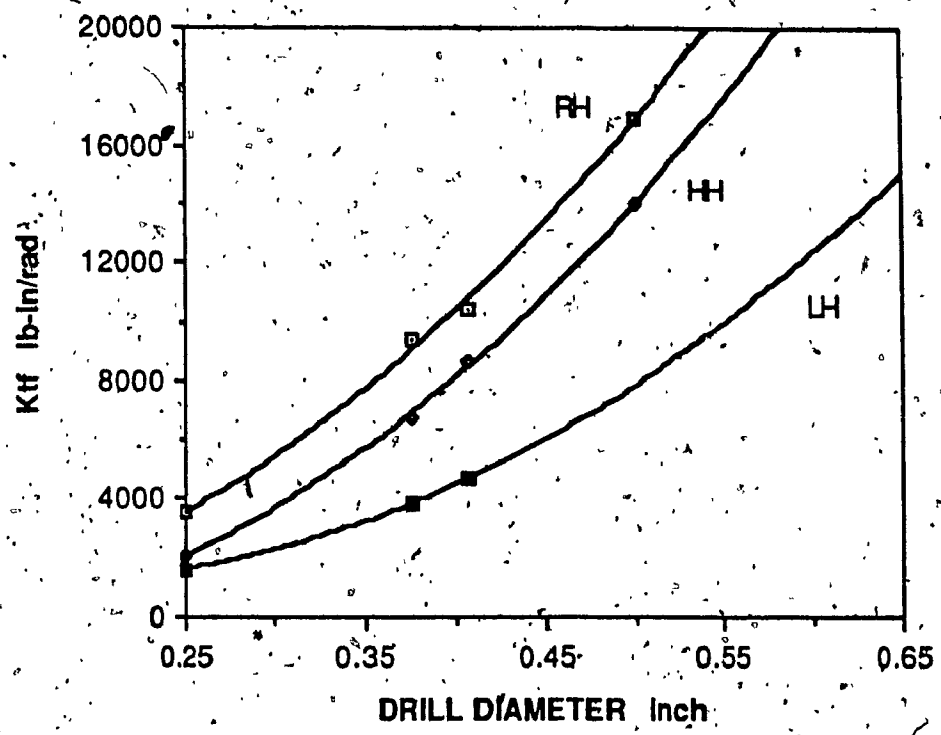

Figure 2.10 Variation of coupling stiffness Ktf, with drill diameter.

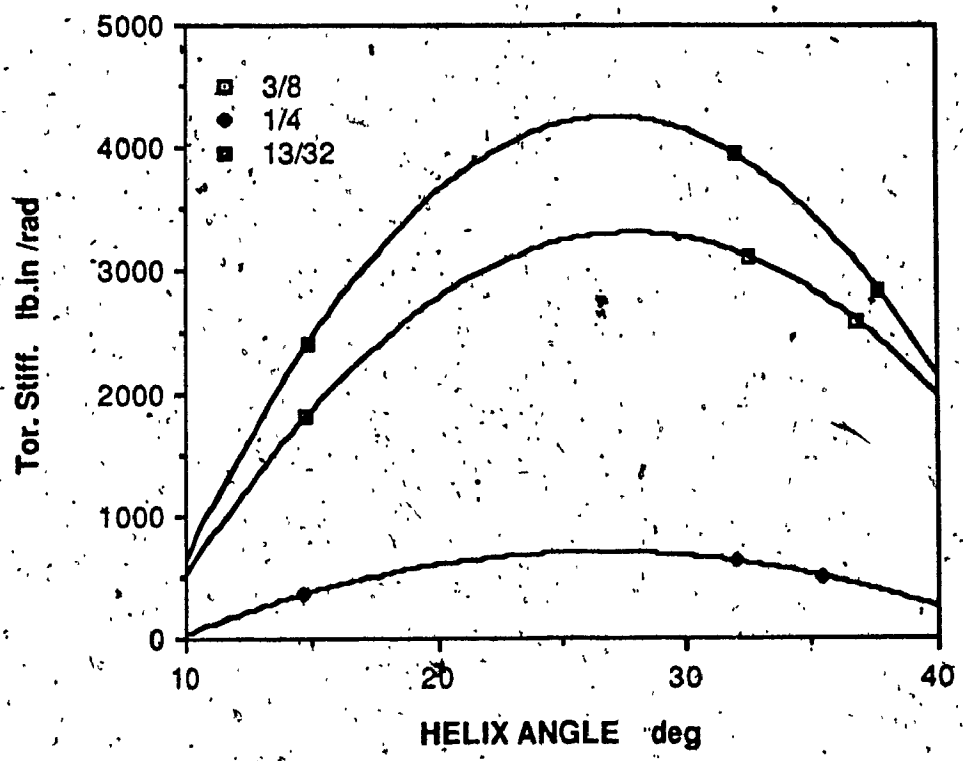

Figure 2.11 Variation of pure torsional stiffness with helix angle.

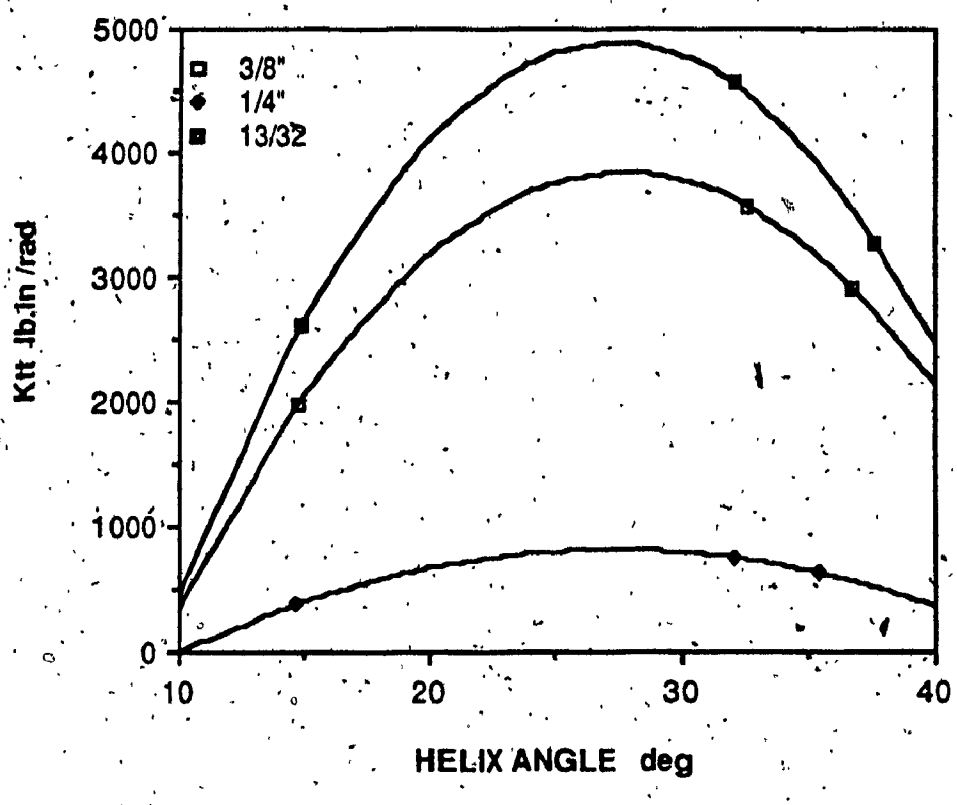

Figure 2.12 Effect of helix angle on torsional stiffness under axial restraint (Ktt).

effect when drills are axially restrained. The indirect effect of helix angle on this stiffening effect is also apparent.

2.7 Corroboration of Past Research

The findings of this investigation may aid in explaining some of the observations made by past researchers on the static deformation behaviour of drills. One may also get a better perspective on certain drill design conventions based on the information.

First of all the profound effect that helix angle has on drill torsional stiffness is clearly shown. This reconfirms Kronenberg's observations (from Lorenz [9]) on twisted profiles.

Spur and Masuha [10] found that indiscriminate increase of web thickness results in a decrease in torsional stiffness. This can be well explained on the basis of the coupling effect. Increasing the web thickness causes a decrease in the torque-thrust interaction [8]. A reduction in the coupling interaction diminishes the beneficial stiffening effect of thrust as shown by the present investigation. The result is a lower torsional stiffness.

The pure torsional stiffness of drills is maximized for a helix angle of around 28 degrees. Also, owing to the coupling effect, the same value of helix angle causes the largest increase in the torsional stiffness under thrust (which simulates drilling conditions). This might be part of the

basis for the traditional popularity of a 28 to 30 degree helix angle for all general purpose drills.

2.8 Conclusions

The torque-thrust coupling effect in twist drills has been investigated with a series of experiments. A set of direct and cross coupling stiffness coefficients are defined for twist drills. It is seen that the coupling interaction is a highly linear phenomenon. The investigation reveals that this interaction (as measured by K_{tf} and K_{ft}) has a distinct maximum around helix angle of 28 degrees. The interaction is more sensitve to helix angle in the case of larger drills. For drills of a given helix type, the coupling interaction increases parabolically with drill diameter.

The torsional stiffness is similarly influenced by helix angle, with a maximum again around 28 degrees, and a steep decline away from this maximum. Smaller drills are relatively insensitive to helix angle in this regard. A study of the torsional stiffness under axial restraint clearly reveals a torsional stiffening effect due to the coupling interaction. The higher the interaction, the higher will be the the torsional stiffness. Thus drills with the 'optimum' helix angle of 28 degrees post the highest torsional stiffness. It is noted with interest that this 'optimum' helix angle of 28 degrees is lower than the value used in current drilling practice (32 degrees), although more tests are needed to confirm the same.

The findings of this investigation are used to corroborate some previous research conclusions, and is proposed as a probable basis for certain drill design conventions.

The following chapter examines in detail, the induced forces aspect and its ramifications on drilling forces, their measurement, and on the drilling process itself.

CHAPTER 3

EFFECT OF TORQUE-THRUST COUPLING ON DRILLING FORCES AND DRILL BEHAVIOUR

The most basic manifestation of the coupling interaction is the inducement of axial strain due to twist, and vice versa. The above would be the sole effect if the induced strains were allowed to occur freely. However, if these strains are physically restrained, reaction forces are induced correspondingly. That is, torque induces thrust and thrust force application results in an induced torque. This effect was employed in the experimentation to study the coupling phenomenon, as described in the previous chapter.

More insight can be gained into the coupling effect by establishing a cause-effect relationship between the applied and induced forces. This can be done by analyzing the results of the coupling experiments from a purely forces point of view.

3.1 Induced-Force Coefficients

From the results of chapter 2 it is clear that the induced force reactions are a linear function of the corresponding applied deformations. Being within the elastic range, the applied deformations in turn are linearly proportional to the applied forces. Therefore the applied forces

and the corresponding induced deformations can be directly related, defining two new coefficients as follows

$$F_i = K_1 T \tag{3.1}$$

$$T_i = K_2 F \tag{3.2}$$

where

F_i = induced thrust

T_i = induced torque

F = applied thrust

T = applied torque

K_1 = coefficient of induced thrust

K_2 = coefficient of induced torque

These coefficients can be obtained by re-plotting the induced forces against the applied forces instead of the corresponding applied deformations. However, in the coupling experiments the applied and induced forces were simultaneously recorded against the applied deformations. This enables the calculation of the induced-force coefficients from the coupling stiffness coefficients, by extending their definitions as follows;

From the definition of the induced-force coefficients,

$$K_1 = dF_i/dT$$

$$K_2 = dT_i/dF$$

We have the coupling stiffness coefficients as

$$K_{tf} = dF_i/d\theta$$

$$K_{tt} = dT/d\theta$$

$$K_{ft} = dT_i/d\epsilon$$

$$K_{ff} = dF/d\epsilon$$

Now we can express

$$\frac{dF_i}{dT} = \frac{dF_i}{d\theta}\frac{d\theta}{dT} = \frac{K_{tf}}{K_{tt}}$$

and

$$\frac{dT_i}{dF} = \frac{dT_i}{d\epsilon}\frac{d\epsilon}{dF} = \frac{K_{ft}}{K_{ff}}$$

Therefore we can express

$$K_1 = K_{tf}/K_{tt} \tag{3.3}$$

$$K_2 = K_{ft}/K_{ff} \tag{3.4}$$

Thus the coupling-force coefficients are simple ratios of the stiffness coefficients determined earlier. This definition is employed to calculate the values of K_1 and K_2 for various drills, and are tabulated below (table

3.1).

In determining the stiffness coefficients with the coupling experiments, absolute rigidity of supports was assumed, with no axial/torsional compliance or slippage. The induced-force coefficients so obtained are maximal values. Any axial or torsional 'relaxation' reduces these values.

3.1.1 Variation of K_1 and K_2 with Drill Diameter

Interesting information is revealed when the induced- force coefficients tabulated above are plotted against the diameter of the drills. Figure 3.1 shows a graph of induced-thrust coefficient K_1 against diameter. It is clearly seen that the coefficient decreases with increasing drill diameter. According to the definition of equation 3.1 this means that for a given applied torque, smaller the drill, the larger will be the induced thrust.

On the other hand it was seen (from the results of the previous chapter) that, plotted against torsional deformation, the induced thrust was higher for drills of larger diameter. This can be explained as follows - Due to their inherently higher torsional stiffness and also due to their higher stiffness under axial restraint, larger drills undergo smaller torsional deformation. Which means the axial deformations induced are also smaller. Therefore the induced thrust reaction is proportionally smaller in larger drills.

Figure 3.2 shows the coefficient of induced torque (K_2) plotted

Table 3.1 Induced-force coefficients of various drills.

DRILL SIZE	HELIX TYPE	K_1 $in^{-1}(m^{-1})$	K_2 in(m)
1/2"	Regular	1.523 (59.96)	0.03051 (7.75E-4)
	High	1.717 (67.60)	0.03239 (8.23E-4)
13/32"	Low	1.741 (68.54)	0.00912 (2.32E-4)
	Regular	2.281 (89.80)	0.01926 (4.892E-4
	High	2.637 (103.8)	0.02058 (5.23E-4)
3/8	Low	1.951 (76.81)	0.008263 (2.10E-4)
	Regular	2.368 (93.23)	0.01698 (4.31E-4)
	High	2.327 (91.61)	0.01668 (4.24E-4)
1/4"	Low	4.284 (168.7)	0.00764 (1.94E-4)
	Regular	4.660 (183.5)	0.01287 (3.27E-4)
	High	4.742 (186.7)	0.01255 (3.19E-4)

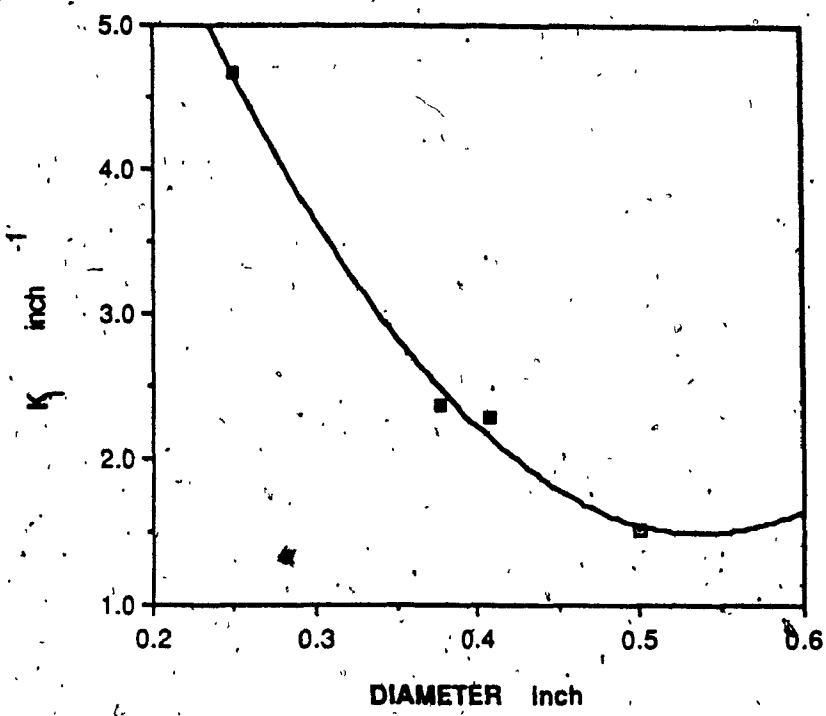

Figure 3.1 Variation of the induced-thrust coefficient with drill diameter.

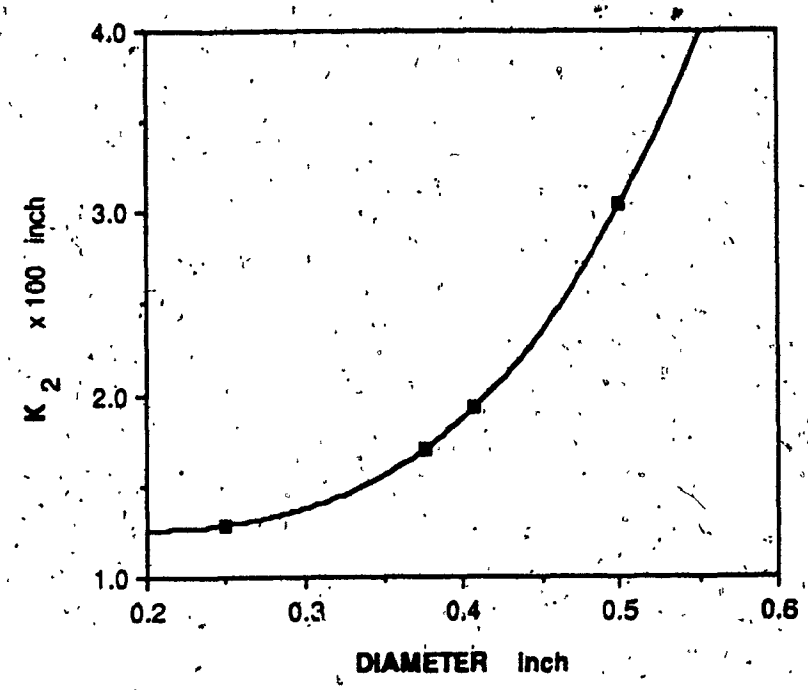

Figure 3.2 Variation of the induced-torque coefficient with drill diameter.

against drill diameters. Contrary to the variation of K_1, it increases with diameter. That is, the larger the drill, the larger will be the induced torque for a given applied thrust.

These observations on the variation of K_1 and K_2 with drill diameter, have important implications which will be explored later.

3.1.2 Effect of Helix Angle on K_1 and K_2

Figures 3.3 and 3.4 show graphs of the induced-force coefficients against the helix angles of the drills. It is seen that the trend of variation of the two coefficients is similar. In general the coefficients increase from low helix angles, reaching a saturation level around 30 degrees. This trend is interesting considering that the coupling interaction as such reaches a maximum around 28 degrees, and shows a decreasing trend beyond. This trend may be attributed to the variation of the direct stiffness coefficients K_{ff} and K_{tt} (equations 3.3 and 3.4) with helix angle.

From the point of view of induced forces, the above observation means that amongst drills of a given size, the lower the helix angle, lower will be the induced torque and thrust values. And for drills of high helix angle, the force-inducement increases and reaches a saturation level.

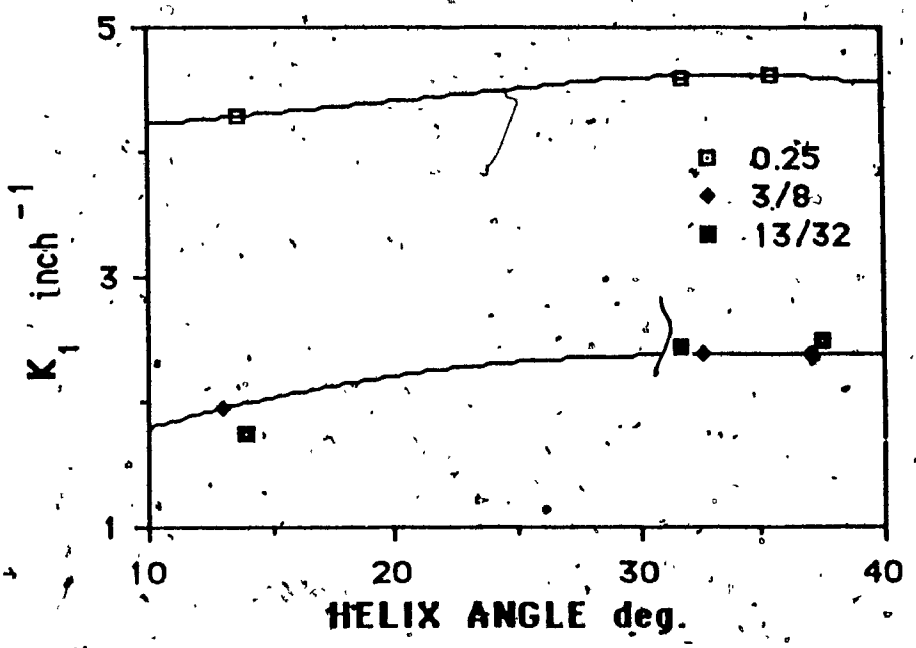

Figure 3.3 Variation of the induced-thrust coefficient with helix angle.

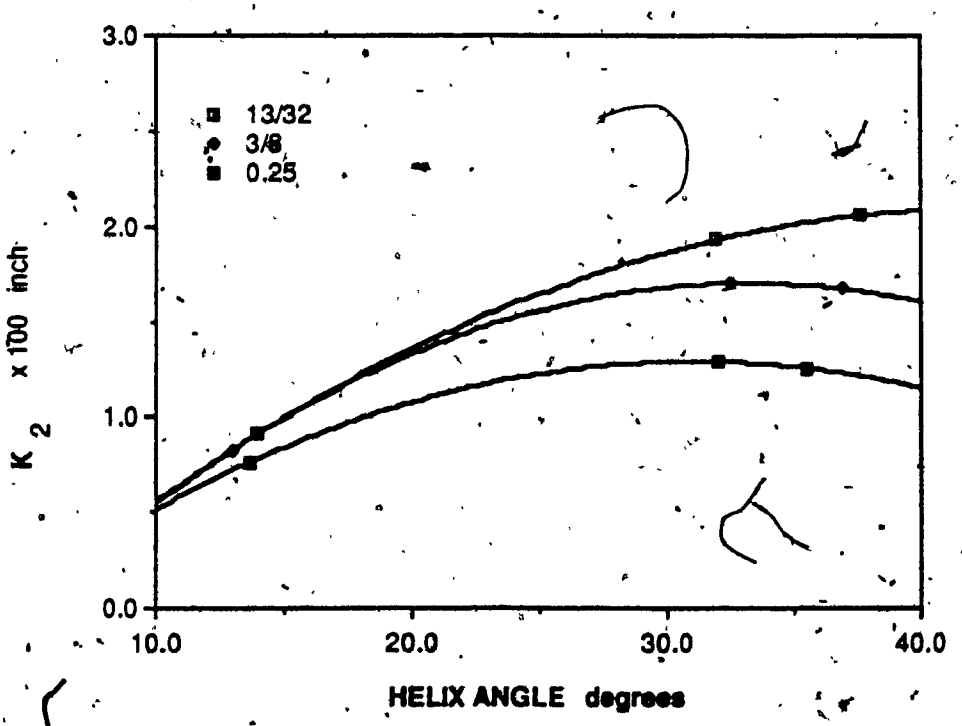

Figure 3.4 Variation of the induced-torque coefficient with helix angle.

3.2 Comparison of Static Test and Drilling Conditions

Drilling process basically involves the plastic deformation of the work material. Particularly in full-hole drilling, at the web of the drill, the metal is removed by a severe, extrusion type of effect which generates a large thrust force. The forces become especially severe when drilling hard materials such as steel, without a coolant. Thus it can be seen that the drilling process creates conditions similar to those in the torsion and compression tests described in the previous chapter. That is, the steady components of cutting torque and cutting thrust restrain the induced static deformations (axial expansion and torsional winding) of the drill.

3.3 Force Inducement During Drilling

Under the rigid support conditions it was seen, particularly from type-II coupling experiments, that the reaction forces inducement is a pronounced effect. For example, with an applied twist of about 7 to 8 degrees, a 1/4-inch diameter drill exerts an induced thrust of 200 pounds. The effect becomes increasingly prominent as drill size increases, with a 1/2-inch drill inducing 300 pounds thrust under a twist of about 3 to 4 degrees.

The fact that the coupling experiments closely simulate drilling conditions (in restraining drill expansion and winding), automatically implies that significant reaction forces are induced during drilling also. In

other words, the axial expansion caused by cutting torque is restrained by cutting thrust (which compresses the drill), inducing a thrust reaction force. Similarly, the torsional winding caused by cutting thrust is opposed by cutting torque (which tends to unwind the drill), resulting in an induced torque reaction. Figure 3.5 illustrates the effect. It is seen that the induced forces add up with the corresponding cutting forces. Therefore in drilling, the measured forces will always be an aggregate of the true cutting and the induced force components. And thus, it is erroneous to attribute the measured forces (torque and thrust) entirely to the cutting process alone.

The above phenomenon has profound consequences on various aspects of drilling, which will be dealt with later. But in order to explore the extent and nature of the induced forces, it is necessary to obtain a means of separating the true cutting and induced components of torque and thrust.

3.4 Separation of Cutting and Induced Components of Forces

Since the induced forces in drilling are due to the coupling effect, the results of the coupling experiments can be employed to separate the true cutting and induced force components.

As stated earlier the induced components of torque and thrust add up with the true components generated due to the work done in cutting

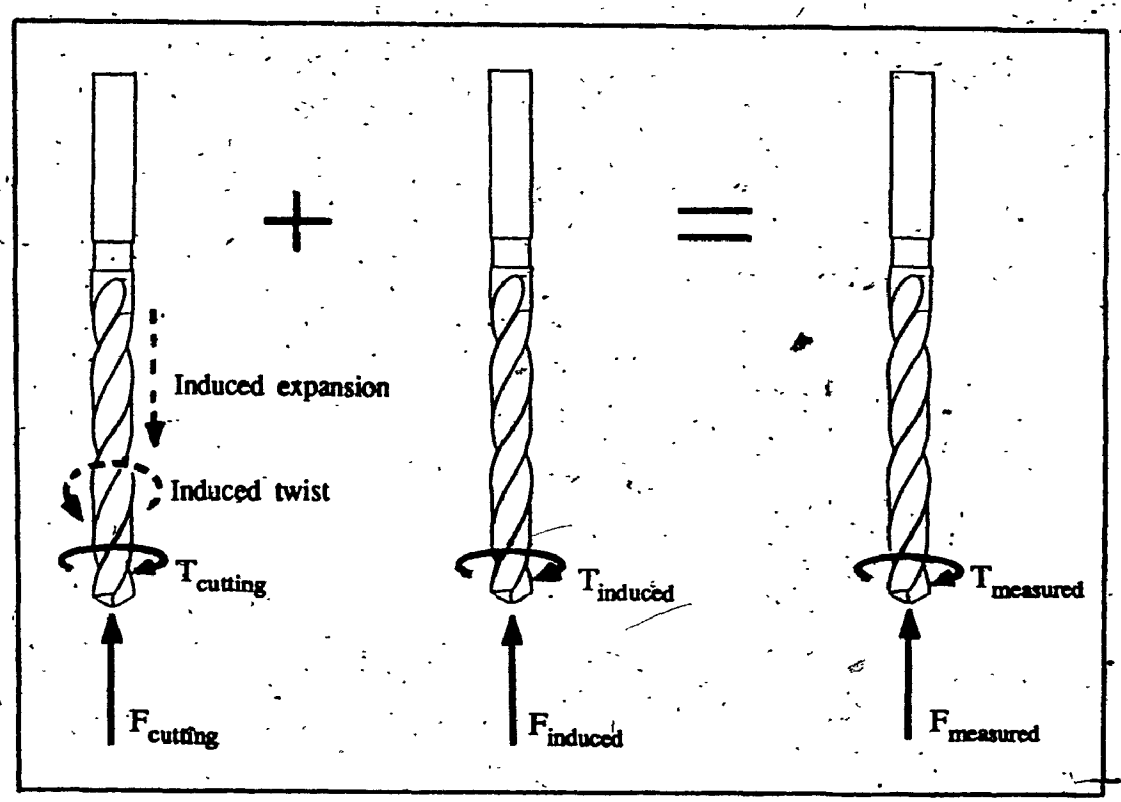

Figure 3.5 Schematic illustration : Force inducement during drilling.

the metal. The measured force values are given by

$$F_m = F_c + F_i \tag{3.5}$$

$$T_m = T_c + T_i \tag{3.6}$$

where

F_c, T_c = true cutting thrust and torque respectively

F_i, T_i = coupling-induced thrust and torque forces

Assuming that the drill encounters rigid restraint conditions during drilling, the induced-force coefficients defined and determined above can be used to relate the cutting forces with the corresponding induced forces as

$$F_i = K_1.T_c \tag{3.7}$$

$$T_i = K_2.F_c \tag{3.8}$$

Substituting equations (3.7) and (3.8) in (3.5) and (3.6), we get

$$F_m = F_c + K_1T_c \tag{3.9}$$

$$T_m = T_c + K_2F_c \tag{3.10}$$

Solving equations (3.9) and (3.10) simultaneously, we get the cutting components of forces given by

$$F_c = \frac{F_m - K_1T_m}{1 - K_1K_2} \tag{3.11}$$

$$T_c = \frac{T_m - K_2 F_m}{1 - K_1 K_2} \tag{3.12}$$

Thus with the knowledge of the induced force coefficients K_1 and K_2 of a particular drill, the above equations enable the separation of the true cutting and the induced force components from the measured total forces.

The numerical values of K_1 and K_2 obtained earlier are substituted above to generate the 'separation equations' for drills of various sizes and tabulated below in table 3.2.

The following points are to be noted about the separation equations:

i) The separation equations tabulated below are valid only for the particular drills tested. Any variation in the drill geometrical features or material, changes the stiffness coefficients and thus the induced force coefficients also.

ii) An observation of the separation equations again reveals the variation of the measurement error with drill size. Particularly from the thrust separation equations it is seen that the measurement error increases with decreasing drill diameters. And the torque separation equations show an opposite trend.

iii) It was mentioned earlier that the induced force coefficients tabulated are maximum values for the drills, obtained experimentally under completely rigid restraint conditions. This also implies that the

DRILL SIZE inch	THRUST SEPARATION EQUATION lb,lb-in (N,N-m)	TORQUE SEPARATION EQUATION lb,lb-in (N,N-m)
1/2	$F_C = 1.049F_m - 1.597T_m$ $(F_C = 1.049F_m - 62.88T_m)$	$T_C = 1.049T_m - 0.032F_m$ $(T_C = 1.049T_m - 8.13E\text{-}4\ F_m)$
13/32	$F_C = 1.046F_m - 2.386T_m$ $(F_C = 1.046F_m - 93.95T_m)$	$T_C = 1.046T_m - 0.020F_m$ $(T_C = 1.046T_m - 5.08E\text{-}4\ F_m)$
3/8	$F_C = 1.042F_m - 2.467T_m$ $(F_C = 1.042F_m - 97.14T_m)$	$T_C = 1.042T_m - 0.018F_m$ $(T_C = 1.042T_m - 4.57E\text{-}4\ F_m)$
1/4	$F_C = 1.063F_m - 4.957T_m$ $(F_C = 1.063F_m - 195.18T_m)$	$T_C = 1.063T_m - 0.014F_m$ $(T_C = 1.063T_m - 3.56E\text{-}4\ F_m)$

Table 3.2 Separation equations for various regular helix drills.

separation equations obtained with these maximal values, will indicate the maximum possible measurement errors of torque and thrust. However, if such rigid axial and torsional restraint conditions are not reached during a drilling operation, lower values of induced forces (and thus lower measurement errors) will be the result. Such a situation may occur in drilling soft metals, where the lower web-generated thrust fails to restrain the drill completely. The case of drilling with a pre-drilled pilot hole may also cause the same effect. The latter is discussed in detail separately.

3.5 Estimation of Force-Measurement Errors

At this stage, some numerical computations of the actual extent of induced forces, may aid in demonstrating their significance. For this purpose, the drilling forces measured and reported by a past investigation (Shaw and Oxford [15]) are used. The specifications of the drills used are identical to those in the present investigation in respect of the helix angle, web-thicknesses, drill lengths and the drill material. Thus it is assumed that the various stiffness coefficients determined presently are valid for the drills and that the above separation equations can be employed without significant error.

Table 3.3 below presents the experimentally measured thrust and torque values, and the corresponding true cutting forces separated using the above separation equations for the particular drills.

Table 3.3 . Separation of actual cutting forces from measured values.

Drill size, in.	Feed in/rev	Measured thrust F_m, lb	Measured torque T_m, lb.in	Actual thrust F_c, lb	Actual torque T_c, lb.in	F_{er} $\%F_m$	T_{er} $\%T_m$
1/2	0.0068	708	125	543	108	23	13
	0.005	575	95	451	81	21	14
	0.0033	482	77	382	65	21	15
3/8	0.0068	557	76	392	69	29	9
	0.005	432	63	295	58	31	8
	0.0033	358	46	259	42	28	9

F_{er} = 'Thrust Measurement Error' = $(F_m - F_c)/F_m$

T_{er} = 'Torque Measurement Error' = $(T_m - T_c)/T_m$

As seen, the induced torque and thrust values (that is, the force 'measurement errors', F_{er} and T_{er}) are of significant magnitude. Particularly, the thrust measurements are prone to large errors. The effect of drill size is also clearly demonstrated.. With decreasing drill diameters, the thrust error becomes increasingly prominent. Whereas, the induced torque value decreases in magnitude for smaller drills, although this change is only slight.

The above effect has important implications on the static deformation behaviour of drills, which will be discussed later.

3.6 Effect of Pilot Holes on Force Measurement

It is often necessary (especially with tough work materials) to drill a small pilot hole before drilling the full size hole. Usually the diameter of the pilot hole is chosen to equal the web thickness of the full size drill. Thus, without the web-generated thrust, the total thrust force during drilling is drastically reduced. This also means that the induced axial strain has very little axial restraint during drilling. The torsional restraint is similarly affected although, to a smaller extent. As a result of this the values of the induced forces in drilling with a pilot hole may be much lower than in full-hole drilling. Consequently, using the separation equations to estimate the induced torque and thrust values in such cases would be erroneous.

Part of the drilling experiments conducted in this investigation will

explore the above expected effect of pilot holes on drilling forces measurement.

The coupling effect and the force inducement due to it have significant implications on the behaviour of the drill and the drilling process itself. These effects have three main aspects namely; the static aspects, the dynamic aspects during drilling, and the effect of force measurement errors.

3.7 Effect of Induced Thrust on Drill Static Behaviour

Drills in general are slender elements by design, and the reduced cross-sectional area along the fluted portion makes them flexible under the forces of drilling. As an inherently slender cantilever subjected to axial and lateral loading at the free end, a drill is highly susceptible to buckling-type bending action.

Under these conditions it can be seen that the extra thrust force induced due to coupling increases the buckling-bending action on the drill. Such a steady static deformation can cause run-out and other errors of the hole. This phenomenon assumes further importance in the case of smaller drills because, as shown earlier, the amount of induced axial force for a given applied torque, is higher for smaller drill diameters. In addition, smaller drills are more slender, thus increasing the chances of buckling.

3.8 Effect of Induced Thrust on Drill Dynamic Behaviour

3.8.1 Effect on Drill Vibration Characteristics

The torque-thrust coupling effect has significant implications on the dynamic behaviour of the drill. Firstly the increased torsional and axial stiffness (owing to the coupling effect) during drilling will result in higher values of the respective resonance frequencies in vibration. This effect may be beneficial, or harmful to the quality of the hole depending on other conditions prevailing during drilling.

Secondly, considering the lateral vibration, the extra thrust force induced by the cutting torque can have detrimental effect on drill dynamic behaviour and thus on hole quality. This is because it is known [13] that increasing the thrust force on a drill decreases the first natural frequency in lateral vibration of a drill.

Spur and Masuha [10], from their experiments on drills with various helix angles, observed that the resonance frequencies increase with decreasing helix angle. This phenomenon can be discerned using the above explanation of the effect of coupling on drill lateral vibration. In section 3.1.2 it was shown that as helix angle decreases from the conventional value, the magnitudes of the induced-force coefficients K_1 and K_2 decrease significantly. This means that the magnitude of induced thrust also decreases significantly. Thus, under this reduced axial loading, the resonance frequency in lateral vibration increases for low-helix drills.

Therefore, the researchers conclude that high helix drills are dynamically weaker.

The same authors cite an earlier researcher who observed torsional vibrations with synchronous, longitudinal vibrations. This phenomenon can be aptly explained by the torque-thrust coupling effect. The drill dynamic behaviour can be envisioned to be identical to its static behaviour. That is, the drill expands when it unwinds, and contracts when it winds back, thus setting up a simultaneous, in-phase torsional-axial vibration. This type of a 'parametric' vibration is more likely to occur in the case of drilling with pilot holes, than in full-hole drilling. The above aspect will be explored with the drilling experiments conducted presently.

3.8.2 Drill Behaviour at Break-through

Based on his experiments with through-hole drilling, Galloway [14] made certain observations and conclusions on drill-behaviour at the break-through stage. These are analyzed and re-evaluated in the light of the coupling effect.

Figure 3.6a shows records of torque and thrust signals of the drilling process. Figure 3.6b shows enlarged records of the fluctuations of the forces. Rapid changes in torque and thrust were observed as the drill broke through the underside of the workpiece. A substantial increase in the actual feed was also seen, and simultaneously the machine began to

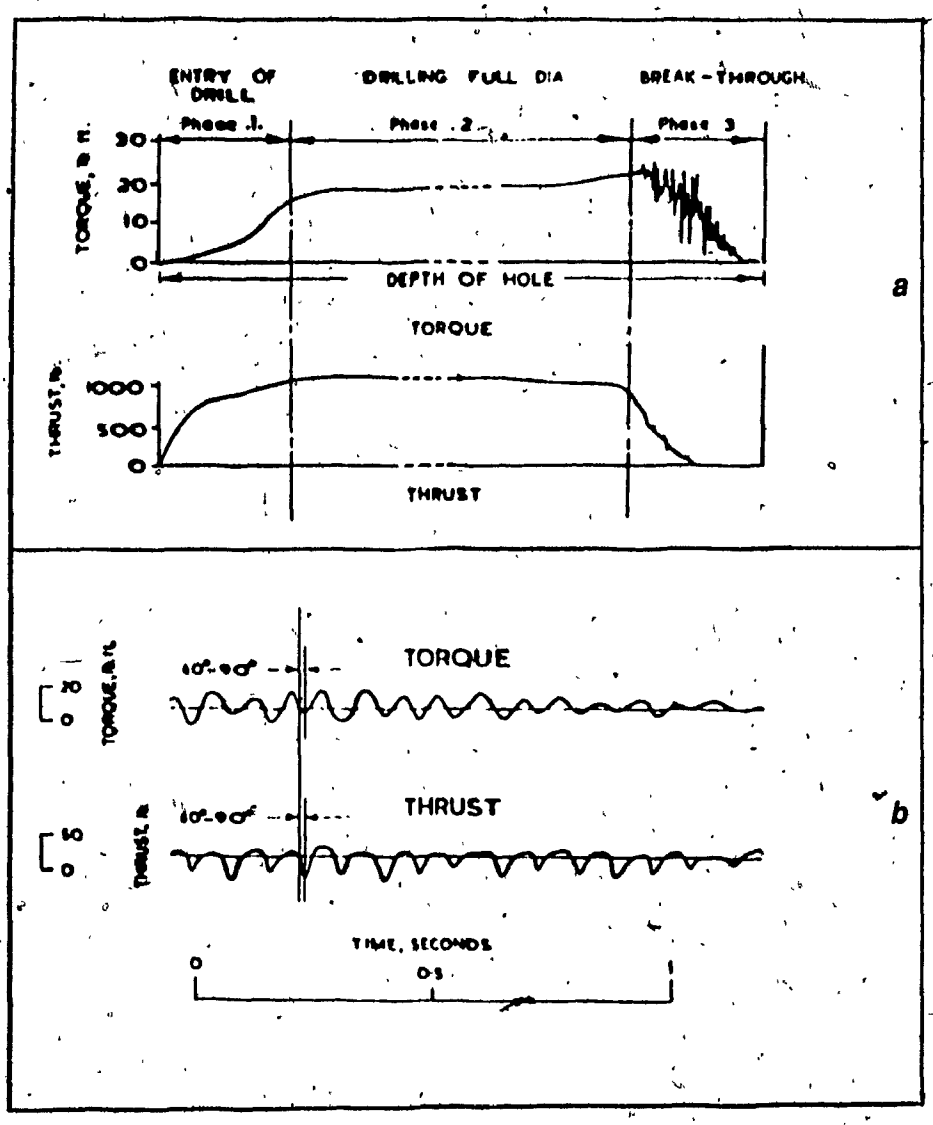

Figure 3.6 (a) Records of torque and thrust in through-hole drilling, and (b) records of force fluctuations.[14]

vibrate and continued until the drill point emerged completely. The vibration of the drill was reflected in both the force signals, particularly in the torque record, where the peak-to-peak fluctuations were almost as large as the average value [14]. The said author concludes that the increase in feed is due to the elastic recovery of the machine tool structure, and that the vibrations at break-through may be due to the regenerative chatter mechanism.

However, it is seen from the record of torque and thrust signals (figure 3.6b) that the fluctuations are of a low frequency (approximately 12 Hz) and high amplitude. Whereas, it is known that chatter is a high frequency phenomenon. Therefore it is the conviction of the present investigator that chatter vibration is not the source of the unstable tool behaviour at break-through. An alternate explanation is offered for the source and mechanism of such vibration.

As explained earlier, during full-hole drilling the cutting torque induces axial expansion, which is restrained by the cutting thrust. In this state, the drill is similar to a compressed spring with its stored potential energy.

At the instant the drill breaks-through as illustrated in figure 3.7, there is a sudden and substantial decrease in thrust. Without the restraint of the web-generated thrust, the drill is now free to unwind and expand axially, simultaneously allowing the elastic recovery of the machine

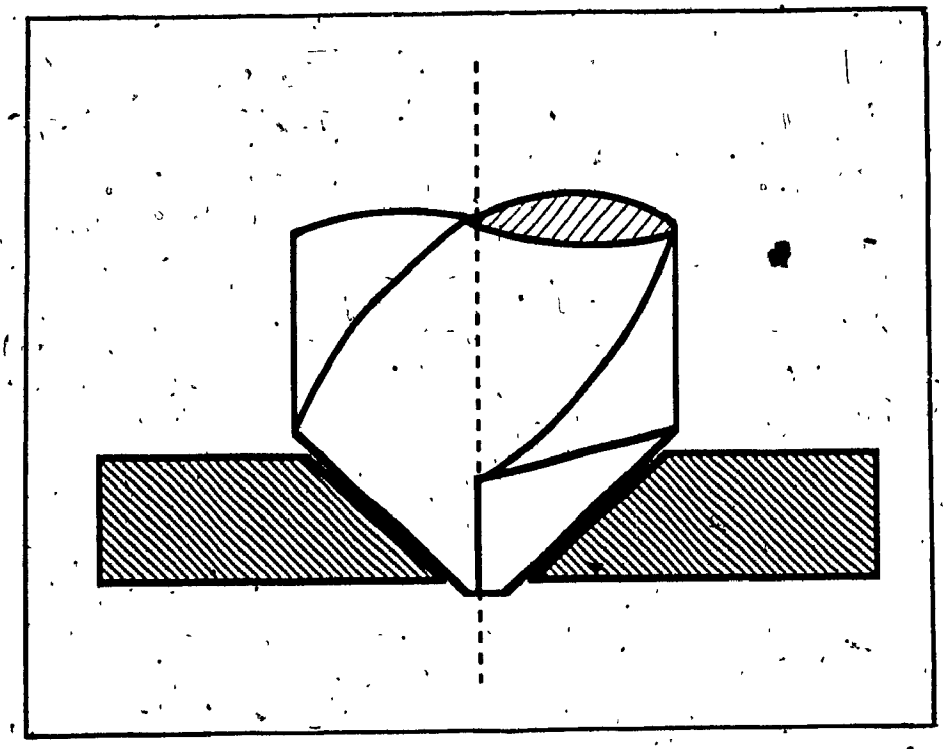

Figure 3.7 Schematic illustration : Drill at break-through in through-hole drilling.

frame also. This results in a sudden increase in the instantaneous feed.

The large pulse of forces caused by such an increase in feed may initiate simultaneous, coupled torque-thrust vibrations of the type described in section 3.8.1. Because of the reduced torsional stiffness, larger torsional deflections may be caused which result in larger axial expansions also. So in each cycle the drill 'digs' into the work material, increasing the forces and sustaining the vibration. Because of the absence of cutting at the web, such simultaneous vibrations cause large fluctuations of torque and relatively small pulses of thrust.

3.9 Implications of Error in Forces Measurement

It was demonstrated by the numerical samples of section 3.5 that the coupling effect may cause significant errors in the measurement of forces during drilling. Especially in the case of thrust, 25 to 30 percent of the measured value (for 1/2" and 3/8" drills) may be that induced by cutting torque. Errors of this magnitude can seriously undermine the utility of experimentation in drilling research.

A substantial research effort has been and continues to be directed at obtaining a theoretical means of predicting the torque and thrust forces in twist drilling. The standard of comparison and evaluation in all such research is obviously the experimental measurement of these forces. In the past, research on this front was limited to the case of drilling with a

pre-drilled pilot hole. In such cases, by the reasoning of section 3.6, minimal or no error may have occurred in the experimental forces-measurement. But recent research has attempted a complete drilling model with no pilot holes. And as discussed above, the measurement errors possible in such cases are significant enough to affect the validation (positively or negatively) of the theoretical models.

Another research area where experimentation is extensively used is the parametric study of the drill geometrical features and their effect on drilling forces. Here, coupling induced error in the forces can cause erroneous conclusions on the effect of a particular parameter-change. Also, where in actuality only one of the forces (torque or thrust) may have changed due to a parameter-variation, coupling produces an illusion of change in the other force also.

Thus the results of experiments to compare drill performance, evaluation of drill life, productivity etc., can all be adversely affected if coupling induced forces are not taken into consideration.

3.10 Computation of Drill Deflections

It is sometimes necessary to compute the twist and axial deformations of a drill under the cutting forces. This is done using equation (2.1) of chapter 2, that is,

$$\begin{Bmatrix} \epsilon \\ \theta \end{Bmatrix} = \begin{bmatrix} \alpha_{11} & -\alpha_{12} \\ -\alpha_{21} & \alpha_{22} \end{bmatrix} \begin{Bmatrix} F \\ T \end{Bmatrix}$$

Following the developments of this chapter, it may be said that the coupling effect will not necessarily affect the drill deformations under all conditions, contrary to the calculations of De Beer [8]. That is, the induced strains and induced forces are mutually exclusive conditions. Therefore the correct approach would be as follows:

i) In the case of full-hole drilling, the deflections under the measured forces are to be computed using only the direct stiffness (or compliance coefficients). In practice there may be small but negligible amounts of induced strains since the restraints are not total.

ii) In the case of pilot-hole drilling, coupling strains are induced. Therefore the total deflections are computed using the above equation, where the Maxwell's coefficients are obtained by inverting the matrix of stiffness coefficients obtained above.

3.11 Conclusions

Two new coefficients K_1 and K_2 are defined, directly relating the applied forces and the corresponding induced forces on drills. The values of these coefficients are computed from the results of the previous chapter.

Values of K_1 increase for decreasing diameter of drills, and the inverse is seen of K_2. Against helix angle, both coefficients show an increasing trend, reaching 'saturation' values later.

It is concluded that, due to the axial and torsional restraint of the cutting forces, the coupling effect induces torque and thrust forces during drilling also, which add up with the corresponding cutting forces. Thus it is erroneous to attribute the entire measured force values to metal cutting.

A simple means of separating the true cutting and the induced force components is obtained by deriving 'separation equations' for the drills, based on the induced-force coefficients K_1 and K_2. Numerical samples computed from the force measurements of past researchers, show that significant errors may occur in the measurement of torque and thrust in full-hole drilling. Particularly, errors in thrust (for 3/8" and 1/2" drills) may be 20 to 30 percent of the measured values. Torque errors are estimated to be 10 to 15 percent. Thrust error increases with decreasing drill diameter and the vice versa holds for torque error. In the case of pilot hole drilling, because of reduced restraint conditions much lower or no errors may be expected.

It is observed that the coupling effect and the induced forces due to it may have significant impact on drill behaviour. Statically, the increased total thrust may increase the chances of the drill bending in buckling, especially in the case of small drills. Dynamically the coupling effect

increases the natural frequencies in torsional and axial vibration. Due to the increased thrust the first natural frequency in bending vibration can be greatly reduced. The same mechanism corroborates the previous research observation that natural frequency increases as helix angle decreases. The coupling induced axial and torsional strains are probably also the cause of the simultaneous torsional-axial 'parametric' vibrations observed during drilling. Based on the coupling effect, a new and more apt description is offered to discern drill behaviour at break-through, in through-hole drilling. Experimental force measurements are of paramount importance in such research areas as drill geometry evaluation, theoretical models for cutting mechanics etc. Therefore, due consideration for coupling induced errors in these measurements is essential.

The following chapter develops a criterion for the selection of pilot-hole sizes in drilling.

CHAPTER 4

A CRITERION FOR THE SIZING OF PILOT HOLES

4.1 Cutting-Edge Geometry

As described in chapter 1, the cutting edges of a twist drill are formed by the intersection of the flute profile and the conical point surface. They have a complex three-dimensional geometry and in addition, are oblique to the cutting velocity vector. Due to these complexities, several planes of view are necessary to visualize their geometry completely.

Figure 4.1 is such an illustration showing the geometrical relationships between the various angles. The normal rake angle α_n, normal clearance angle Cl_n and the angle of inclination i for a point Q on the cutting edge are shown. The helix angle δ at Q is defined in a plane perpendicular to the radius r (view A), and is given by

$$\tan \delta = 2\pi r/L \tag{4.1}$$

where L is the lead of the helix. Therefore, the helix angle δ varies along the length of the cutting lip. The peripheral value of it is used as a drill specification [19].

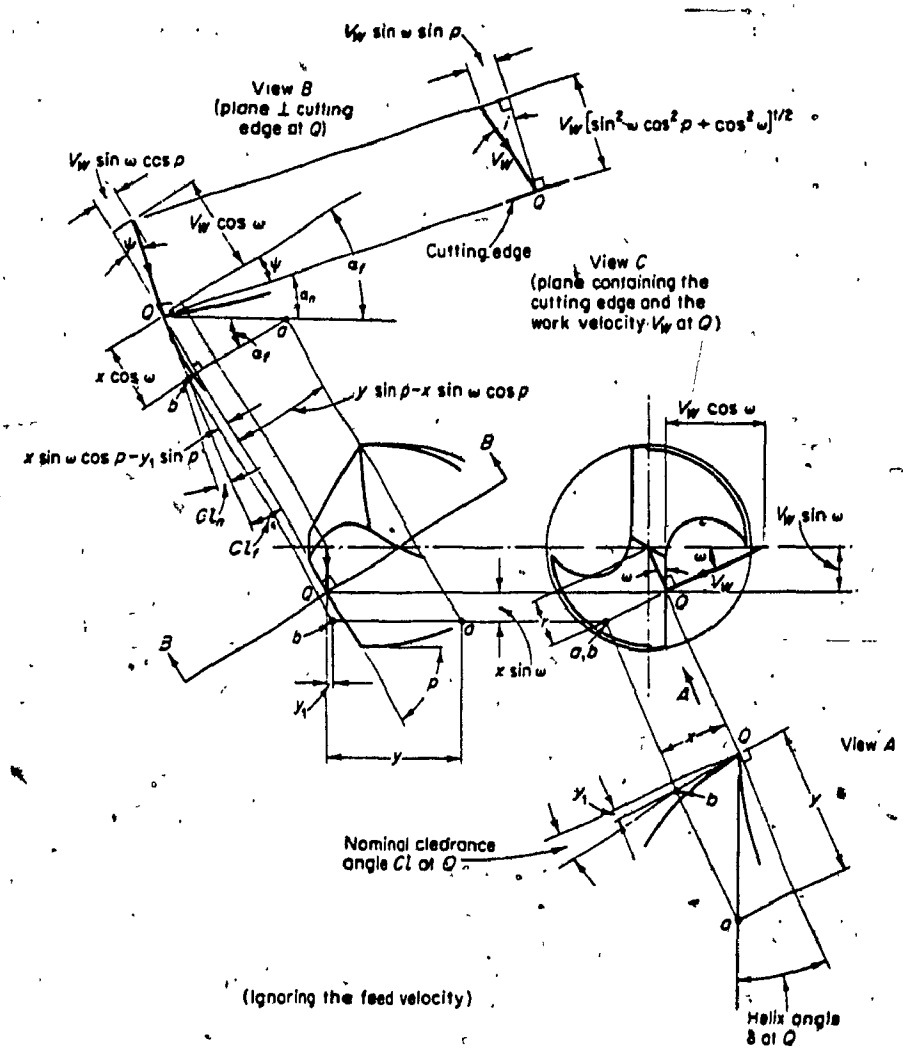

Figure 4.1 Geometrical relationships between various twist drill angles.[18]

The normal rake angle at Q is measured in a plane perpendicular to the cutting edge at Q and is defined by

$$\alpha_n = \alpha_f - \psi \tag{4.2}$$

where α_f is a reference rake angle in the normal plane, given by

$$\tan \alpha_f = \frac{\tan \delta \cos \omega}{\sin p - \tan \delta \sin \omega \cos p} \tag{4.3}$$

and angle ψ in the normal plane, given by

$$\tan \psi = \tan \omega \cos p \tag{4.4}$$

In the above expressions, p is the half-point angle, and angle ω at the point is given by

$$\sin \omega = W/r \tag{4.5}$$

where W is the half web thickness and r the radius at the point. Substituting equations (4.3) and (4.4) into (4.2), we get the expression for the normal rake angle as

$$\tan \alpha_n = [\cos \omega + \sin \omega \tan \omega \cos^2 p] \frac{\tan \delta}{\sin p} - \tan \omega \cos p \tag{4.6}$$

From equation (4.6) it is apparent that for any given drill geometry, the normal rake angle varies continuously along the cutting edge [18].

When numerical values of the rake angle are plotted against radius, interesting information is revealed.

Figure 4.2 is a typical plot of the normal rake angle variation along the cutting edge. Starting near the chisel edge (or web region) the normal rake angle has a high negative value. As radius increases, the rake angle increases and reaches a high positive value at the periphery of the drill. Therefore, at some radius along the cutting edge, the normal rake angle assumes a value of zero.

4.2 Cutting Mechanics and Cutting Edge Geometry

Due to the complexities of geometry and the variation of the cutting angles along the cutting edges, the mechanics of cutting are highly complex in drilling.

Figure 4.3 schematically shows the chip formation in different areas of cutting on the drill point. Section AA is in the positive rake angle region of the cutting edge, and the chip formation resembles that of a normal single-point cutting tool. Section BB shows the cutting mechanics in the negative rake angle region. Here, the cut chip is turned backwards onto the rake-face through a large angle. The excessive plastic deformation thus required, makes the cutting conditions in this region to be severe.

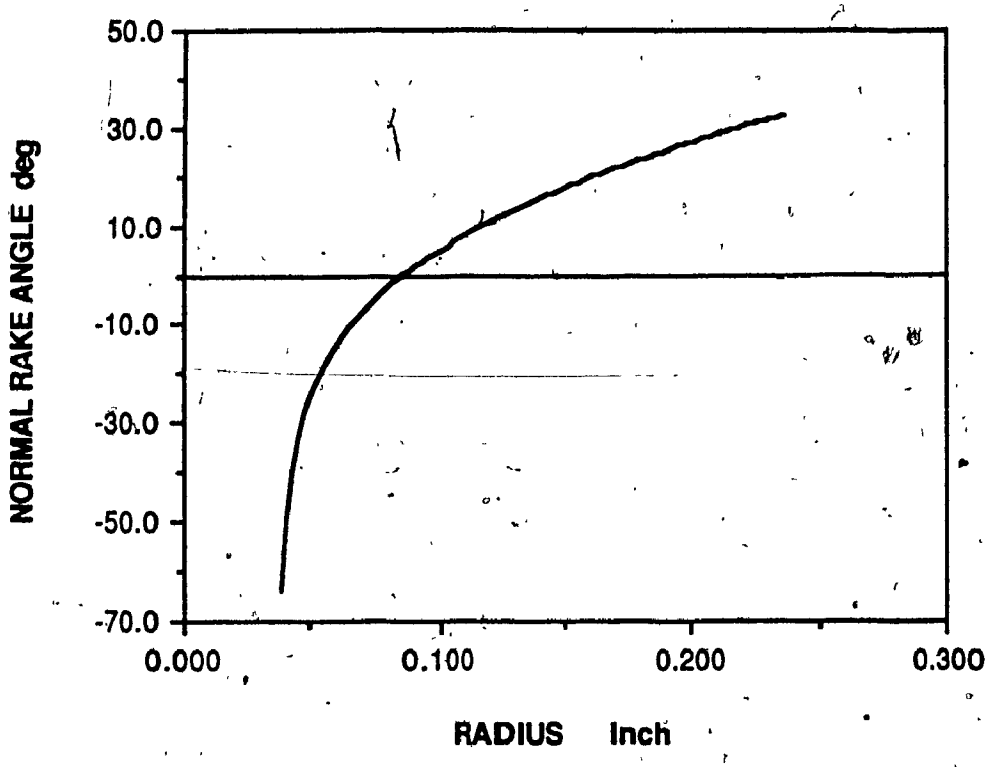

Figure 4.2 Typical variation of the normal rake angle along the cutting lips.

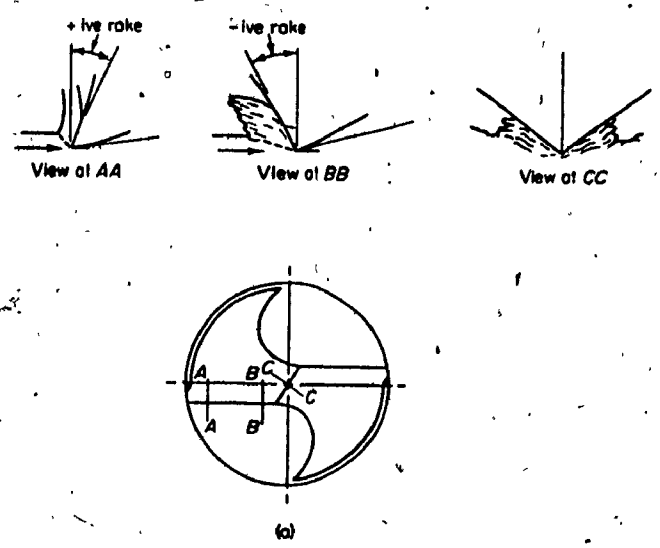

Figure 4.3 Chip formation in various cutting regions.[18]

But the most severe conditions of all prevail at the chisel-edge region, shown by section CC. The cutting action in this region is likened to that of a wedge-shaped indentor [19] with a high negative rake angle (-50 to -55 degrees). Due to the proximity to the drill axis, the tangential cutting velocity is extremely low. Thus the material removal is effected by a severe extrusion-type of plastic flow of the metal.

The cutting geometry and the resulting mechanics of metal removal have a direct and significant influence on the forces generated in drilling a given metal. It is well known that the power force (the radial plane force-couple in drilling) is directly proportional to the normal rake angle [18]. When the rake angle of a cutting edge is increased from a nominal positive value, the power force decreases, and a decrease of rake angle has the inverse effect. Consequently, the excessive plastic deformation at the negative rake angle region of the lips, generates large tangential as well as thrust forces. It is well known that, owing to its cutting mechanics the web (or chisel edge) of a standard drill generates more than 50 percent of the thrust force (and 20 percent of torque) in drilling [20]. In addition, the large amount of energy consumed by the plastic flow of metal is dissipated as heat, which causes built-up edges and a further increase in the forces.

4.3 Necessity of Pilot Holes

When drilling holes of large diameter and/or when a tough work material is involved, it is impossible or unadvisable to directly start the full-size hole. The common drilling practice in such cases is to pre-drill a 'pilot hole' of a smaller diameter. The purpose of such a pilot hole being

i) To reduce the thrust force requirements when drilling the full size hole.

ii) To prevent excessive stresses and heat generation at the web, and thus increase the tool-life.

4.4 Present Sizing Criterion for Pilot Holes

In the perception of current drilling practice, the severe cutting process at the chisel edge and the resulting high thrust force, are the only reasons that necessitate a pilot hole. Therefore, the standard practice is to size the pilot hole diameter to equal the web-thickness of the full size drill, eliminating cutting in that region.

However, it is well known from drilling practice and past research [14,20] that drilling with a pilot hole so sized, results in poor hole-quality in terms of roundness error. Therefore, in most cases subsequent processing (that is, reaming, boring etc.) is required to improve the hole profile. The following presents a reasoning for such a deterioration in hole

quality.

As found by the cutting-geometry analysis, negative rake angle is not restricted to the chisel edge region of the drill. For a substantial length on each cutting edge (starting from the web), the normal rake angle remains negative. It was also pointed out that the cutting mechanics associated with such a negative rake angle, are inherently severe and unstable.

Therefore, pre-drilling a pilot hole of diameter equal to the chisel-edge length, does not completely solve the problem of excessive forces. The severe cutting process in this region of the lip continues to generate large forces. Combined with the inherent errors of point geometry, substantial radial (or 'drift') forces are produced on the drill. In addition, under the drastically reduced restraint of the thrust force, the rigidity of the drill is lost. The combination of these factors, causes the drill to easily deflect (radially), producing higher roundness error of the hole.

Yet, drilling with a pilot hole improves the straightness of the final hole [14]. Therefore, if the deterioration of roundness is prevented, the process of pilot hole drilling may be more widely prescribed to obtain high quality holes.

In this pursuit, a more appropriate criterion is proposed for the selection of pilot hole size for a given drill. This criterion is based on

the cutting mechanics in the various regions of the lips, as described above.

4.5 A New Criterion for Sizing Pilot Holes

Following the deficiencies of the currently practiced criterion, the principle of the proposed criterion for sizing pilot holes is simply, to eliminate metal-cutting in all of the negative rake regions on the drill point. That is, the diameter of the pilot hole should be large enough to exclude cutting in the negative-rake region of the lips also (figure 4.4). The ideal pilot hole diameter should be within certain minimum and maximum values, determined for each drill as follows.

For the given full-size drill to be used, equation (4.6) above is set-up and solved for the root, to obtain the radius at which the normal rake angle becomes zero. This gives the diameter within which the rake angle is negative, and defines the minimum recommended diameter of pilot hole.

The minimum diameter so determined is the ideal size for a pilot hole. However, with this size, it may be impossible to reach the depth required of the full size hole, necessitating the choice of a larger size of pilot hole.

On the other hand, the pilot hole diameter cannot be increased indiscriminately. Because, with a large pilot hole the rim of the pilot hole contacts a sharp (high positive rake angle) region of the lips when

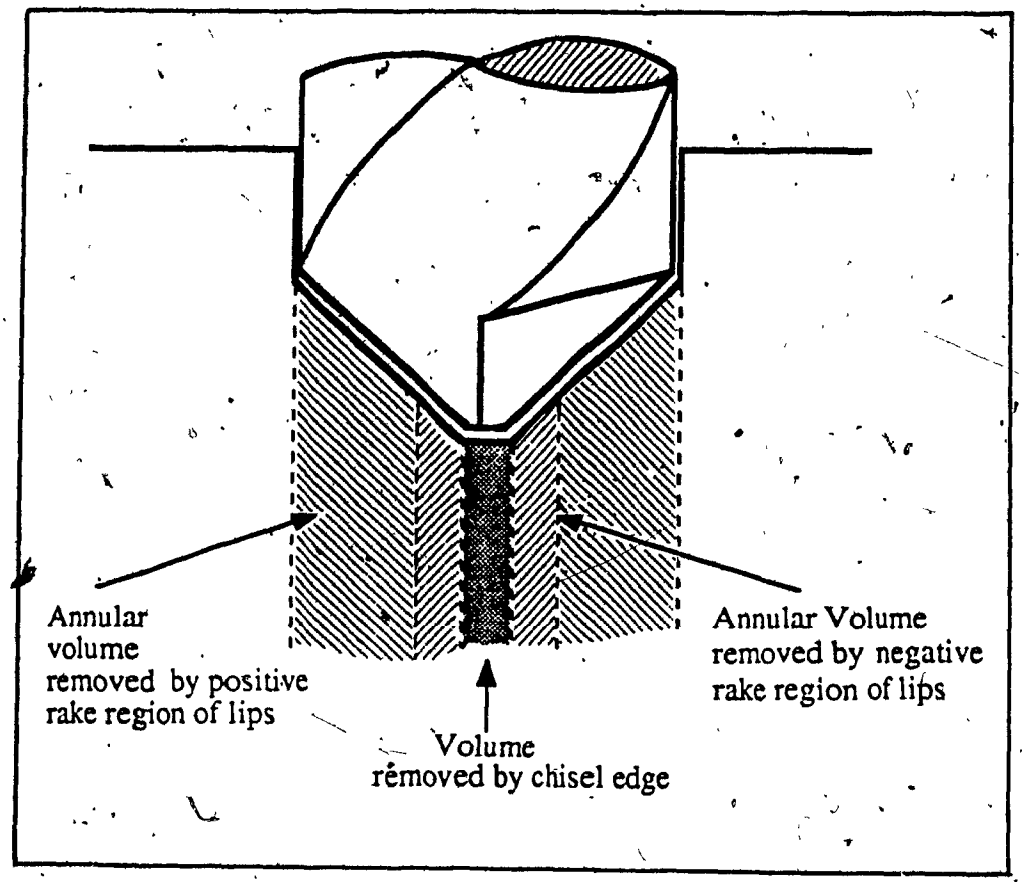

Figure 4.4 Schematic illustration : Rake-regions of cutting.

drilling commences (Figures 4.2 and 4.4). This can cause 'digging-in' of the cutting edges, in turn result in large force fluctuations and poor hole quality.

Based on the proposed criterion, table 4.1 lists the 'critical size' of pilot hole diameters recommended for several common sizes of drills. The chosen size must be the nearest convenient drill size, without being smaller than this recommended minimum size. If the required depth of hole cannot be achieved with this recommended size, the larger size chosen should be as close as possible to the same.

It is to be noted that the standard twist drill profile varies continually from the point-end towards the shank (the web thickness increases). Correspondingly, the cutting-edge geometry also changes. Therefore, as a drill is shortened by successive point-grindings, a substantial variation occurs in the cutting-geometry. Hence, the above recommended sizes of pilot holes are only for new drills, and would be invalid for drills significantly shortened by successive point-grindings. In such a situation the ideal size of pilot holes must be re-calculated by the user, employing the criterion.

The following section discusses the choice of pilot hole sizes in the experiments conducted to validate the sizing criterion developed above.

Table 4.1 Recommended size of pilot holes for various common drills.

Full size drill inch	Web thickness at point end inch	Critical diameter of pilot hole inch
3/8	0.060	0.137
1/2	0.075	0.172
9/16	0.095	0.219
5/8	0.100	0.238
11/16	0.105	0.250
3/4	0.115	0.272
13/16	0.125	0.300
7/8	0.130	0.316
15/16	0.135	0.332
1	0.140	0.346

4.6 Pilot Hole Sizing for Present Experimentation

The drilling tests in this investigation are carried out with a 1/2-inch and a 3/8-inch diameter drills. The critical pilot hole diameters for these sizes are as given in table 4.1.

The 1/2-inch drilling experiments are designed so as to clearly isolate the effect of the 'critical diameter' of pilot hole defined above. Several experiments (varying the feed as well as the feed method) are done with a pilot hole of diameter slightly larger than the 'critical' value. Termed as drilling with a 'right size' pilot hole, these experiments are designed to show the beneficial effects of proper pilot hole sizing. The same experiments are repeated with a pilot hole of size slightly less than the critical value. These are designated as 'wrong size' pilot holes and, show the detrimental effects of cutting with a negative rake. A comparison of these two sets of experiments will reveal the validity of the criterion proposed. It is to be noted that in practice the pilot hole is sized to equal the web-thickness, which is a more extreme case of the 'wrong size' pilot-hole. Also, the same experiments are repeated without a pilot hole, to determine the general effects of pilot holes.

A more detailed description of the experimentation is presented in the following chapter.

4.7 Conclusions

The cutting edges of a twist drill are of a complex three-dimensional geometry. The normal rake angle α_n, on the cutting lips are of utmost importance to the cutting mechanics, and is shown to vary widely with radius. Starting with a high negative value near the web of the drill, α_n reaches a value of zero degree at some radius, and continues to increase, reaching a high positive value at the periphery of the drill.

The varying geometries also produce varying cutting mechanics in the different regions of the drill-point. The web (or chisel-edge) is likened to a wedge-shaped indentor. The large negative rake angle and the low cutting velocity in the region result in the metal being removed by a severe extrusion type of effect, which generates excessive forces and heat. The cutting in the negative rake region of the lips is also inefficient, with a high degree of plastic deformation, heat and forces.

The high thrust forces and heat generated at the web are undesirable when drilling with a large diameter drill and/or when tough work materials are involved. Therefore, it is standard drilling practice to pre-drill a pilot hole of a smaller diameter. However, this invariably results in poor quality of holes.

The criterion used for sizing the pilot holes, is suggested as the reason for the deterioration of hole-quality. The current practice is to

drill a pilot hole of size equal to the web-thickness of the drill. However, it is shown that this still leaves the negative rake region of the lips to generate deflecting drift forces, which cause roundness errors of the hole.

Therefore, a new criterion is proposed that eliminates cutting in all of the negative rake regions of the drill point. For this, the diameter at which the rake angle reaches zero (on the lips) is determined and defined as the 'critical diameter' of pilot hole for the given drill size. Based on this criterion, a set of recommended pilot hole sizes is presented for common drill sizes.

Drilling with a pilot hole is shown to improve the straightness of the final hole. If the stumbling block of poor hole-roundness that also accompanies, is eliminated by employing the proposed criterion, then the process of pilot hole drilling may be prescribed more often to obtain high quality holes.

CHAPTER 5

EXPERIMENTAL MEASUREMENT OF THE FORCES DURING DRILLING

5.1 Experimental Measurements of Cutting Forces

In all conventional machining processes, the experimental measurement of cutting forces enables one to comment on the qualitative and quantitative aspects of

i) the design of the cutting tool

ii) the process parameters

iii) and the performance of the machine tool itself.

The resultant cutting forces are closely related to cutting-edge geometry, tool and workpiece materials, feed and speed, the rigidity and power of the machine tool, and so on. And in a closed loop fashion all these factors together determine the quality of the machined surface.

In drilling, the measurement and understanding of the cutting forces is most critical because, as described earlier, the severe cutting mechanics generate large forces on the tool. In addition, since a drill is inherently slender, the deflecting forces of cutting directly affect the quality of the hole, in spite of a rigid machine.

The direct measurement of the cutting forces at their origin is impossible, therefore the reactions are measured at some distant plane. So, a measuring system is required which measures the forces accurately, independent of the point of application of the forces[1]. Such a system has three basic parts [2] as shown by the schematic of figure 5.1 :

i) A detector transducer stage where the physical variable (such as force, acceleration etc.) is detected. The detection automatically causes a proportional change/output of some measurable quantity (e.g. charge, displacement etc.).

ii) An intermediate signal conditioning stage which involves one or more of the following changes- Conversion to another physical variable, signal amplification, filtration, modulation/demodulation, stabilization etc..

iii) A read-out stage using analog or digital instruments for reading, recording and monitoring the output signal.

In order to obtain true measurements, the measuring system should satisfy the following requirements [1] :

i) Original rigidities should be maintained, if not exceeded

ii) Dynamic characteristics should be as similar as possible to those of the original set-up

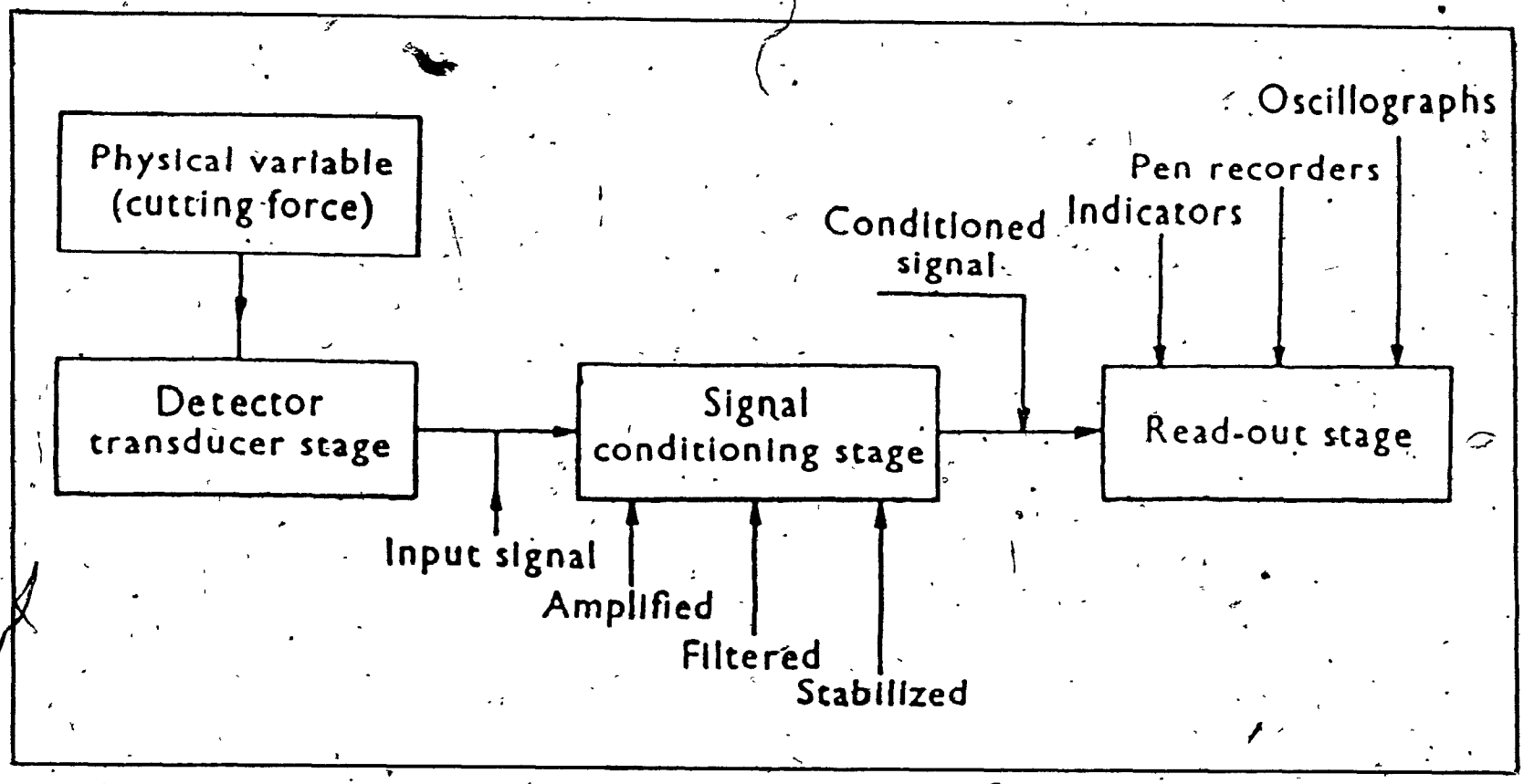

Figure 5.1 Schematic illustration : Force measuring system.[2]

iii) The mounting of the tool or the workpiece should be as close as possible as before

iv) Frequency response should be as wide as possible

v) Cross-talk between components of the forces and moments should be minimal

vi) Sensitivities of transducers should be unaffected by time, temperature and mounting of the tool and workpiece

vii) High resolution, that is, the capability of measuring small variations in an important force or moment

viii) Non-critical adjustments of zero-points, sensitivities, measuring ranges and so on.

5.2 Transducers to Measure Forces

Forces and moments are measured by transducers that employ various principles of operation. Common among them are

i) Strain gage-based transducers in which minute changes in electrical resistances is detected and amplified through a bridge circuit, to produce a proportional voltage output.

ii) Capacitive load cells wherein the measured forces produce deflections, which change the gap capacitance between two elements,and this is

suitably metered.

iii) Piezoelectric transducers which are described below.

Piezoelectric transducers are the most widely used force sensors today. Their operation is based on the property of certain crystals (most commonly, Quartz) that electric charges appear on their surfaces under mechanical loading. The electrical charges are collected with elctrodes and transformed by a charge amplifier into an analog voltage signal. Individual transducers (or 'load washers') are made by mounting suitably cut quartz elements in a steel housing. Elements sensitive to different orthogonal normal and shear directions can be cut and mounted in one unit to make multi-component load washers[1]. In order to be used, load washers require to be held by a specified compressive pre-load. Complete, ready-to-use dynamometers are also available.

Piezoquartz force transducers offer excellent rigidity and dynamic response. Load cells measuring up to four components of forces and/or moments can be had in compact units, with minimal cross-talk between the various measuring axes. Quasi-static forces can also be measured by increasing the system time constant at the charge amplifier. For these reasons piezoquartz transducers are particularly popular for measuring forces in metal cutting.

5.3 Experimental Set-up

The experimental set-up to measure and record the cutting forces in drilling (figures 5.2a, b, and c) consists of the following components

a) The radial drilling machine

b) The dynamometer

c) Charge amplifiers

d) An X-Y-Z compensator

e) FM magnetic taperecorder

f) Digital Voltmeters

g) An FFT analyzer

The radial drilling machine has a 14 horsepower capacity and is equipped with auto-stop depth setting. It has six choices of feed, from 0.0016 inch/revolution to 0.016 inch/revolution. Eight choices of spindle speeds between 340 and 2700 RPM are available.

5.4 Drilling Dynamometer

Two orthogonal components of radial (or 'drift') forces, a thrust force and a torque are required to be measured. These force components completely describe the force system in drilling (figure 5.3). Most readily available drilling dynamometers measure merely the torque and the thrust forces. Therefore for the present investigation, a dynamometer was specifically designed and built using two available multi-component load

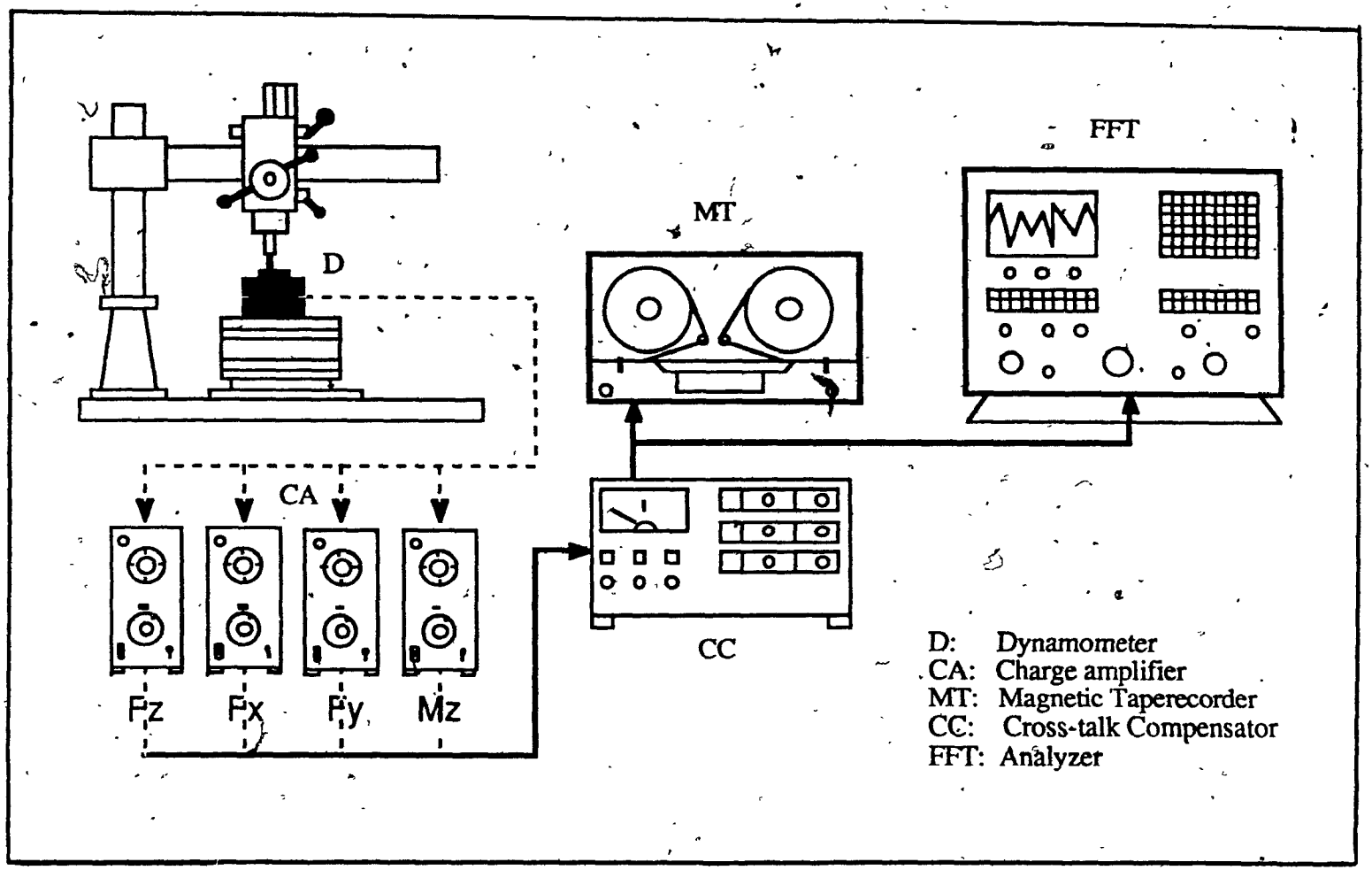

Figure 5.2 a) Schematic illustration : Set-up for drilling experiments.

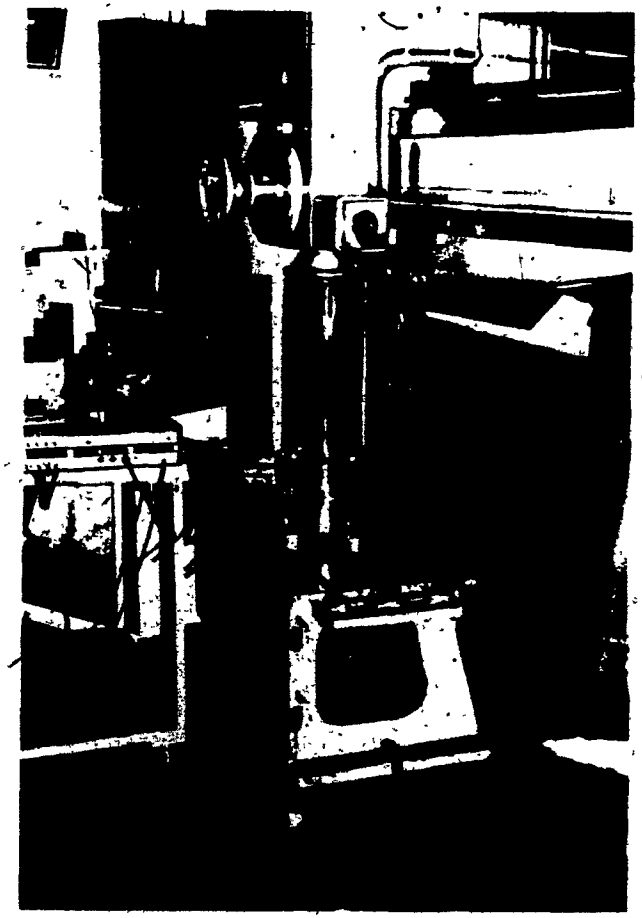

b

c

Figure 5.2 b) and c) Photographs of set-up and instruments used.

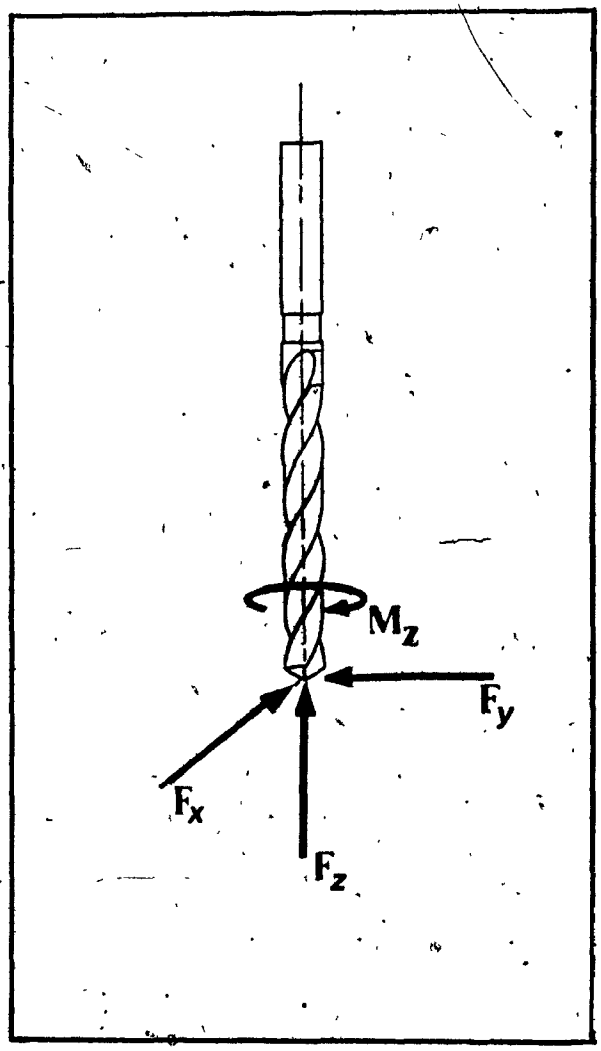

Figure 5.3 Force system in drilling.

washers.

Figure 5.4a shows a schematic of the dynamometer in cross-section. The Z10917 load washer measures the two in- plane radial forces F_x and F_y, and the thrust force F_z. The smaller load washer (Z9065) measures the torque M_z. Tables 5.1 and 5.2 describe the main specifications of the load washers. The massive bottom and middle plates ensure minimal deflections under the large compressive pre-load (157000 pounds) specified for the Z10917 load washer. The pre-load is achieved with a calculated amount of torque applied evenly on six bolts by means of a metering torque-wrench.

The Z9065 load washer is compressed to 27000 pounds between the middle and the top plates, also by applying a specific amount of torque on six bolts. The four bearing surfaces of the pre-loading plates are surface-ground to ensure uniform load distribution. The top plate has an axially centered threaded hole to allow the workpiece specimens. Figure 5.4b shows a pictorial view of the dynamometer.

The function of the charge amplifiers is to convert the charge outputs from the load washers into proportional voltages using the respective charge sensitivities. The amplifiers used in the experiments were Kistler model 5001 or similar types, wherein the load washer charge sensitivities can be directly dialed in. Output voltage amplifications can be achieved with a large choice of steps.

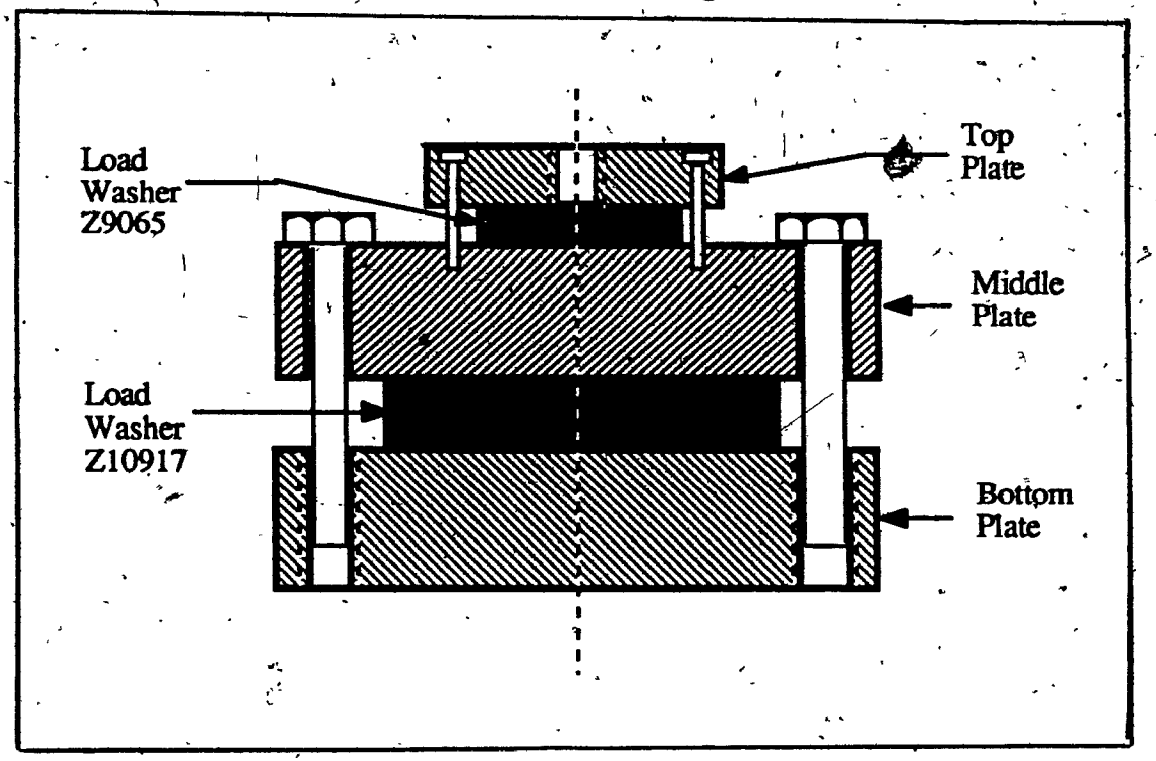

Figure 5.4 a) Drilling force dynamometer: Cross-section schematic

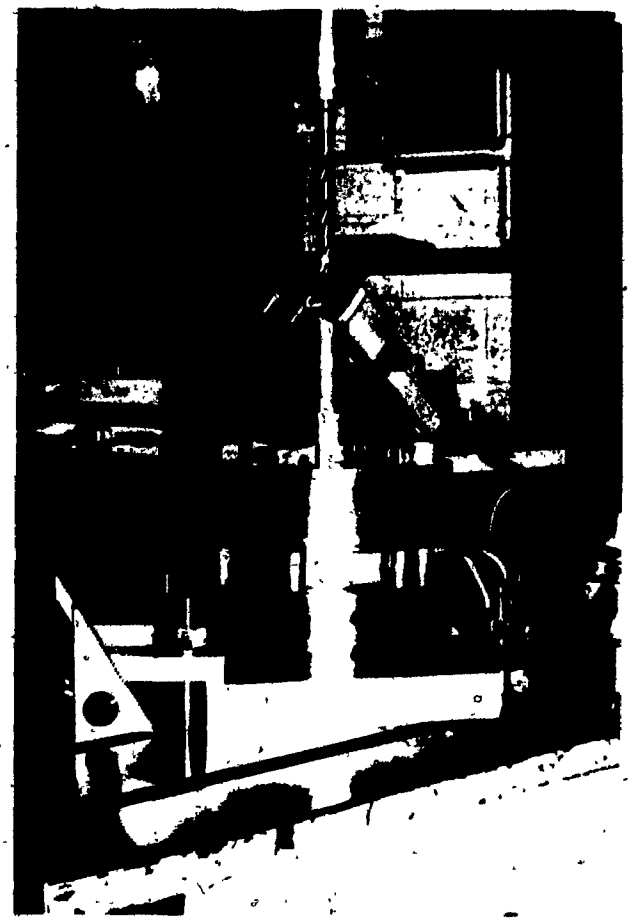

Figure 5.4 b) Drilling force dynamometer: photograph.

Table 5.1 Specifications of load cell Z10917.[3]

SPECIFICATIONS		Z10917
Measuring range: F_x, F_y	k lb	±17*
F_z	k lb	±90*
Overload	%	20
Maximum normal force	k lb	270
Maximum moment M_z & $M_{x,y}$	ft-lb	±1,800 & 5,200*
Resolution	lb	0.002
Sensitivity (nom.): F_z & F_x, F_y	pC/lb	−9 & −16
M_z	pC/ft-lb	−2
Linearity	%FS	≤±1
Cross talk: $F_x \rightarrow F_y$	%	≤±2
$F_{x,y} \rightarrow F_z$	%	≤±3
$F_z \rightarrow F_{x,y}$	%	≤±1
Operating temperature range	C	−50 to 150
Temperature sensitivity shift	%/C	0.02
Capacitance	pF	2,300
Insulation resistance	Ω	>10^{13}
Weight	g	2,500

*Standard mounting with 157k lb preload

Table 5.2 Specifications of load cell Z9065.[3]

SPECIFICATIONS		9065
Measuring range: F_z	lb	±4,500*
M_z	ft-lb	±148*
Overload	%	20
Maximum normal force	lb	32,400
Maximum moment M_x, M_y	ft-lb	±148*
Maximum total shear $F_{x,y}$	lb	±2,700*
Resolution: F_z	lb	≈0.004
M_z	in-lb	≈0.002
Sensitivity (nom.): F_z	pC/lb	−8
M_z	pC/in-lb	−18
Linearity & hysteresis	%FS	≤±1.0 & ≤1.0
Cross talk: $F_z \rightarrow M_z$ & F_x, $F_y \rightarrow M_z$	in-lb/lb	≤±0.008 & ≈±0.04
$M_z \rightarrow F_z$	lb/in-lb	≤±0.025
F_x, $F_y \rightarrow F_z$	%	≤±2.0
Rigidity: x, y, & z directions	lb/μin	≈7.4 & ≈37
torsion z axis	ft-lb/m rad	≈368
Natural frequency (nom.)	kHz	40
Operating temperature range	°C	−196 to 150
Temperature sensitivity shift	%/°C	~0.02
Shock & vibration	g	<2,000
Capacitance (each channel)	pF	350
Insulation resistance	Ω	>10^{13}
Weight	g	150

*Standard mounting with 27k lb preload

Measurement of fast-varying dynamic processes, which is the main application for piezoelectric transducers, is done with a 'short' time constant setting. Selection of a 'long' time constant instead, allows the measurement of quasi-static processes.

The function of the X-Y-Z compensator is to nullify the undesirable cross-talk between nominally independent measuring channels. Since only three channels can be accommodated on the compensator, the thrust channel was excluded from the compensation process. The outputs of the charge amplifiers are connected to the inputs of the compensator. Any desired portion of the output voltage of any one channel may be tapped and fed as a compensation signal to the input of the other channels [4]. When this is done for all three channels, the outputs from the compensator are the true measured forces along the respective axes.

The FM taperecorder stores the four channels of force signals measured, on a magnetic tape, to be retrieved repeatedly for analysis later. The FFT analyzer is a tool for dynamic signal analyses, used at this stage merely to monitor the force signals during the experiments.

The sensitivities and other specifications given in the above tables are only nominal values for the load washers. In practice, the design of the dynamometer, the value of pre-load applied and other factors affect the static and dynamic performance of the dynamometer. Therefore, a thorough calibration of the dynamometer-workpiece system is imperative.

The calibration procedure is two-fold :

i) Static calibration

ii) Dynamic calibration

5.5 Static Calibration of the Dynamometer

The purpose of static calibration is to establish the relationship between the input variable and the outputs of the dynamometer. In other words, the charge sensitivities of each measuring channel is to be established. In addition the extent of cross-talk between the measuring channels is also established so that compensation can be effected.

The procedure basically involves applying known values of the input force variable with a set of calibrated weights or other means, and measuring the voltage outputs from all channels. Due to the high insulation resistance of the load washers and also the 'long' time constant setting, sufficient time is available for reading the voltage outputs accurately before they decay. The actual charge outputs of the load washers are calculated using the following equation

$$Q = S_v \; S_c \; V \tag{5.1}$$

where

Q = charge output of the load washer, pCb

S_v = voltage sensitivity setting, lb/volt

S_c = nominal charge sensitivity setting, pCb/lb

V = voltmeter reading, volts

The charge values are then plotted against the corresponding input force values to obtain the calibration curves.

5.5.1 Static Calibration Along the Thrust Direction

In order to apply the relatively large calibration load required, a TINIUS OLSEN tension/compression tester was used. Figure 5.5 shows a schematic of the calibration set-up. A workpiece specimen was put in place to imitate the drilling set-up as nearly as possible.

Readings were taken during loading as well as unloading cycles, and repeated readings were taken to ensure consistency. The charge outputs so obtained were plotted against the applied load to obtain the calibration graph of the thrust channel as shown by figure 5.6.

As seen in the graph, the input-output relationship is highly linear with no hysteresis or off-set errors. It was also observed by tests that the cross-influence of thrust on the other three channels (F_x, F_y & M_z) was negligible and thus has not been reported here. The equation shown on the graph describes the input-output relationship, with the coefficient of the first order term being the charge sensitivity.

5.5.2 Static Calibration along Shear Directions

The dynamometer can measure two orthogonal, in-plane shear forces

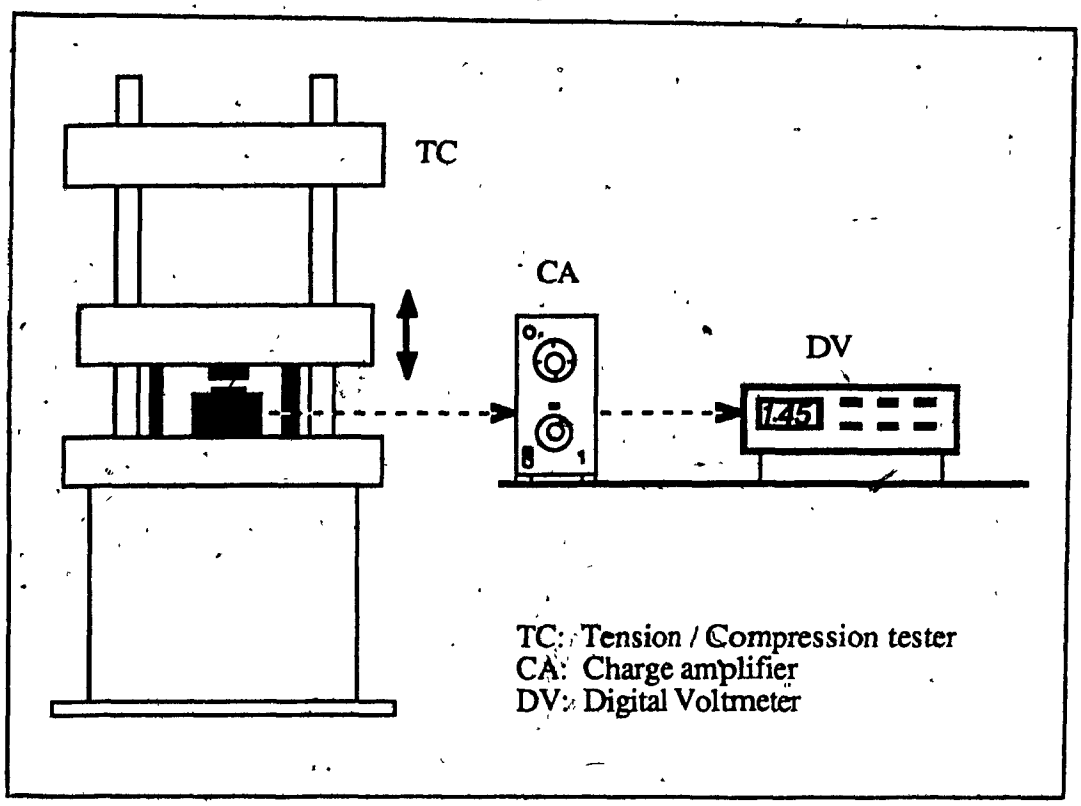

Figure 5.5 Schematic : Set-up for static calibration along axial direction.

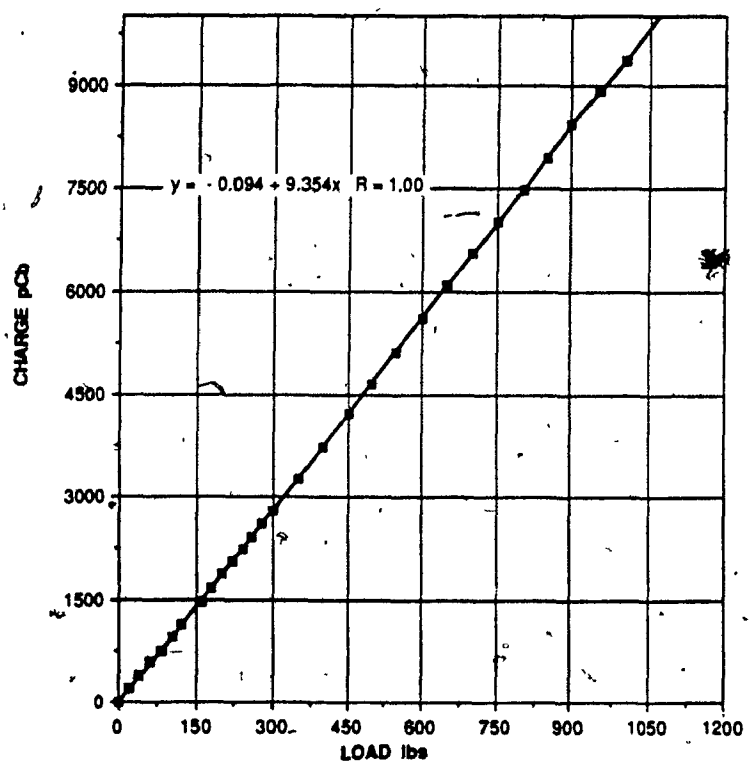

Figure 5.6 Static calibration : Thrust direction.

F_x and F_y. Calibration along these directions was carried out using a set of calibrated dead weights. The dynamometer was mounted with its base on the side of the machine table (figure 5.7), with the measuring axis aligned vertically. The weights were hung from a short stem that simulates the work specimen. Discrete weights were added and the voltage outputs of all channels noted. The experiment was repeated for the second shear axis.

Figures 5.8 and 5.9 are the direct calibration curves of the shear force channels. The mutual cross-influence of the shear channels, and the influence of the shear channels on the torque and thrust channels were investigated and found to be linear functions of loading. Table 5.3 shows the percentage cross-talk values of the various channels.

5.5.3 Static Calibration along Torque Axis

The calibration was carried out in the same set up as that of shear-calibration, except that the loading was applied eccentrically, on a moment arm. Figure 5.10 shows the calibration graph. Because of the moment being applied with a single force on an arm, a resultant shear force is automatically read by the dynamometer (application of a 'pure' torque by means of a shear force couple, requires an elaborate calibration fixture). Therefore the cross-talk of torque on other channels has been assumed to be minimal and omitted.

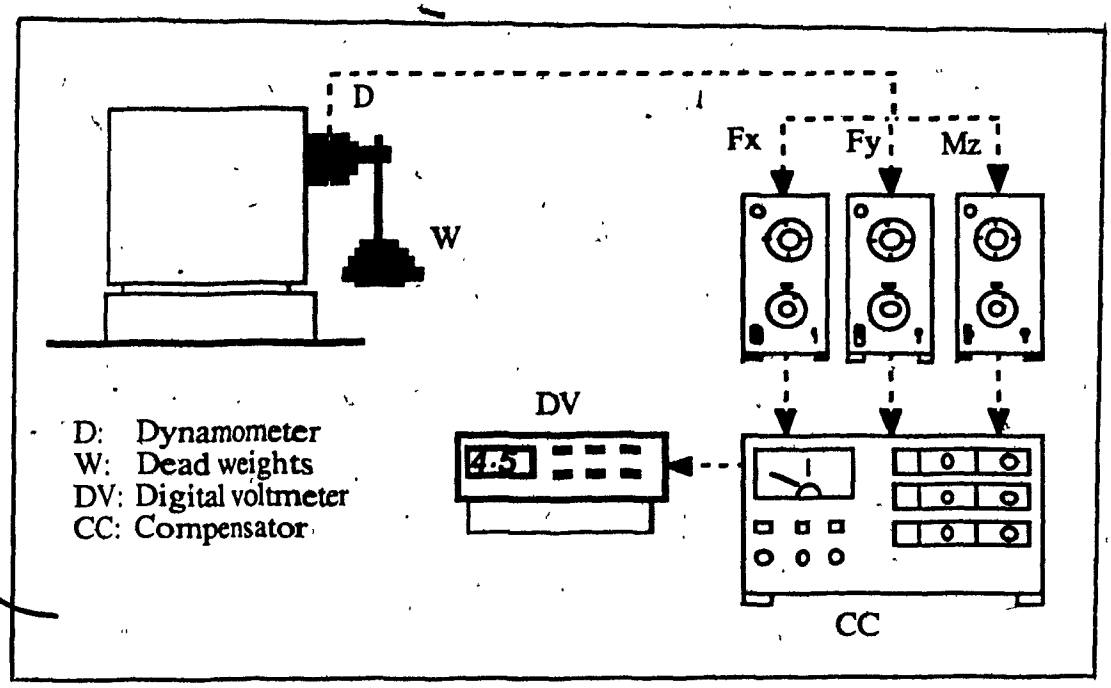

Figure 5.7 Schematic : Set-up for static calibration along shear directions.

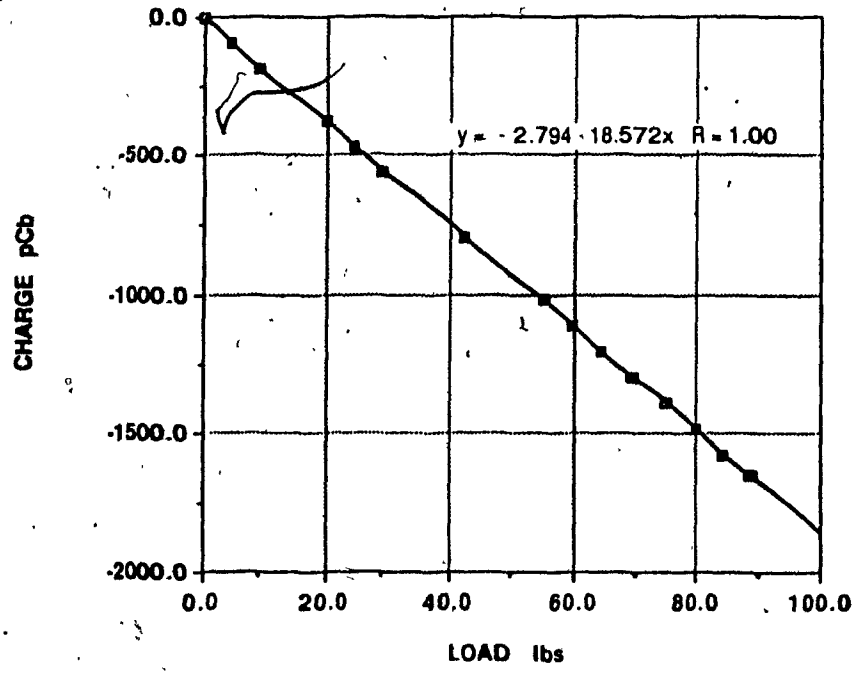

Figure 5.8 Static calibration : Shear axis - Fx.

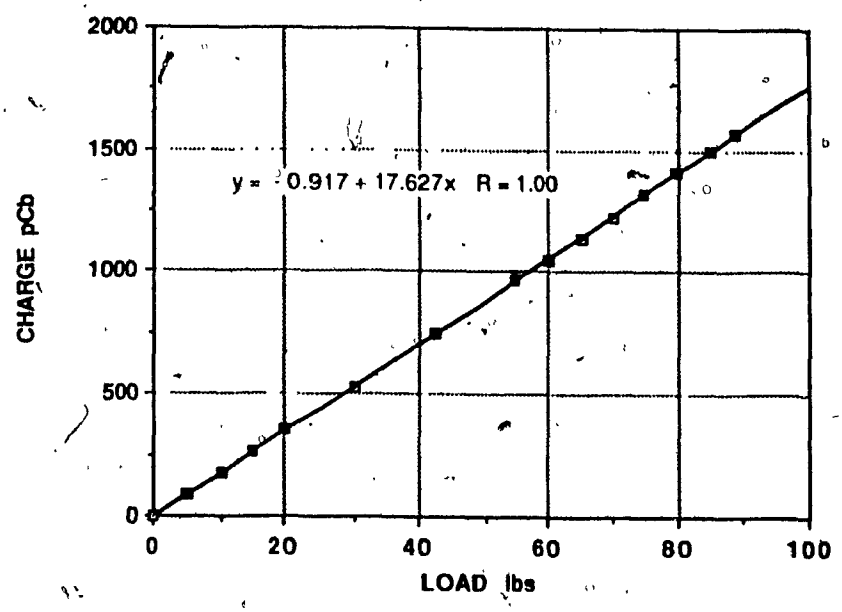

Figure 5.9 Static calibration : Shear axis - Fy.

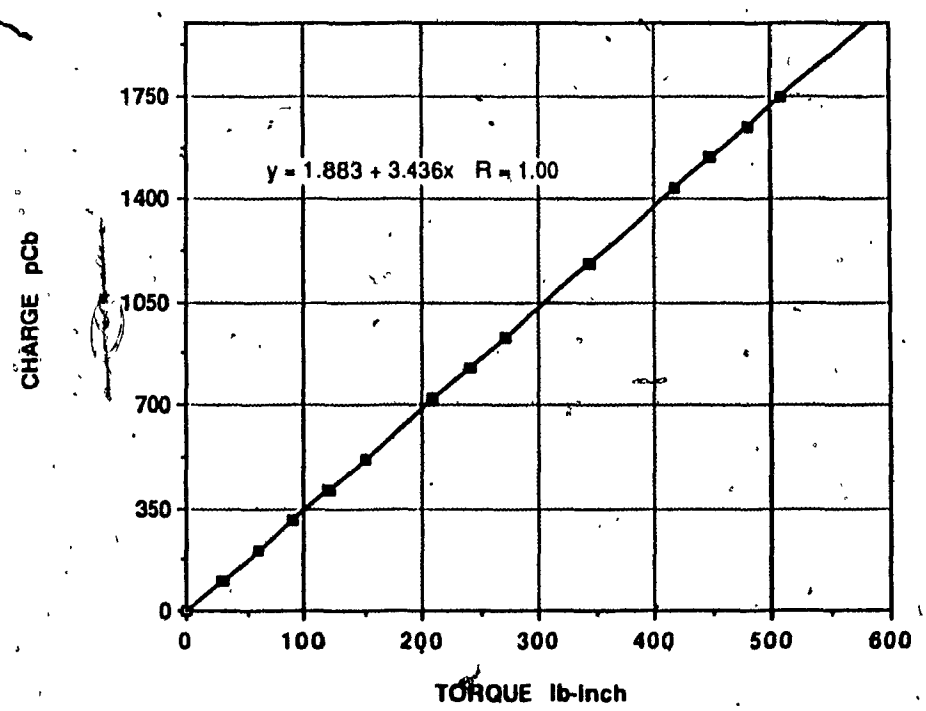

Figure 5.10 Static calibration : Torque direction - Mz.

Table 5.3 Static calibration : Cross-talk magnitudes.

Channel	Cross-talk magnitude
F_x on F_y	0.095 lb/lb
F_y on F_x	0.017 lb/lb
F_x on M_z	0.14 lb-in/lb
F_y on M_z	1.2 lb-in/lb
F_x on F_z	0.26 lb/lb
F_y on F_z	0.035 lb/lb

5.5.4 Cross-talk Compensation

After establishing the direct and cross-calibration of all channels, the procedure was repeated to make the settings on the X-Y-Z compensator to minimize the cross-talk between channels. Since the compensator has only three channels, the torque channel and the two radial force channels were chosen, and the thrust channel excluded from the compensation process. This choice was based on the following factors :

i) The magnitudes of radial forces are small in drilling and accuracy in their measurement is essential. Therefore, the cross-influence of other channels on them must be minimized by compensation.

ii) From the results of static calibration, it is seen that the torque measuring channel is strongly influenced by shear force F_y (1.2 lb-in/lb), and must therefore be included in the compensation process.

iii) The thrust channel reads a significant portion of shear force F_x (about 25%). However, due to the high thrust forces and low radial forces in drilling, the actual error caused on thrust readings is very low (about 2%). Therefore, the thrust channel need not be compensated for cross-talk.

Loading was applied to each of the three loading axes (F_x, F_y & M_z) and the appropriate potentiometers tuned until the cross-talk voltages on the other two channels (at the output of the compensator) were nullified.

5.6 Dynamic Calibration

Static calibration would be sufficient when measuring quasi-static processes at best. But the measurement of fast-varying processes requires an understanding of the dynamic characteristics of the measuring system and the original system. The piezoelectric dynamometer is a multi-element system which experiences natural vibration phenomenon under the fluctuating cutting forces in machining. Such vibratory behaviour may cause

i) error in the measured values of forces

ii) distortion of the frequency content of the force signals due to a mix-up with the system dynamics

iii) alteration of the cutting process itself in terms of change in parameters such as depth of cut, feed etc.

Therefore, a thorough dynamic calibration of the dynamometer, workpiece, and machine-tool system along all measuring axes was carried out to ascertain the following

i) Accuracy of the measuring channels under dynamic conditions

ii) the dominant natural frequencies of the system, so as to determine the usable frequency range

iii) the extent of cross-talk between channels under dynamic conditions.

The procedure basically consists of a frequency response test wherein, sinusoidal forces of known magnitudes and frequencies are applied and the dynamometer outputs compared to the input. The resonance frequencies are reconfirmed with transient excitation tests.

5.6.1 Experimental Set up for Dynamic Calibration

The experimental set up for dynamic calibration consists of the following (figure 5.11)

1. Electrodynamic shaker
2. Exciter control unit
3. Reference transducer
4. FFT analyzer
5. Plotter.

The shaker is an electrically driven linear actuator which outputs force signals. It is controlled by the Exciter-control unit, using the reference transducer for feedback. The control unit also generates the source waveform which is then amplified to drive the shaker. A swept frequency sine wave signal is used as input to the dynamometer and its outputs are fed into the FFT analyzer. Using the output of the reference transducer as the standard, the FFT analyzer computes the frequency-averaged ratio of output to input across the dynamometer. The computed function is then plotted by the digital plotter.

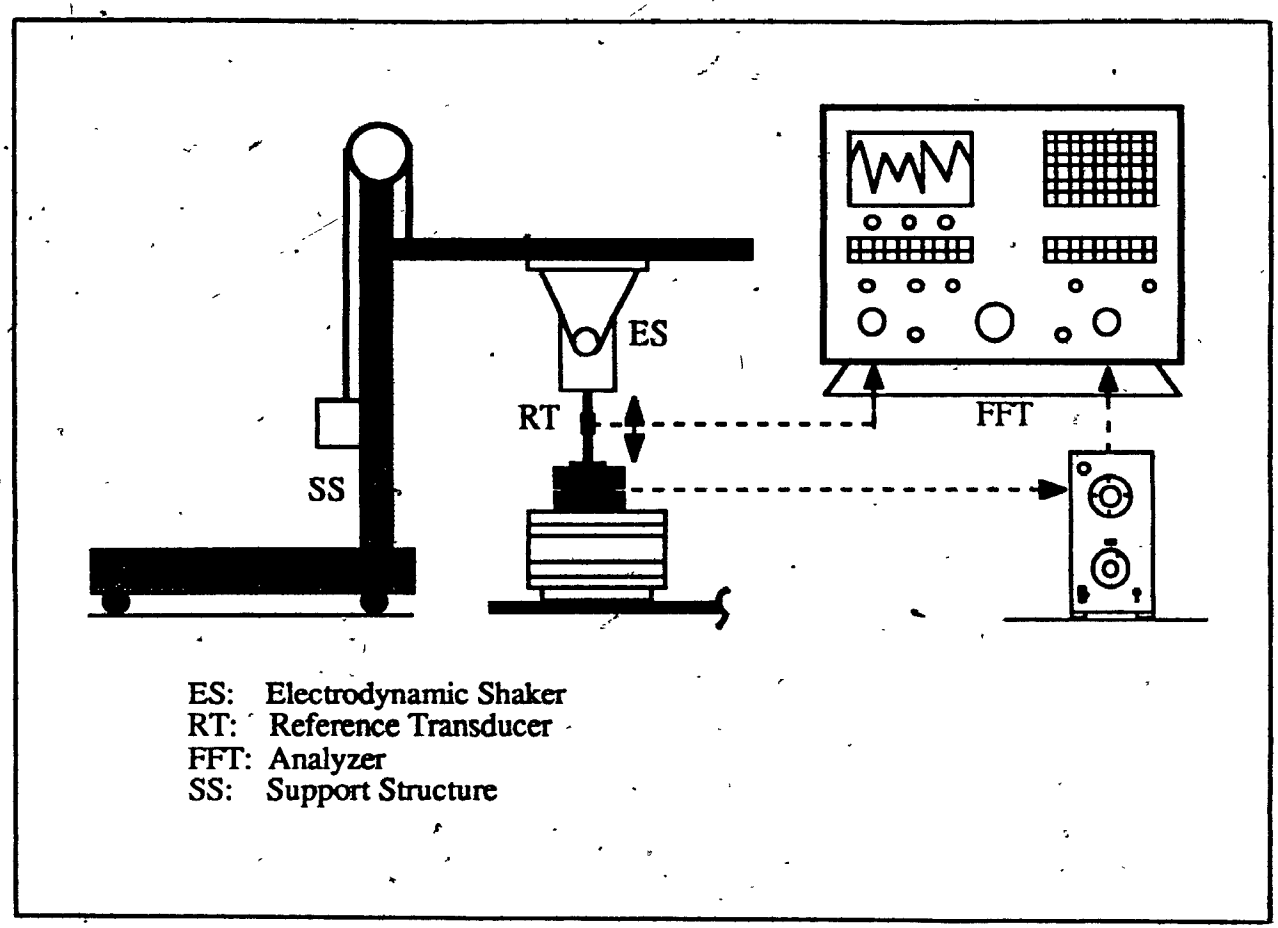

Figure 5.11 Schematic : Set-up for dynamic calibration.

The frequency sweep range for all tests was selected to be between 10 Hz and 500 Hz. This choice is based on the results of a previous investigation [5], which showed that most of the power in drilling forces is distributed within 200 Hz frequency.

5.6.2 Dynamic Calibration of Shear Force Directions

Figures 5.12 and 5.13 show pictorial views of the set up for dynamic shear force calibration. The shaker spindle was aligned along the shear axis to be calibrated, and both the dynamometer and the shaker clamped rigidly to the machine base. A short stem was affixed on the dynamometer, simulating the workpiece, and the shaker spindle connected to it through the reference transducer.

The frequency sweep was applied and the averaging process commenced simultaneously on the FFT analyzer. The process was continued until no change was observed in the computed transmissibility function. First the direct calibration was computed and then the cross-calibration on the other channels was conducted.

Figure 5.14 shows the direct calibration graph of shear force channel F_x. The peaks signify the resonance frequencies of the system, one at about 360 Hz, and a more prominent one around 450 Hz. Behind these resonances there is a flat region where the transmissibility ratio remains unity. This means that in this range, the dynamometer measures the

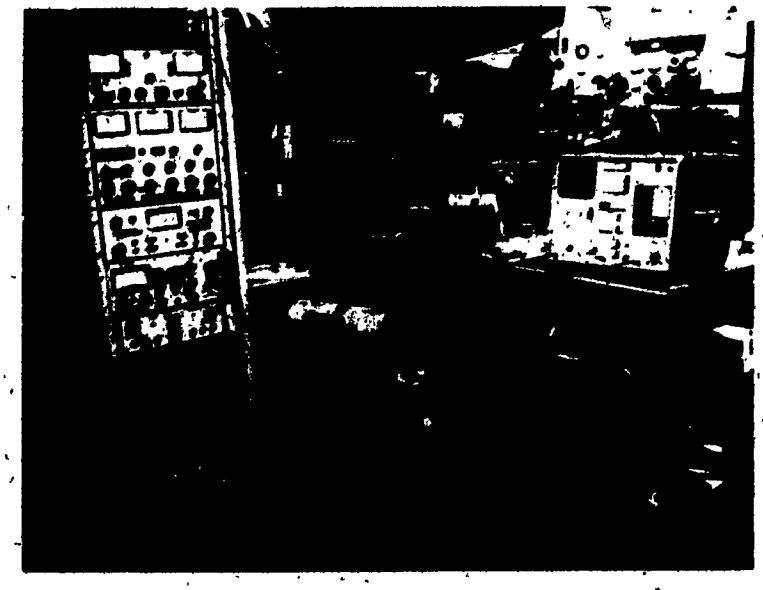

Figure 5.12 Photograph : Set-up and instruments for dynamic calibration.

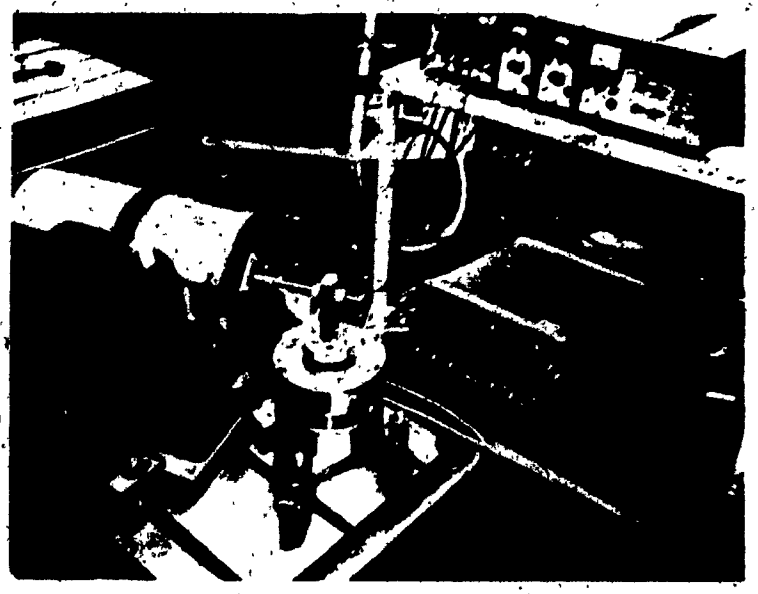

Figure 5.13 Photograph : Set-up for dynamic shear calibration.

forces faithfully. The sharp peak around 4 Hz seen in this and other graphs, was found to be due to the switching pulse of the averager.

The cross-calibration curve of F_x on F_y (figure 5.15) shows resonances identical to the direct calibration and the magnitude of cross-talk is generally found to be low. The cross-calibration on torque channel (figure 5.16) also shows minimal cross-talk and the same resonance frequency.

The direct and cross calibration procedures were repeated for the y-axis of the dynamometer, figures 5.17, 5.18 and 5.19 show the calibration curves.

5.6.3 Dynamic Calibration along Axial Direction

For calibration along the axial direction, the dynamometer was clamped on the machine table and the shaker was held in an overhung structure. A sinusoidal sweep was applied as before to establish the direct calibration shown in figure 5.20. Because of flexibility in the shaker-support, clearances at the various joints etc., it was not possible to align the shaker spindle to be perfectly parallel with the F_z axis of the dynamometer. This invariably caused the shaker to apply force components in the shear directions. Therefore the cross-talk calibration of thrust on radial force channels was not attempted. Cross-talk on the torque channel was investigated and found to be minimal.

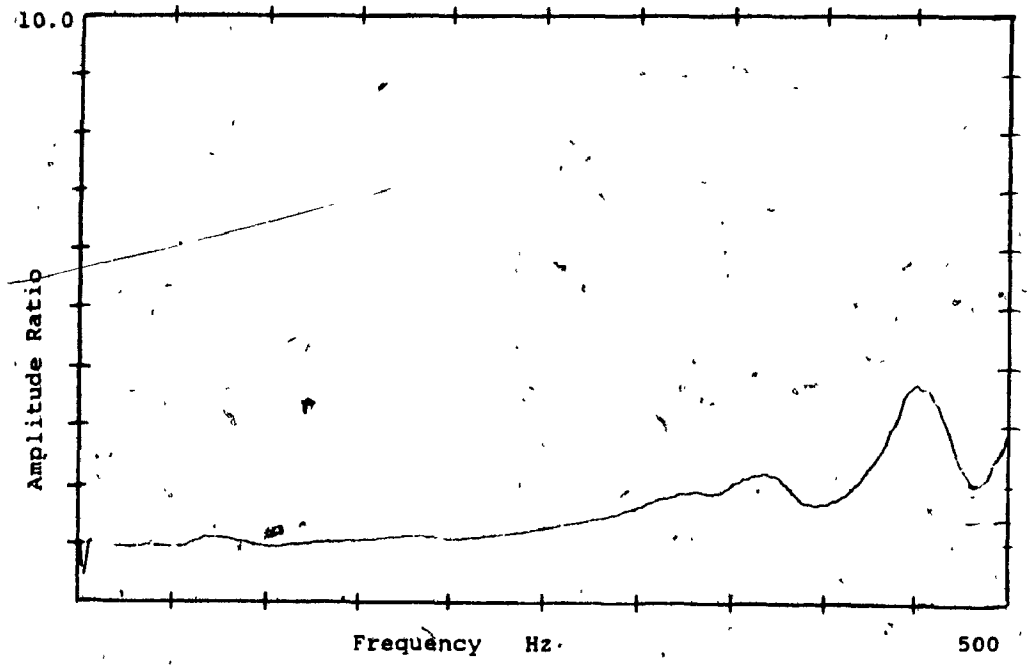

Figure 5.14 Direct dynamic calibration : Shear axis Fx.

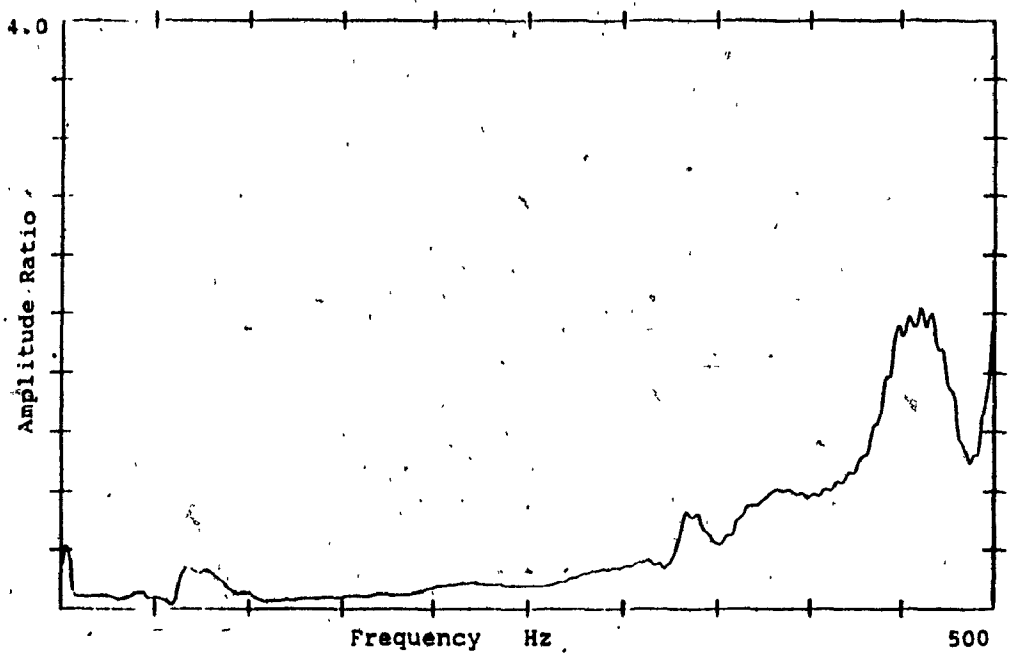

Figure 5.15 Dynamic cross-calibration : Fx on Fy.

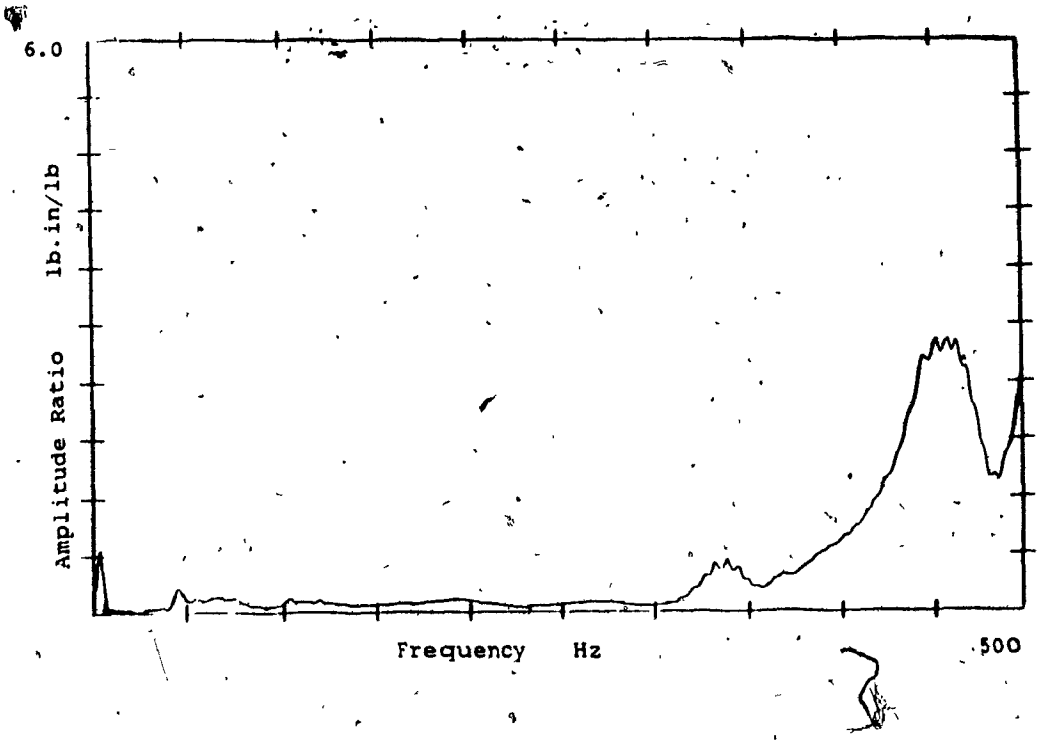

Figure 5.16 Dynamic cross-calibration : Fx on Mz.

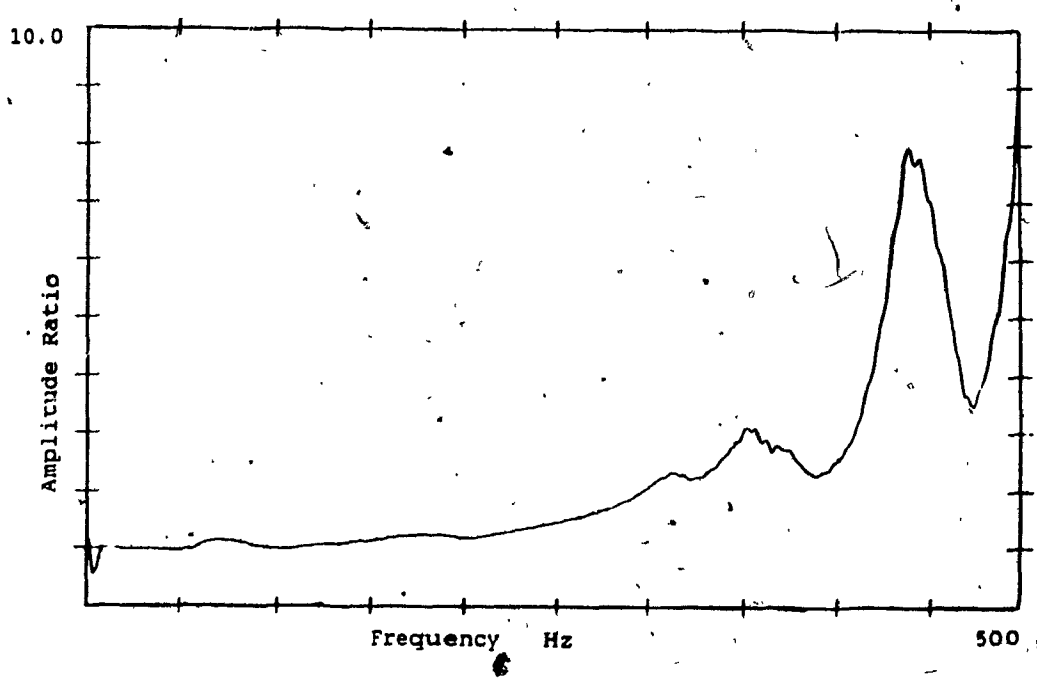

Figure 5.17 Direct dynamic calibration : Shear axis - Fy.

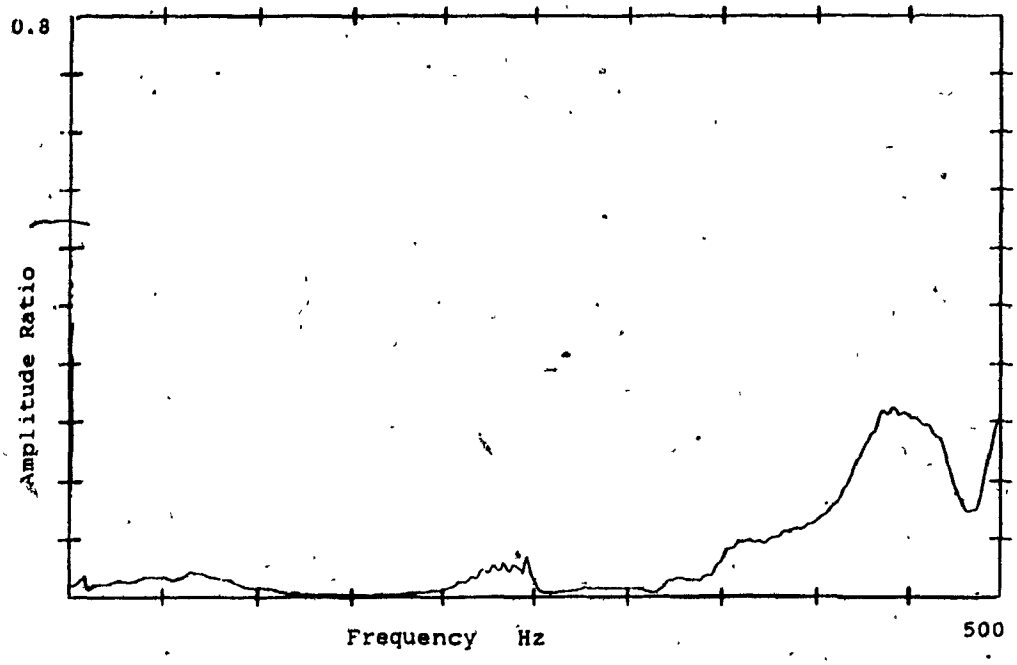

Figure 5.18 Dynamic cross-calibration : Fy on Fx.

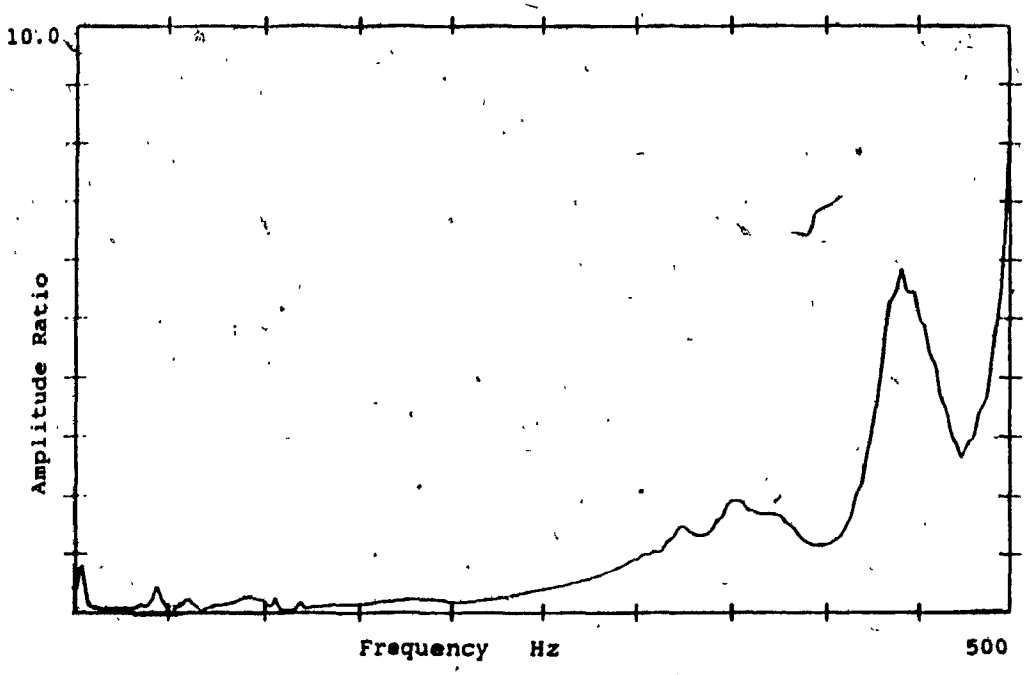

Figure 5.19 Dynamic cross-calibration : Fy on Mz.

5.6.4 Dynamic Calibration along Torque Direction

Dynamic torque was applied by connecting the shaker to the dynamometer through a moment-arm. A frequency-swept torque was applied and the response investigated. Figure 5.21 is a plot of the function, and it shows a dominant resonance around 175 Hz. But this resonance was suspected to be that of the moment arm and the mounting fixture on it, as they were vibrating noticeably. In order to find out the true resonance frequency of the torque channel and as well reconfirm those of the others, impact tests were carried out.

5.6.5 Resonance Frequencies with Impact Tests

In order to eliminate the possible interference of the shaker itself on the frequency response of the dynamometer, the resonance frequencies were reconfirmed by transient excitation with a light steel hammer.

Figure 5.22 shows the instant spectrum of the torque channel output due to a torsional impact. It is seen that the true resonance frequencies of the torque channel are 350 Hz and higher.

Similar impact tests were carried out on all other channels, the results reconfirm the resonance frequencies to be as obtained by the shaker tests. Figure 5.23 shows a sample calibration, for the shear force direction F_x.

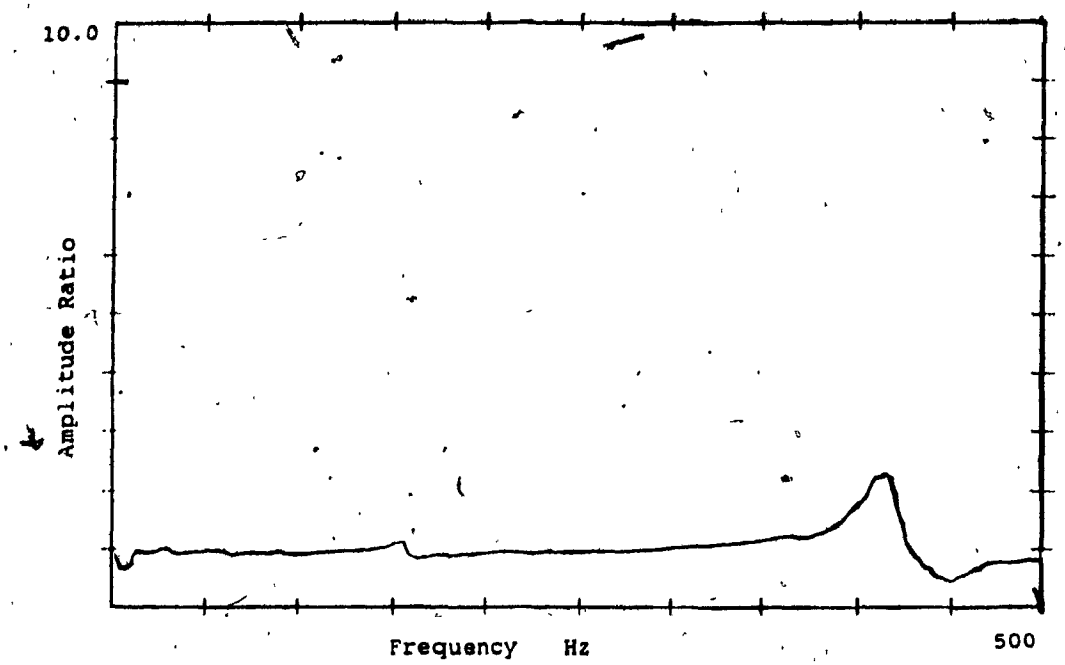

Figure 5.20 Direct dynamic calibration : Thrust axis Fz.

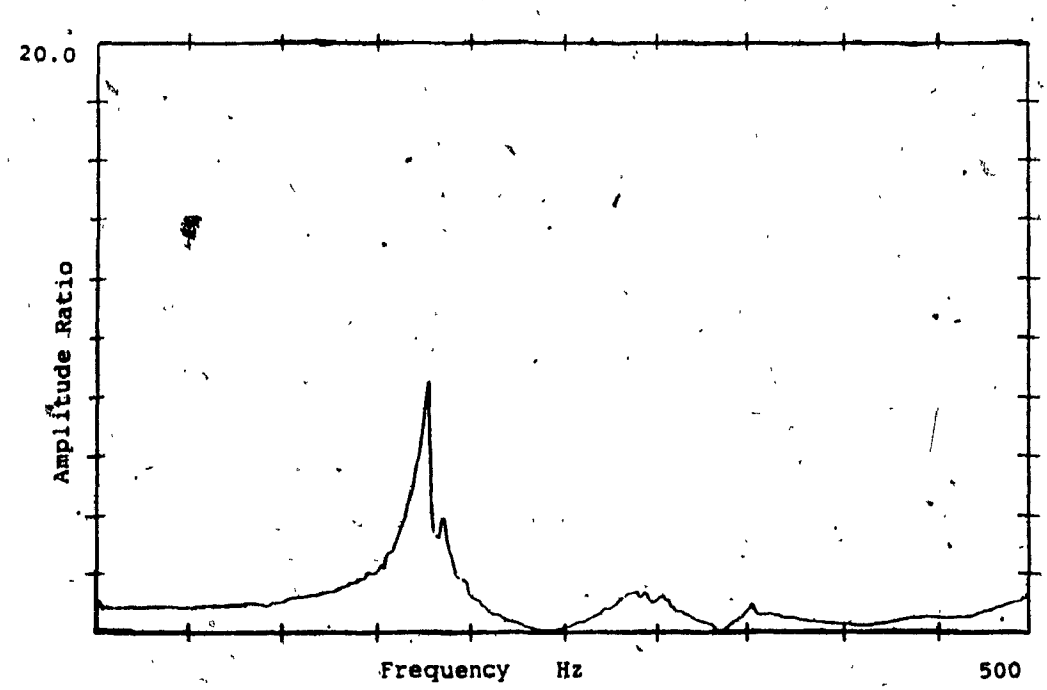

Figure 5.21 Direct dynamic calibration : Torque, Mz.

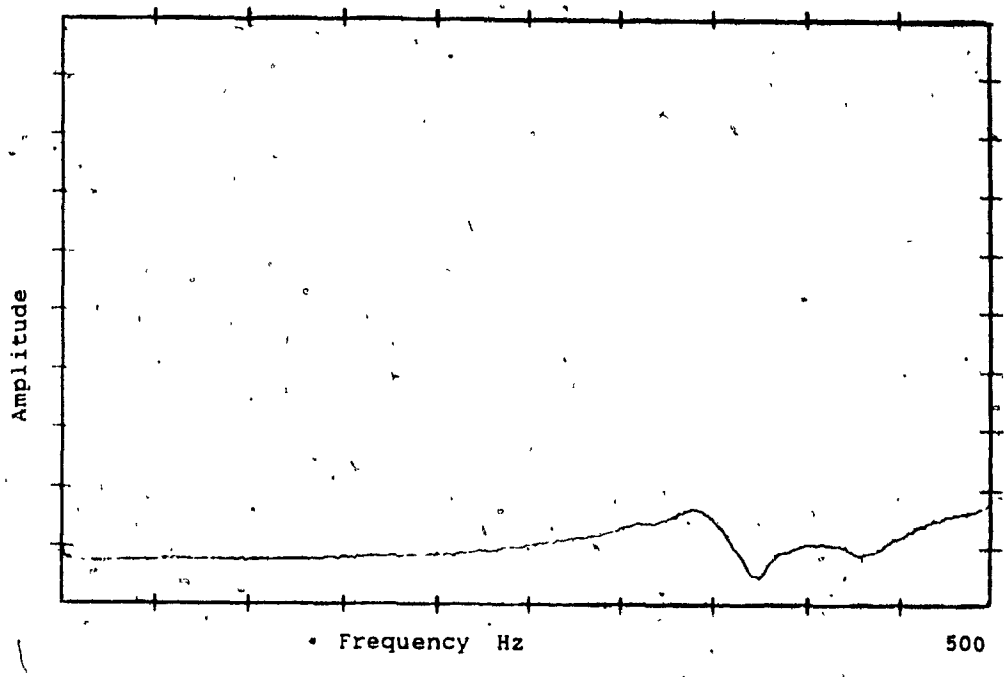

Figure 5.22 Transient response test : Torque, Mz direction.

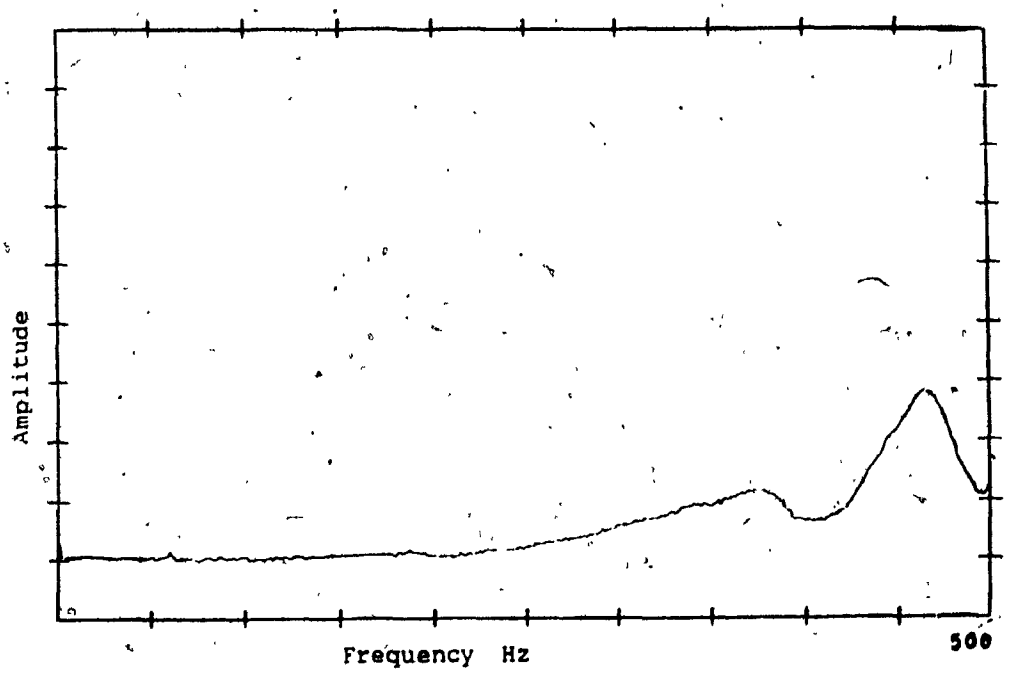

Figure 5.23 Transient response test : Shear axis - Fx.

5.7 Usable Frequency Range of the Dynamometer

An examination of the dynamic calibration plots enables us to make the following comments :

i) The first significant resonance of the dynamometer is around 350 Hz. Another, more dominant resonance occurs around a frequency of 450 Hz.

ii) 'Flat transmission' with minimal amplitude errors is seen to occur in all channels between 0 and 200 Hz. Beyond this range there is a gradual distortion of the signal due to resonance.

iii) Cross-talk between channels is found to be small in general, table 5.4 lists the average values.

It can be concluded that the dynamometer senses and faithfully reproduces the cutting force components in the frequency range of interest in this investigation.

5.8 Design of the Experiments

The drilling experiments have been designed so that the information sought in the investigation would be clear from the results. Yet the tools and process parameters chosen, reflect the conditions encountered in routine drilling practice.

Table 5.5 gives details of the experimental conditions and parameters chosen. The two sizes of drills selected are commonly used in drilling practice [6] as well as in past drilling research. Taper-shank ends were chosen to minimize drill axis run-out. The spindle speeds selected give cutting a speed of about 70 feet per minute. These lower-than-recommended speeds [7] were used since no coolant was applied. The feeds used are recommended values for the particular drill sizes [7]. The '2-step' feed consists of starting the drilling with a slow hand-feed, and after the drill-tip enters the workpiece, automatic feed is engaged.

The criterion behind the pilot hole sizes selected was explained in chapter 4. Only one axially-centered hole is drilled in each workpiece. This avoids the problem of mis-read force components that is inevitable when drilling several holes in a single workpiece (for example, radial forces read into the torque channel due to the eccentricity of the hole from the dynamometer axis).

5.9 Experimental Procedure

In setting up the radial drill for the experiments, the arm position on the column and the drilling-head position on the arm, were kept at their lower extremities to ensure machine rigidity during drilling. The dynamometer and the workpiece on it were rigidly clamped. The machine and the instrumentation were given a sufficient warm-up period before commencing the experiments.

Table 5.4 Dynamic calibration : Cross-talk magnitudes.

Channels	Cross-talk magnitude
F_x on F_y	0.10 lb/lb
F_x on F_z	0.18 lb/lb
F_x on M_z	0.15 lb-in/lb
F_y on F_x	0.03 lb/lb
F_y on F_z	0.03 lb/lb
F_y on M_z	0.25 lb-in/lb
F_z on M_z	0.07 lb-in/lb

Table 5.5 Experimental parameters chosen

Drill sizes	1/2 and 3/8 inch diameter. HSS, tapershank regular helix, jobbers length drills
Feeds	0.0045 inch/revolution 0.007 inch/revolution 2-step feed (0.007 in/rev)
Speeds	1/2" drilling : 531 RPM 3/8" drilling : 723 RPM
Pilot hole sizes	1/2" drilling : #28 (0.1405") and #9 (0.196") 3/8" drilling : #10 (0.1935)
Workpiece	AISI 1020 mild steel, 1.5" dia. bar stock

Several trial holes were drilled to 'break-in' the new drills used, and also to verify the functioning of the dynamometer and the various instrumentation used. The drilling experiments were then commenced, carefully monitoring the force signals, the chip flow out of the hole, etc.. In required experiments, the pilot holes were drilled and the full holes drilled in the same set up to ensure concentricity. Each distinct experiment was repeated three times, once to measure the static components of all forces, and twice to measure the dynamic components. With each change of voltge sensitivity setting, the compensation ratios were appropriately re-adjusted.

5.10 Conclusions

A methodology for the measurement of the cutting forces in drilling is presented. The design of the piezoquartz dynamometer used for the purpose is detailed. A thorough static and dynamic calibration is carried out. The frequency response measurement reveals that fluctuating components of the drilling forces can be measured without distortion up to 200 Hz. A three-channel compensation procedure is employed to minimize the cross-talk between measuring channels. A detailed description of the experimental variables and procedures is also presented.

CHAPTER 6

DATA REDUCTION, ANALYSIS AND DISCUSSION OF EXPERIMENTAL RESULTS

The previous chapter described the equipment and procedure for measuring and recording the cutting forces during the drilling experiments. This chapter presents the analysis of the recorded signals and a detailed discussion of the results relevant to the various objectives of this investigation.

Figure 6.1 shows a schematic of the set up used for the analysis of the force signals. The signals recorded on magnetic tapes are played back on the FM recorder and fed into the FFT analyzer, wherein the signals are analyzed for time, frequency and statistical characteristics. The results of such an analysis are plotted using the direct digital plotter connected to the FFT analyzer.

6.1 Analysis Procedure

There are two major aspects in the analysis of the force signals;

1) Static component analysis
2) Dynamic component analysis.

Static component analysis is performed on torque and thrust signals to

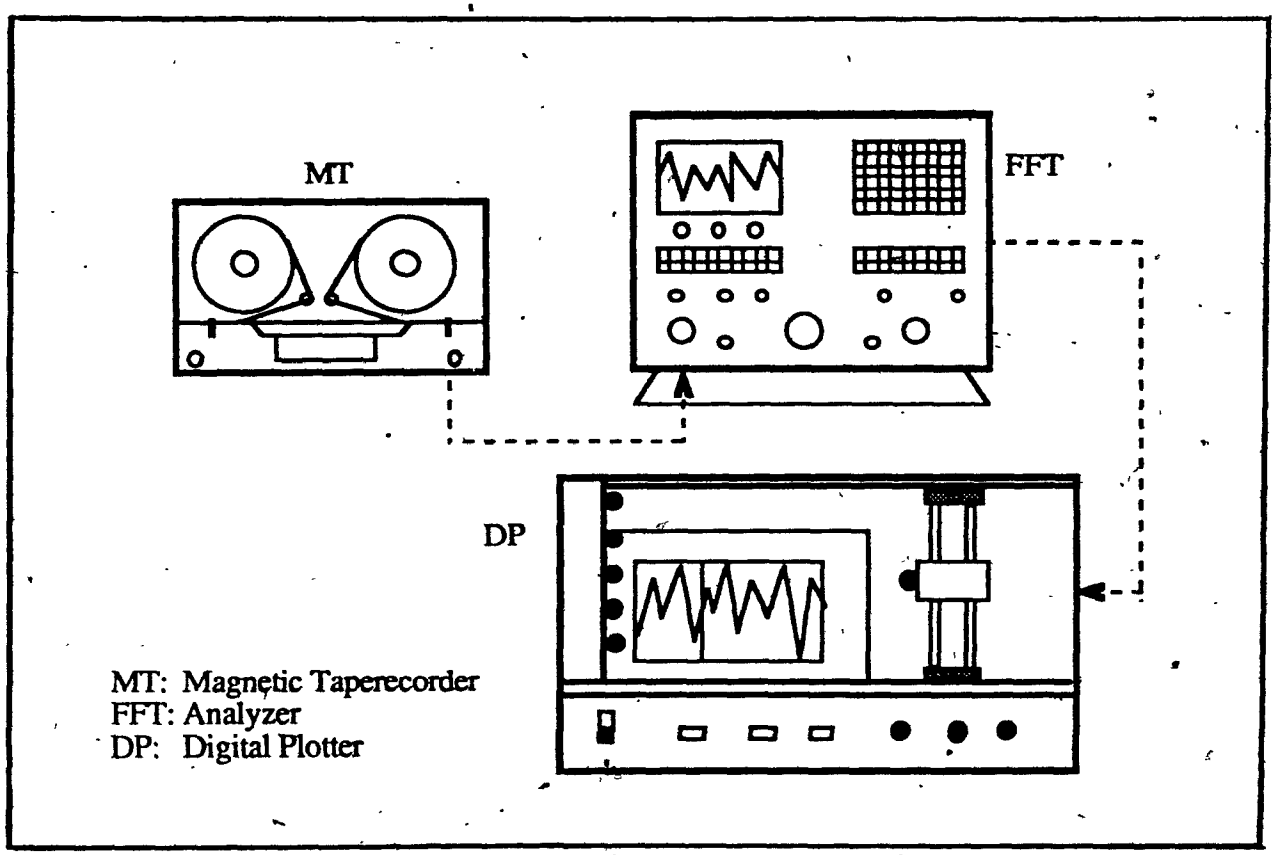

Figure 6.1 Schematic : Set-up for data analysis.

determine the steady or 'DC' values of the forces. The FFT analyzer inputs are set in the DC mode and a very low frequency range (5 or 10 Hz) is chosen. This gives a large time window (40 or 80 seconds) so that the general trend of the signals can be observed.

The dynamic component analysis is performed on all four force signals (F_x, F_y, F_z and M_z). Three major characteristics of the fluctuating components are observed,

1) Root Mean Square (RMS) spectra
2) Probability density analysis
3) Auto Correlation functions

The PSD function $S_f(\omega)$ or mean square spectral density function as it is also called, is a distribution of the mean square values (MSV) of the variable in the frequency domain [16]. Therefore,

$$MSV = E[x^2] = \int_0^\infty S_f(\omega)\, d\omega \qquad (6.1)$$

The RMS spectral density function is a distribution of the RMS value of the variable. Therefore the two spectral density magnitudes are related by

$$|S_{RMS}| = \sqrt{|S_f(\omega)|}$$

The spectral density functions are computed in the FFT analyzer by statistically sampled averages in the frequency domain. Therefore, particular values of the function at dominant frequencies give a close approximation of the actual signal amplitudes at those particular

frequencies. All signals in the present investigation had a dominant frequency, relative to which the remainder of the spectra were negligible. Therefore, values of the RMS spectra at these dominant frequencies have been used as an index of comparison between the signals.

The Auto Correlation Function (ACF) is an averaged-time statistic which describes the randomness of a signal and is given by,

$$R_f(\tau) = < f(t).f(t+\tau) >$$

where τ is a time delay. The ACF and PSD functions are Fourier transform pairs such that,

$$S_f(\omega) = \int_{-\infty}^{\infty} R_f(\tau).e^{-i\omega\tau}.d\tau \qquad (6.2)$$

Putting τ=0, we get

$$R_f(0) = <f^2(t)> = \text{Mean Square Value}$$

The probability distribution function P(f) of the continuous random variable f(t) is defined by

$$P(f) = P[f(t) < f]$$

The probability density function p(f) is the derivative of P(f). It has been shown by a previous researcher [5] that the torque and thrust force fluctuations in drilling are stationary random processes with a Gaussian probability distribution, which is described by

$$P(f) = \frac{1}{\sqrt{2\pi}\sigma} \exp\left[-\frac{1}{2}(f-\mu)^2/\sigma^2\right] \tag{6.3}$$

where μ is the mean value and σ the standard deviation. The above characteristics have been assumed to be valid for the torque and thrust signals of the present investigation and comparisons are performed on the basis of the standard deviation values.

In order to compute the above mentioned statistical properties, data-sampling was carried out employing the sampler-averager in the FFT analyzer. As established by the dynamic calibration procedure on the dynamometer, a frequency range of 0 to 200 Hz was selected to analyze most signals. For radial force signals, a lower range was selected to suit their frequency content. Selection of the frequency range automatically sets a particular data sampling rate of the averager. Therefore, the required number of samples were obtained by repeated replay of the signals, with cumulative averaging. Also the averaging was carried out on signals of single experiments (temporal averaging). This presumes the properties of stationarity and ergodicity of the random process [16].

6.2 Averaged Static Values of Measured Forces

Static values of the measured signals were obtained by time-averaging the DC signals. Table 6.1 shows the averaged values of the torque and thrust along with the parameters and coding of the various experiments with the half-inch diameter drill.

Table 6.1 Static torque and thrust : 1/2-inch drilling.

EXPT CODE	PARTICULARS	THRUST lbs (N)	TORQUE lbin (N-m)
H1-S	f = 0.007 ϕ_{ph} = 0	603 (2682)	94 (10.62)
H2-S	f = 0.0045 ϕ_{ph} = 0	405 (1801)	73 (8.25)
H3-S	f = 2-step ϕ_{ph} = 0	660 (2936)	107 (12.10)
H4-S	f = 0.007 ϕ_{ph} = ϕ_1	205 (912)	76 (8.59)
H5-S	f = 0.0045 ϕ_{ph} = ϕ_1	140 (623)	55 (6.21)
H6-S	f = 2-step ϕ_{ph} = ϕ_1	230 (1023)	82 (9.26)
H7-S	f = 0.007 ϕ_{ph} = ϕ_2	142 (632)	66 (7.46)
H8-S	f = 0.0045 ϕ_{ph} = ϕ_2	95 (423)	49 (5.54)
H9-S	f = 2-step ϕ_{ph} = ϕ_2	155 (689)	72 (8.13)

'ϕ_{ph}' = pilot hole diameter

Experiments H1, H2 and H3 were done without a pilot hole. The designations ϕ_1 and ϕ_2 for the pilot hole diameter correspond to the 'smaller than critical' ('wrong' size) and 'larger than critical' ('right' size) diameters respectively, as determined in chapter 4.

6.2.1 Effect of feed on static torque and thrust: 1/2 inch Drilling

It is seen from the values of table 6.1 that torque and thrust increase drastically with feed. Amongst experiments of a given pilot hole condition, an increase of feed from 0.0045"/rev to 0.007"/rev, increases the measured thrust force by about 50 percent and the measured torque by approximately 30 percent.

The feed method has an interesting effect on the measured forces. The experiments with 2-step feed are identical to those at high feed, except during the tip-entry period. However, the static torque and thrust values in the two cases are not the same. The measured torque and thrust values in the 2-step feed experiments are about 10 percent higher than in the corresponding high-feed experiments.

6.2.2 Effect of pilot hole on forces : 1/2-inch drilling

Comparing experiments of a given feed with various pilot hole conditions, the following effects are observed on the measured torque and thrust forces : Between experiments with no pilot hole and those with the

'right' size pilot hole, a drastic change in forces is observed. The web of the drill together with the negative-rake region of the cutting lips are seen to generate about 75 percent of the measured thrust and 30 percent of the measured torque.

Between experiments with two different pilot hole sizes, a 30 percent decrease is seen in thrust. This is significant since the reduction in pilot hole diameter is only marginal. Correspondingly, the torque values decrease by 14 percent. Figure 6.2 shows the variation of static torque and thrust for various pilot hole conditions.

6.2.3 Effect of feed and pilot holes on static torque and thrust : 3/8-inch drilling

Table 6.2 shows the parameters and the measured values of torque and thrust in experiments with 3/8-inch drills. Two sets of experiments were conducted, one without a pilot hole (expts. T1 to T3) and one with a 'right' size pilot hole (expts. T4 to T6).

Similar to 1/2-inch diameter experiments, an increase in feed from 0.0045"/rev to 0.007"/rev, increases the static thrust by approximately 50 percent and the torque by 40 percent. The feed method has a similar effect. The torque and thrust values are higher by 10 percent with a 2-step feed, and a pilot hole. The increase is only marginal when drilling without a pilot hole.

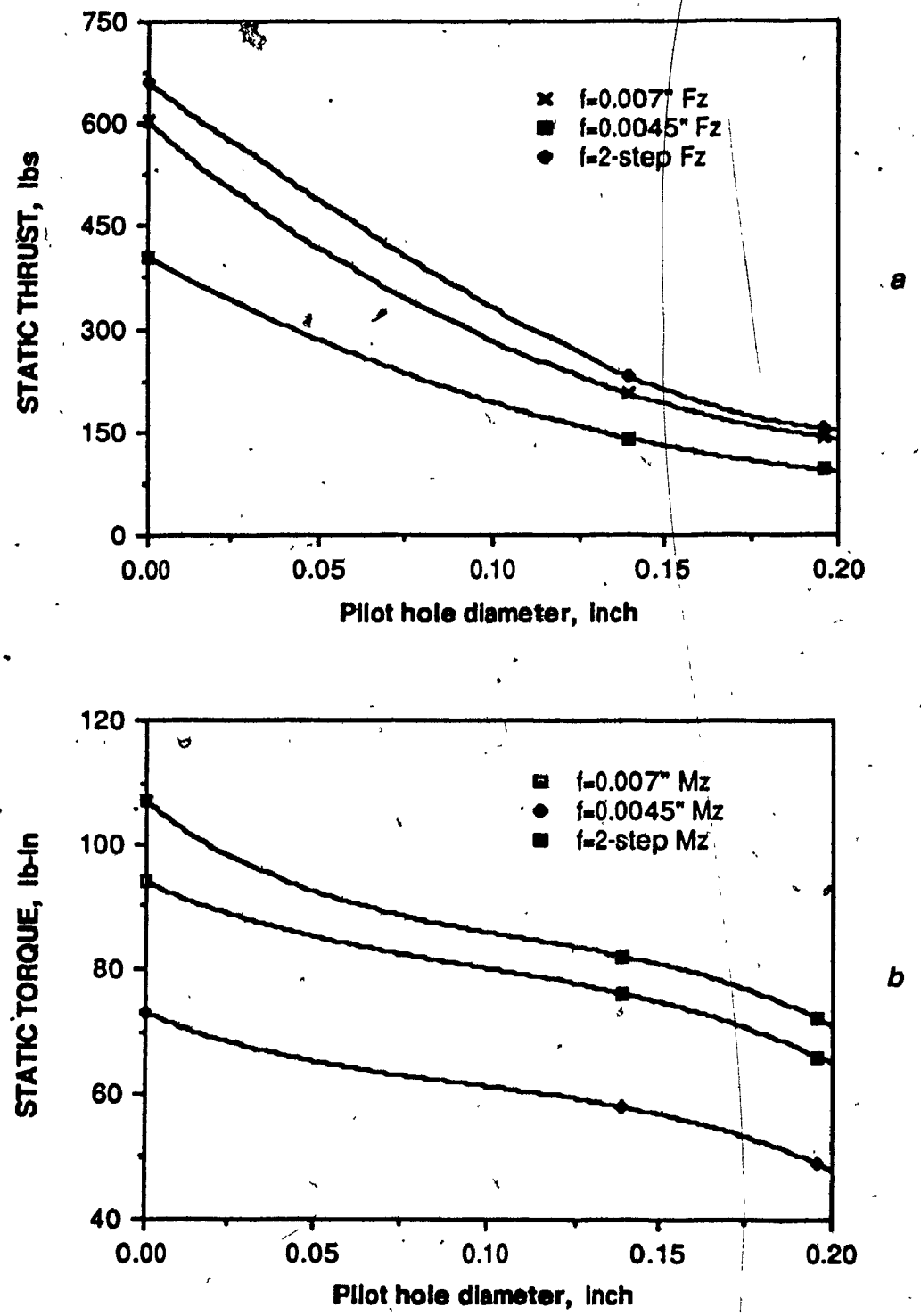

Figure 6.2 Graphs of static thrust (a), and static torque (b) against pilot hole diameters.

Table 6.2 Static torque and thrust : 3/8-inch drilling.

EXPT CODE	PARTICULARS	THRUST lbs (N)	TORQUE lb.in (N-m)
T1-S	f = 0.0045 ϕ_{ph} = 0	260 (1157)	40 (4.52)
T2-S	f = 0.007 ϕ_{ph} = 0	402 (1788)	58 (6.55)
T3-S	f = 2-step ϕ_{ph} = 0	410 (1824)	61 (6.89)
T4-S	f = 0.0045 ϕ_{ph} = ϕ_1	52 (231)	23 (2.60)
T5-S	f = 0.007 ϕ_{ph} = ϕ_1	78 (347)	31 (3.5)
T6-S	f = 2-step ϕ_{ph} = ϕ_1	86 (382)	34 (3.84)

Again, a comparison of the two sets of experiments reveals that approximately 80 percent of thrust and 45 percent of torque are generated by the drill-web and the negative rake region of the lips together.

The above observations highlight the drastic effect of cutting mechanics in terms of normal rake angle, on the cutting forces generated. Thus the basis of the pilot hole sizing criterion of chapter 4 is also demonstrated.

6.3 Estimation of Coupling Error in Measured Forces

In chapter 3 it was proposed that the torque-thrust coupling effect can induce torque and thrust forces which add up with the true cutting forces during drilling. With some previous experimental results, it was illustrated that in solid drilling (that is, without a pilot hole) significant error can be incurred in the measurement of torque and thrust. Again, the phrase 'measurement error' refers to the induced forces mixed up with the true cutting forces.

The separation equations derived in chapter 3 are used again to isolate the true cutting forces from the measured forces, and thus estimate the measurement error in the present experiments.

Tables 6.3a and 6.3b list the measured torque and thrust values, the corresponding true cutting forces and the induced force components ('error') for the two drill sizes tested.

Table 6.3 Estimated torque and thrust measurement errors in full hole drilling.

a) 1/2-inch drilling

EXPT CODE	T_m lb-in	F_m lb	T_{cut} lb-in	F_{cut} lb	T_{er} % T_m	F_{er} % F_m
H1-S	94	603	79	482	16	20
H2-S	73	405	63.6	308	13	24
H3-S	107	660	91	521	15	21
Separation equations	$T_{cut} = 1.049\ T_m - 0.032\ F_m$ $F_{cut} = 1.049\ F_m - 1.597\ T_m$					

b) 3/8-inch drilling

EXPT CODE	T_m lb-in	F_m lb	T_{cut} lb-in	F_{cut} lb	Torque Error % T_m	Thrust Error % F_m
T1-S	40	260	37	172	7.5	33
T2-S	58	402	53.3	276	8.1	31
T3-S	61	410	56.3	277	7.7	32
Separation equations	$T_{cut} = 1.042\ T_m - 0.0177\ F_m$ $F_{cut} = 1.042\ F_m - 2.467\ T_m$					

The induced thrust or 'thrust error', constitutes approximately 22 percent of the measured value and the 'torque error' forms about 15 percent, when drilling with a 1/2-inch drill. As noted in section 3.1.1, the thrust error increases for the smaller diameter (3/8") drill, with the induced thrust at 32 percent of the measured value. Correspondingly, the torque error decreases to about 8 percent. It is seen that the above estimates of torque and thrust error are nearly identical to the numerical samples computed in chapter 3, using previous experimental results.

When the induced forces are expressed as a percentage of the true cutting forces, their prominence increases further. The thrust error constitutes 28 percent of cutting thrust for a 1/2-inch drill and about 48 percent for the smaller drill.

A comparison of the above 'true' values of cutting forces reveals that with an increase in feed, the actual increase in thrust and torque values are approximately the same percentages as those of the corresponding measured values. The increase in forces between the high feed and 2-step feed experiments are also nearly the same.

6.4 General Trend of Torque and Thrust Signals

Interesting characteristics are revealed in the general trend of the static torque and thrust signals when each process signal is presented in its entirety in a single time window of the analyzer.

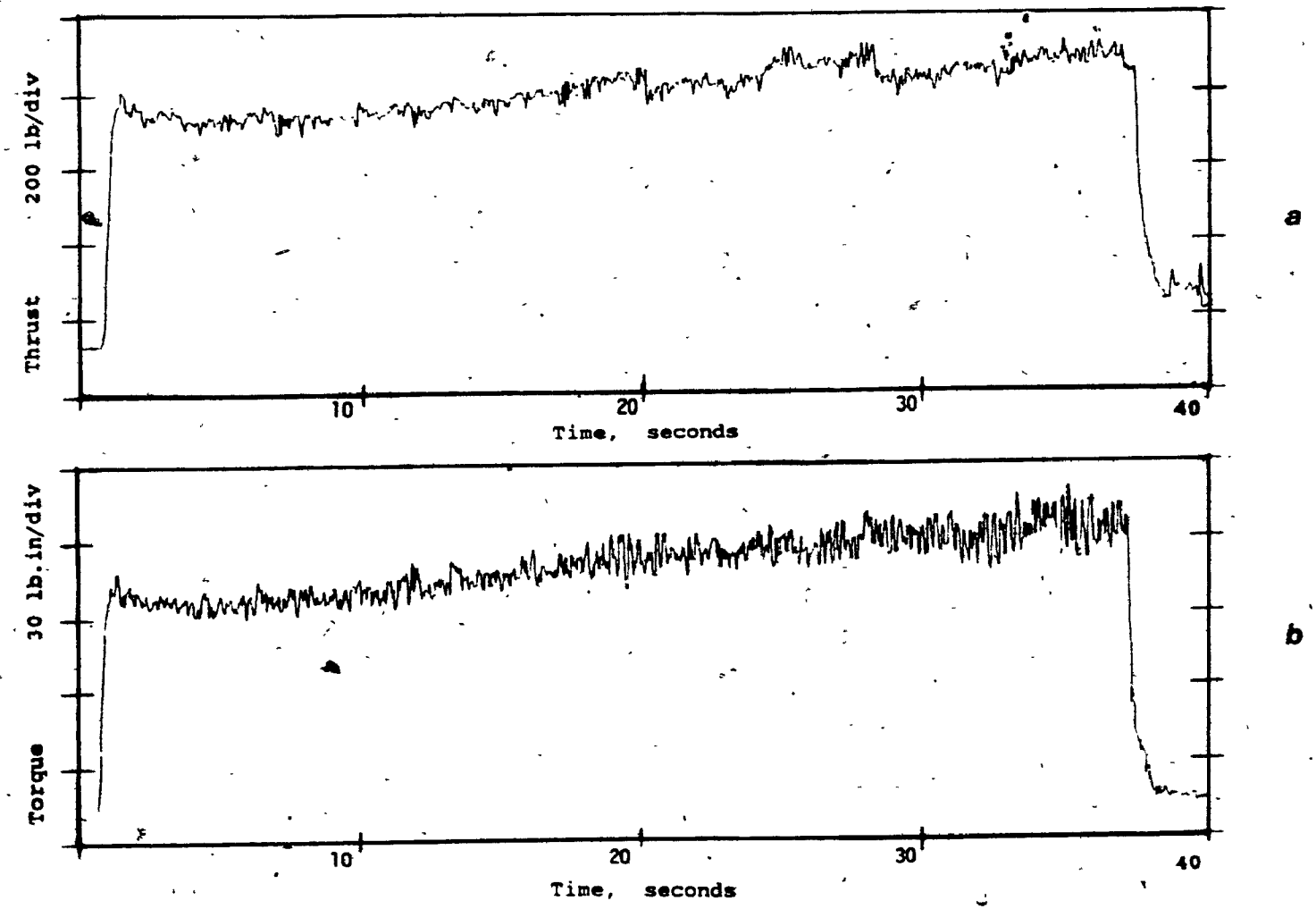

Figure 6.3 Typical plots of thrust (a), and torque (b) in full-hole drilling : Experiment H3-S.

Figure 6.3 shows the typical trend of the force signals when drilling without a pilot hole. It is seen that the static torque and thrust values increase gradually and continuously, throughout the duration of drilling. The following is the reasoning behind the phenomenon.

In drilling, the chips produced at the drill point are removed from the hole solely due to the pumping action of the helical flutes. As the drill penetrates deeper into the material, the chips have to be pumped a longer distance before being ejected from the hole-mouth. This causes accumulation of chips along the flutes. In manual drilling the problem is remedied by frequently withdrawing the drill from the hole and then re-starting. However, in the present experiments each hole was drilled entirely without interruption. This causes chip-clogging and hence the gradual increase in torque and thrust forces.

In addition, since the web thickness of a drill increases substantially towards the shank, the amount of flute profile area available for chip-flow is correspondingly reduced. This aggravates the problem of chip-accumulation and clogging as the hole depth increases, and further increases the torque and thrust forces. Figure 6.4 shows a similar trend in the torque and thrust forces while drilling with the smaller drill.

6.5 General Trend of Static Forces in Pilot Hole Drilling

Figure 6.5 is a typical plot of the torque and thrust signals in

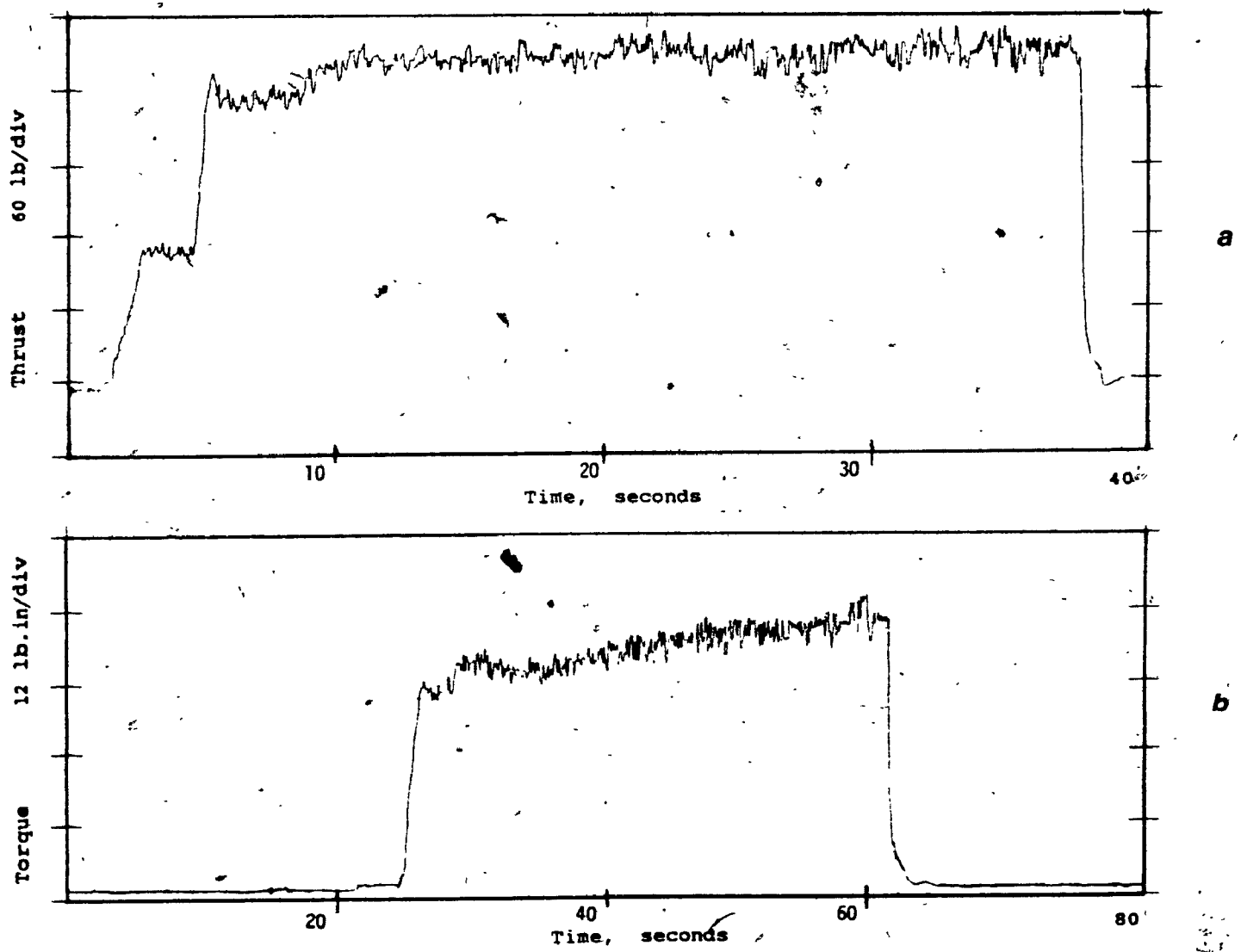

Figure 6.4 Typical plots of thrust (a), and torque (b) in full-hole drilling : Experiment T1-S.

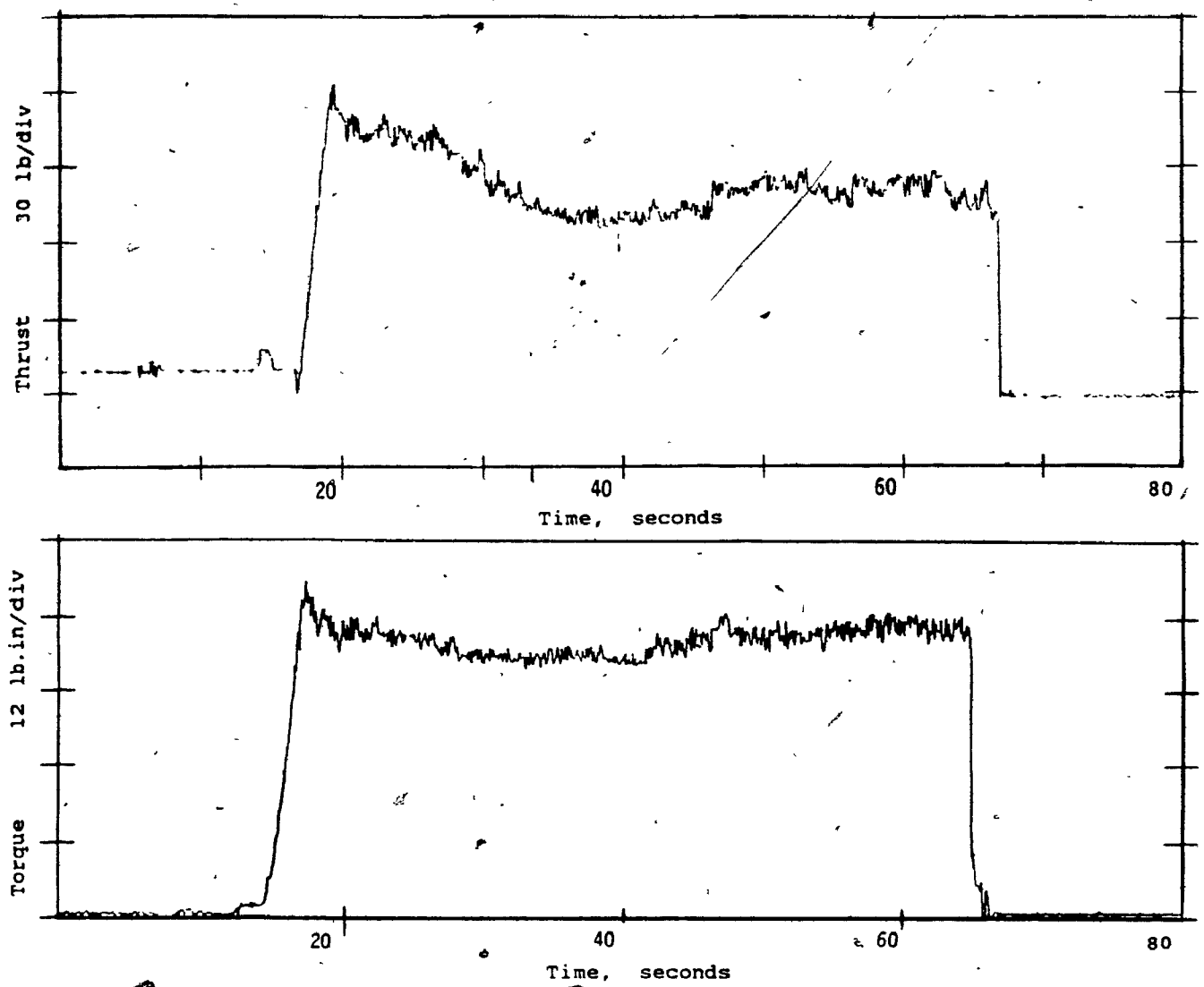

Figure 6.5 Typical plots of thrust (a), and torque (b) in pilot-hole drilling : Experiment H8-S.

drilling with pilot holes. It is clear that the trend illustrated is drastically different from those of full-hole drilling. Here the measured static torque and thrust forces decrease gradually as drilling progresses and reach certain minimum values in some period of time. After this, in most experiments, the force values begin to show a gradual increasing trend until drilling is terminated.

Figure 6.6 presents another sample of the torque and thrust signals in pilot hole drilling. The following is proposed as the reasoning for the 'decay' phenomenon in the torque and thrust signals. In doing so, the proposal has some significant implications, as seen further.

6.6 Mechanism Behind Torque-Thrust Decay Phenomenon

In chapter 3 it was argued that, owing to the coupling effect, the cutting forces induce axial and torsional strains during drilling. Because the conditions in full-hole drilling restrain these induced strains, it was proposed that significant induced torque and thrust may result instead.

In pilot hole drilling the absence of cutting at the web drastically reduces the forces (especially thrust) and changes the cutting conditions (rate of increase of thrust with feed). The result can be that the drill encounters reduced axial and torsional restraint.

When drilling commences, the restraint is sufficient enough that some torque and thrust forces are yet induced, leading to higher measured forces

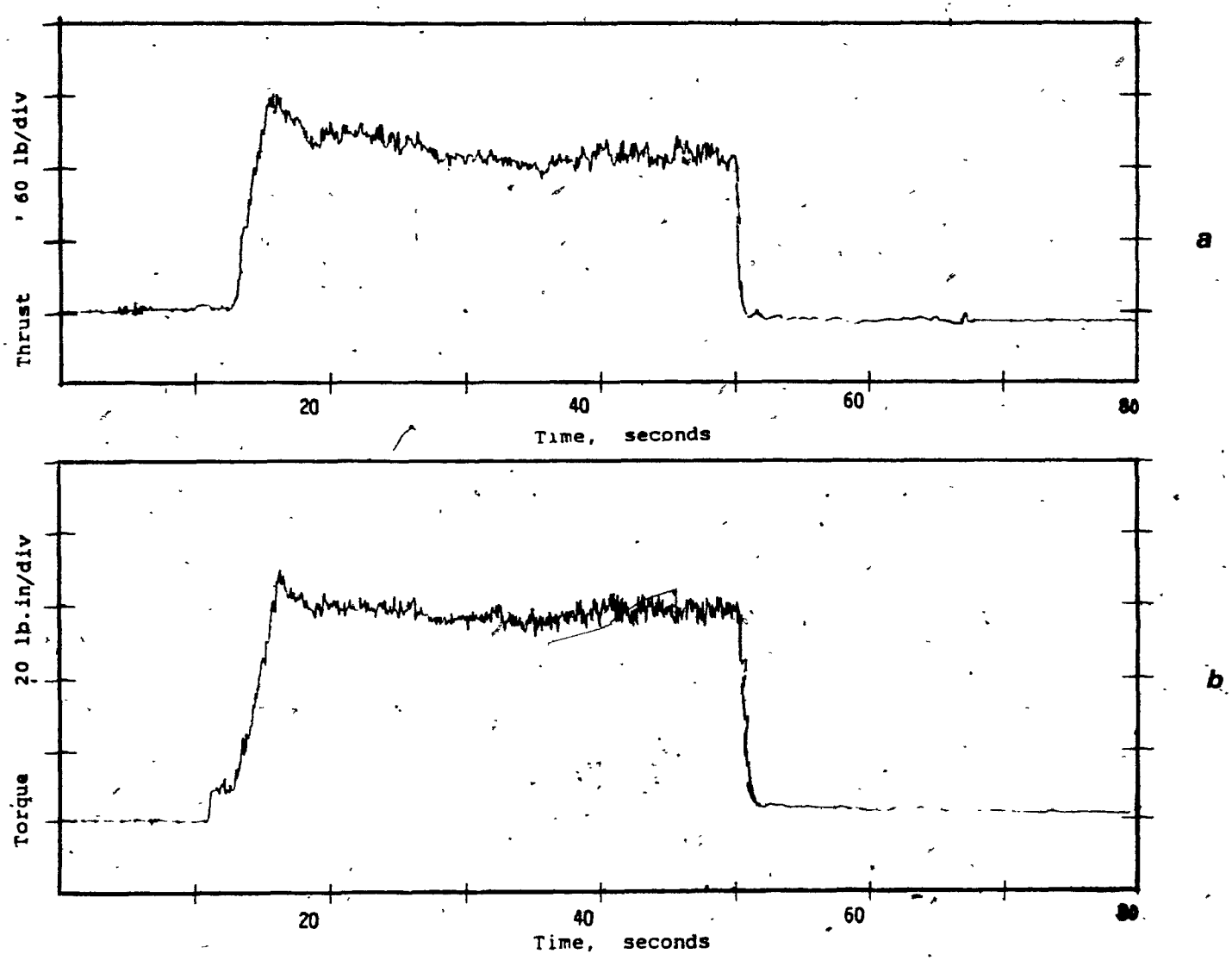

Figure 6.6 Typical plots of thrust (a), and torque (b) in pilot-hole drilling : Experiment H5-S.

initially. However, the reduced restraint is ineffective in totally preventing the induced strains. So the drill begins to expand axially and wind torsionally. When the drill 'relaxes' in such a way, the induced force reactions reduce correspondingly. This process occurs gradually due to the metal-cutting (plastic deformation) process acting similar to a viscous damper in mechanical motion. As a result, a gradual 'decay' phenomenon is produced on the measured force signals.

The decay phenomenon continues until all of the induced strains are exhausted, at which time the measured torque and thrust values reach certain minima. The force values remain stable for a short time as seen in the above figures. Thenceforth, the force records show (in most experiments) an increasing trend similar to those in full-hole drilling. The latter effect is again because of the chip-clogging effect explained earlier.

The above explanation of the decay phenomenon implies that the initial values of torque and thrust in pilot hole drilling are aggregates of the true cutting forces and the corresponding induced force components. The minimum values attained by the forces at the end of the decay process, may be considered as the true cutting components of the forces. Therefore the amounts of decay measured correspond to the induced force components.

6.7 Torque-Thrust Decay Magnitudes

The initial values of forces, and the amounts of decay for all pilot hole drilling experiments are tabulated in table 6.4. As said above, the final values (minima) of the forces are regarded as the true cutting forces, and the decay values (equal to the induced forces) are expressed as percentages of these true forces.

The magnitudes of torque decay at about 13 percent (8 percent for 3/8" drills), are seen to be highly consistent amongst the various experiments. Whereas, the thrust decay values vary widely, ranging between 12 and 50 percent of the true cutting thrust force. These variations (or lack of them) may be entirely attributed to the torsional and axial restraint conditions during drilling. In this regard feed appears to have an effect on the extent of decay. The high feed experiments (including 2-step feed) show significantly lower values of thrust decay than the low feed experiments. The reason for this is considered to be, that the higher static thrust values of the former, provide a higher axial restraint against the induced strains.

Since according to the above proposal, the decay phenomenon is actually the release of the induced forces, it implies that their magnitudes may be estimated employing the force separation principle developed in chapter 3.

Table 6.4 Observed values of torque and thrust decay.

EXPT CODE	T_i lb-in	T_f lb-in	F_i lbs	F_f lbs	TORQUE DECAY $\%T_f$	THRUST DECAY $\%F_f$
H4-S	78	69.5	222	188	12.2	18.0
H5-S	56	49	164	122	14.3	34.5
H6-S	89	78	--	--	14.1	NIL
H7-S	72	64	155	138	12.5	12.3
H8-S	50	44	109	72	13.6	51.0
H9-S	74	67	170	146	10.4	16.0
T4-S	25	23	57	44	8.7	29.5
T5-S	32	29.8	--	--	7.0	NIL
T6-S	34	31.3	--	--	8.6	NIL

'T_i', 'F_i' = Initial values of torque and thrust

'T_f', 'F_f' = Final values of torque and thrust

6.8 Prediction of Torque-Thrust Decay Magnitudes

The following aspects are to be noted before the analysis of chapter 3 may be applied to the task of predicting the torque and thrust decay magnitudes :

i) Since the torsional and axial restraint conditions in pilot hole drilling are deemed to be insufficient in preventing the induced strains, it also implies that a portion of the induced strains may occur immediately as drilling commences. That is, the drill may instantaneously expand and wind, causing a 'leakage' of the induced forces. This means that the initial values of thrust measured comprise of only a portion of the possible amount of induced thrust corresponding to the cutting torque. The same is true of the initial value of measured torque. As such it would be erroneous to use these values to predict the induced forces employing the separation equations.

ii) By definition, the coefficients K_1 and K_2 relate the applied and induced forces. Therefore a change in the torsional and axial restraint conditions as described above, would automatically affect the values of these coefficients. That is, the numerical values obtained for the coefficients under the perfect restraint conditions of the static tests, cannot be used in the present case for predicting the torque-thrust decay.

In view of the above factors, the only means of predicting the induced forces (decay) is by using the direct-force coupling equations (3.7 and 3.8) of chapter 3. That is,

$$F_i = K_1 T_c \tag{6.4}$$

$$T_i = K_2 F_c \tag{6.5}$$

where the true cutting forces T_c and F_c are those measured from the pilot hole experiments.

The coefficients K_1 and K_2 are re-computed for the pilot hole drilling case, using one reliable set of experimental measurements. Specifically, the force measurements of experiment H5-S (table 6.3) is used for 1/2-inch drills, which yields,

$$K_1 = F_i/T_{cut} = 42 \text{ lb}/49 \text{ lb.in} = 0.8571 \text{ inch}^{-1}$$

$$K_2 = T_i/F_{cut} = 7 \text{ lb.in}/122 \text{ lb} = 0.0574 \text{ inch}$$

For 3/8-inch drills the measurements of experiment T4-S are used, which gives,

$$K_1 = 0.565 \text{ inch}^{-1}$$

$$K_2 = 0.455 \text{ inch}$$

Using these values of coefficients together with the cutting torque and thrust values, the induced torque and thrust forces are computed and tabulated below. In experiments where no thrust decay was observed

(H6-S, T5-S and T6-S), it is assumed that the initial thrust forces recorded are the 'measured' values, F_m. Therefore, F_{cut} is computed by subtracting F_i ($= K_1.T_{cut}$) from this F_m. Then the thrust error percentages are calculated.

From the values of table 6.5, it is observed that the predicted induced forces (decay) are highly consistent amongst themselves, especially that of torque. The average torque decay predicted for 1/2-inch drills (12.4 percent) agrees very well with the experimentally observed average (12.6 percent). Close predictions are also obtained for the torque decay values of 3/8-inch drills.

Accuracy in thrust decay prediction is obtained in low feed experiments (H8-S). In the case of high feed experiments, the experimentally observed decay values (table 6.4) are substantially lower than the corresponding predictions. The experimental conditions as explained earlier, are considered to be the reasons for these discrepancies. That is, firstly, due to partial expansion of the drill, the measured initial thrust consists of a lower amount of induced thrust. Secondly, the higher static thrust in these experiments permits only a small amount of axial expansion. The above two factors cause a lower thrust decay to be apparent in the experiments.

Table 6.5 Predicted values of torque and thrust decay (Induced force magnitudes).

EXPT CODE	T_{cut} lb-in	T_{ind} lb-in	F_{cut} lb	F_{ind} lb	T_{er} %	F_{er} %
H4-S	69.5	10.8	188	59.6	15.5	32.0
H6-S	78	9.4	163.2	66.8	12.0	41.0
H7-S	64	7.9	138	54.9	12.4	40.0
H8-S	44	4.1	72	37.7	9.5	52.0
H9-S	67	8.4	146	57.4	12.5	39.0
T5-S	29.8	2.8	61.2	16.8	9.3	27.5
T6-S	31.3	3.1	68.3	17.7	9.8	26.0

$T_{er} = T_{ind}/T_{cut}$ = Torque error

$F_{er} = F_{ind}/F_{cut}$ = Thrust error

6.9 Validity of the Force-Inducement Hypothesis

From the experimental results of the pilot hole drilling tests, it is clear that the torque and thrust decay phenomena are highly consistent. Definite correlation is observed between the decay magnitude of one force and the final minimum value of the other force. Thus the coupling effect is seen as the most plausible explanation of the decay phenomenon, as presented in section 6.6. Further, the analysis of the preceding section establishes that the torque and thrust decay magnitudes are accurately predictable using the concepts and results of chapter 3. Where discrepancies are seen between the predicted and observed decay values, credible reasoning is presented for the same.

The accuracy and consistency of the predictions is considered as proof for the validity of the reasoning proposed for the decay phenomenon. More significantly, the results above are proof that indeed, substantial torque and thrust forces are induced during drilling. To reiterate the analysis of section 6.3, these coupling-induced forces form a significant portion of the measured values in full-hole drilling.

6.10 Dynamic Signal Analysis

The fluctuating components of the forces are captured by setting a short time constant at the charge amplifier, which automatically suppresses the steady (or 'DC') portions of the signals. The following is a general

description of the statistical characteristics of the dynamic torque and thrust signals. Further analysis of these as well as the radial force signals is presented later, in the context of the various objectives of this investigation.

6,10.1 Probability Density Functions of Torque and Thrust

As mentioned earlier, it has been shown by a previous researcher [5] that the dynamic components of torque and thrust in drilling are stationary, Gaussian random processes. Therefore, the present analysis presumes the randomness of the said force signals.

Figures 6.7a and 6.7b are two samples of the probability density obtained for half-inch full-hole drilling conditions. It is seen that the plots very closely resemble the bell curve of a Gaussian distribution. The distributions of torque signal show a smooth trend throughout, whereas those of thrust show a jagged variation. This trend is typical of thrust signals, as has been observed in previous investigations. Figure 6.8 shows the PDF plot for a 3/8-inch drill, and an identical trend is seen.

Interestingly, a similar analysis of the torque and thrust signals of pilot hole drilling shows a drastically different characteristic. Figure 6.9 is a sample PDF (experiment H4T1) and it is clear that the distribution is highly non-gaussian. A similar behaviour is exhibited by all signals from pilot hole drilling.

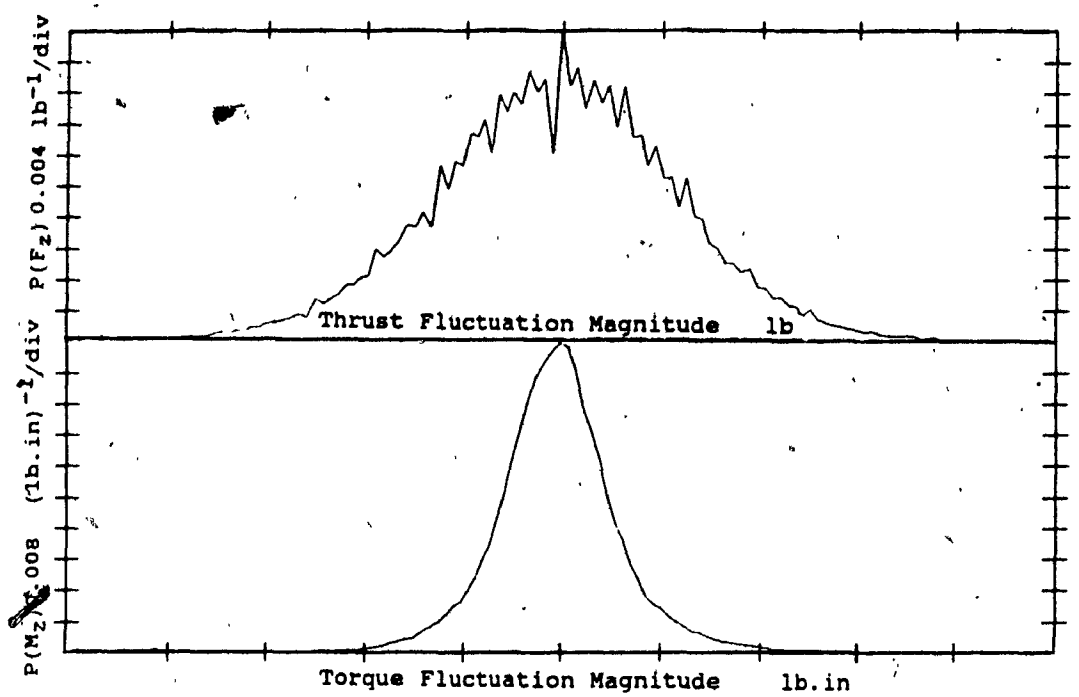

a

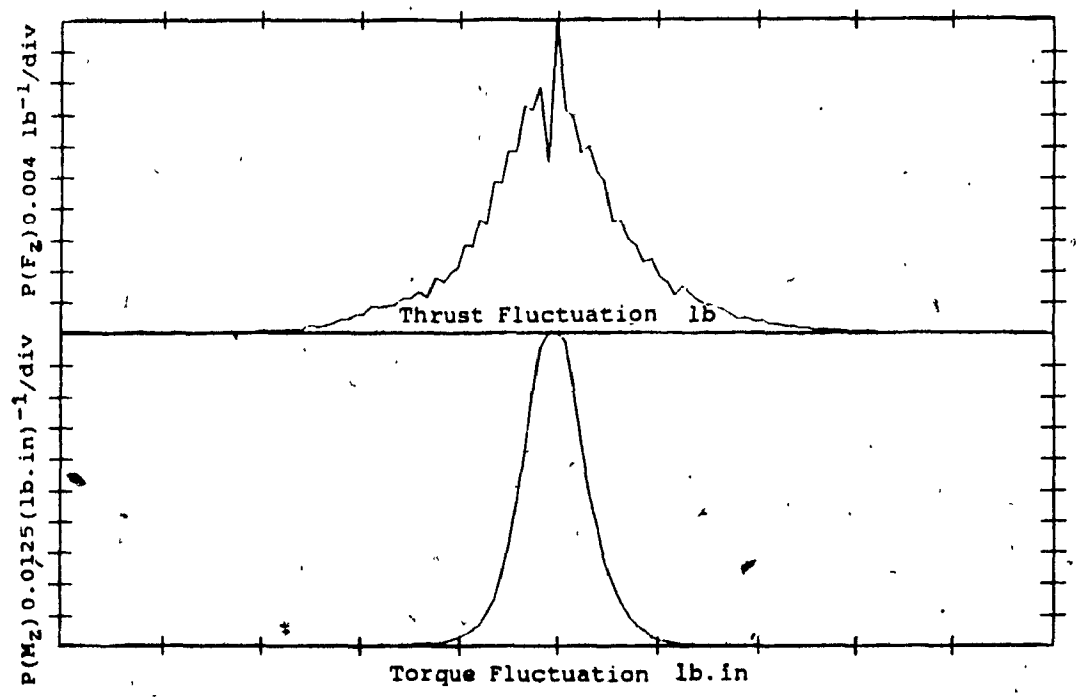

b

Figure 6.7 Probability density functions of torque and thrust : a) Experiment H1, and b) experiment H2.

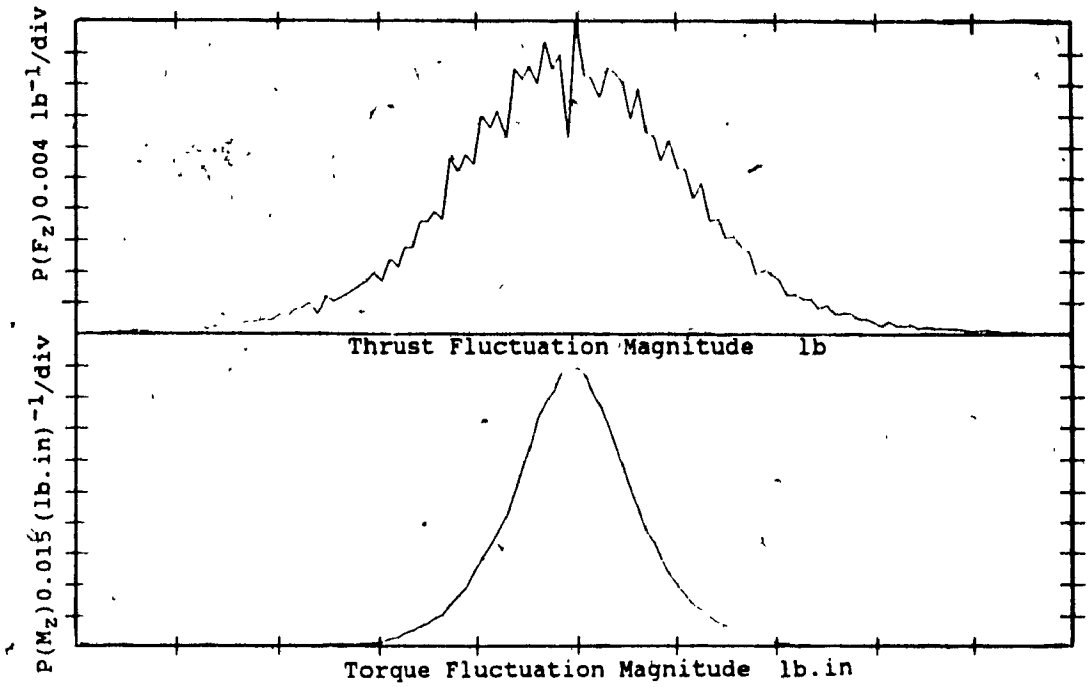

Figure 6.8 Probability density functions of torque and thrust : Experiment T1.

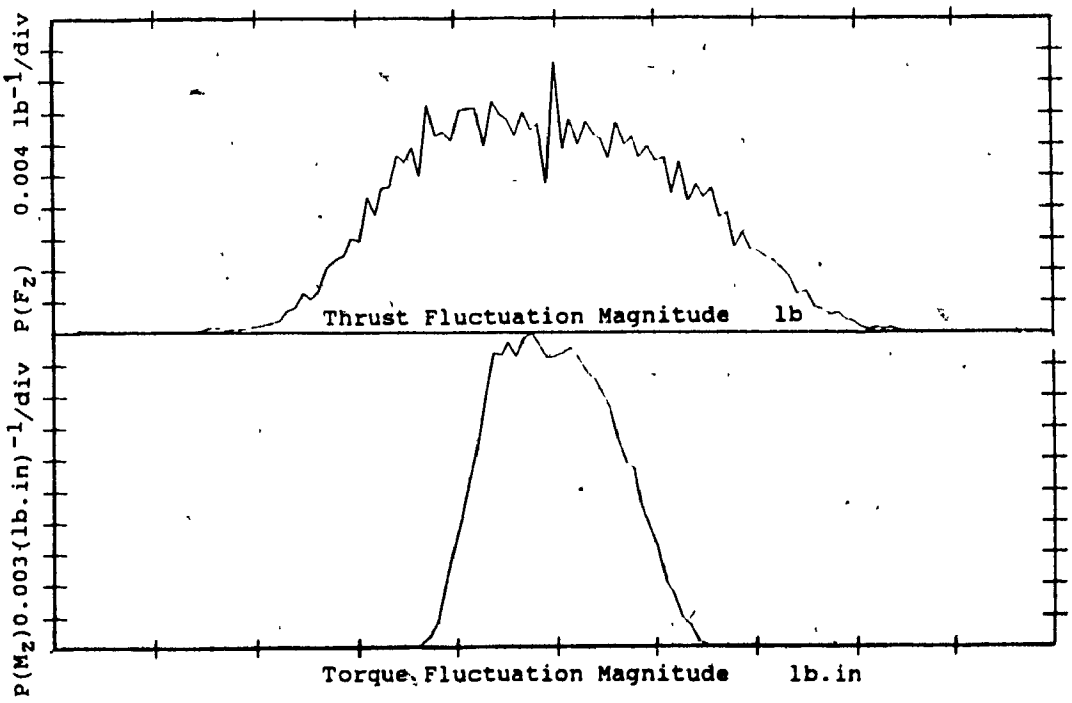

Figure 6.9 Probability density functions of torque and thrust in pilot hole drilling : Experiment H4.

Considering the torque and thrust fluctuations (in full-hole drilling) to be Gaussian processes, the density functions are integrated to obtain the probability distribution functions. The probabilities associated with the occurrence of individual values can then be determined. The standard deviations of the force fluctuations obtained this way are tabulated below (table 6.6).

For half-inch diameter drilling, there is a very slight increase in σ_f and σ_t when feed is increased. But in drilling with 3/8-inch drill, the fluctuating components increase substantially with feed. No appreciable difference is seen between the force-fluctuations of the high-feed and 2-step feed drilling.

6.10.2 Autocorrelograms of Torque and Thrust Fluctuations

An examination of the autocorrelogram gives further insight into the randomness of a signal. Figure 6.10 is the typical autocorrelation function of the torque and thrust fluctuations. A double decaying-exponential envelope on the functions can be clearly discerned. A comparison with standard autocorrelograms (figure 6.11) leads to the conclusion that the torque and thrust fluctuations are narrow-band random processes. As mentioned earlier, the value of the correlation function at $\tau=0$ corresponds to the mean square value of the signal.

Table 6.6 Standard deviation values of torque and thrust.

EXPERIMENT CODE	THRUST FLUCTUATIONS Standard deviation σ_f, lbs	TORQUE FLUCTUATIONS Standard deviation σ_t, lb-in
H1	10.2	3.5
H2	9.4	2.8
H3	10.0	3.7
T1	12.5	3.3
T2	20.0	6.7
T3	20.0	6.3

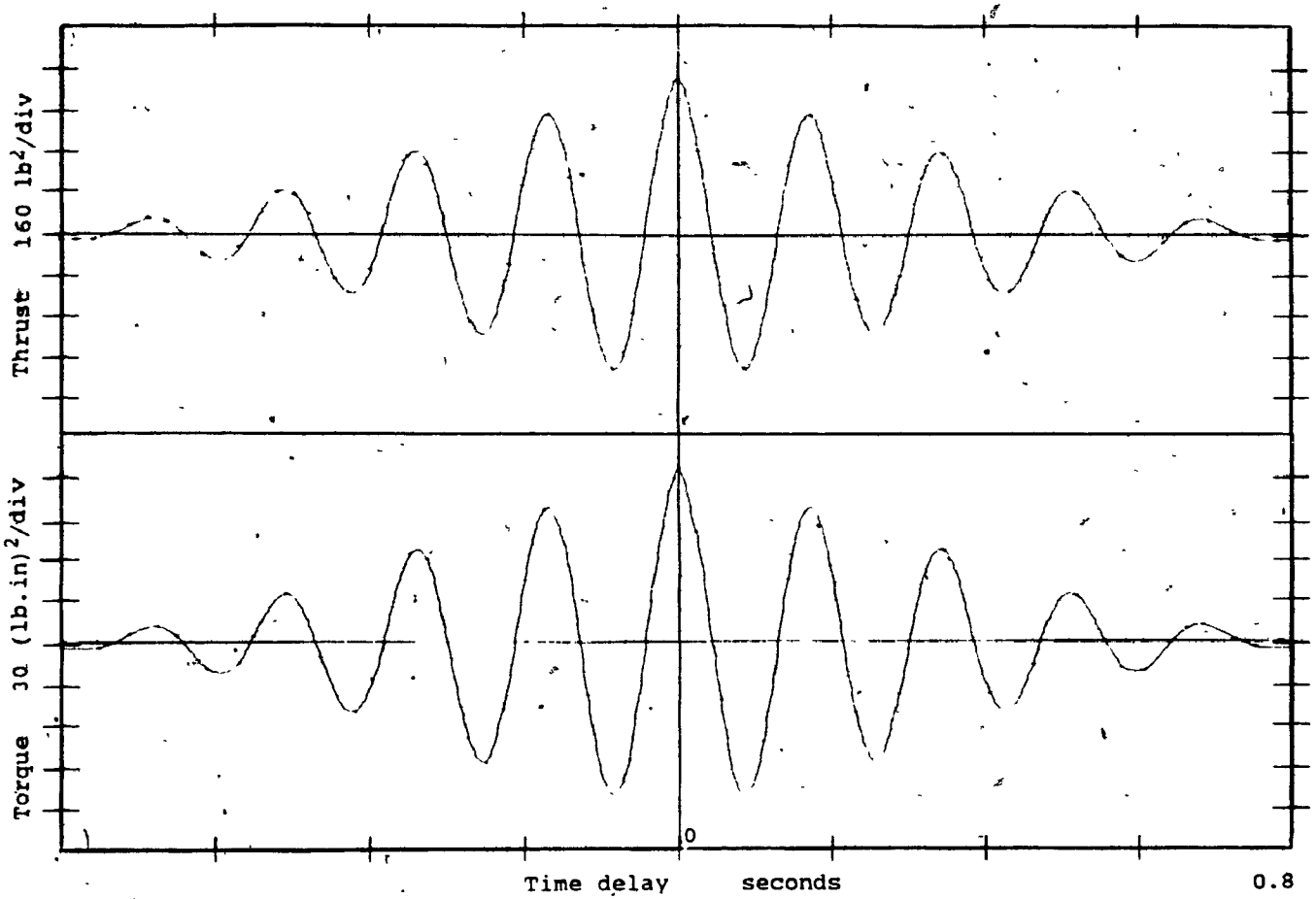

Figure 6.10 Autocorrellogram of torque and thrust : Expt. H4.

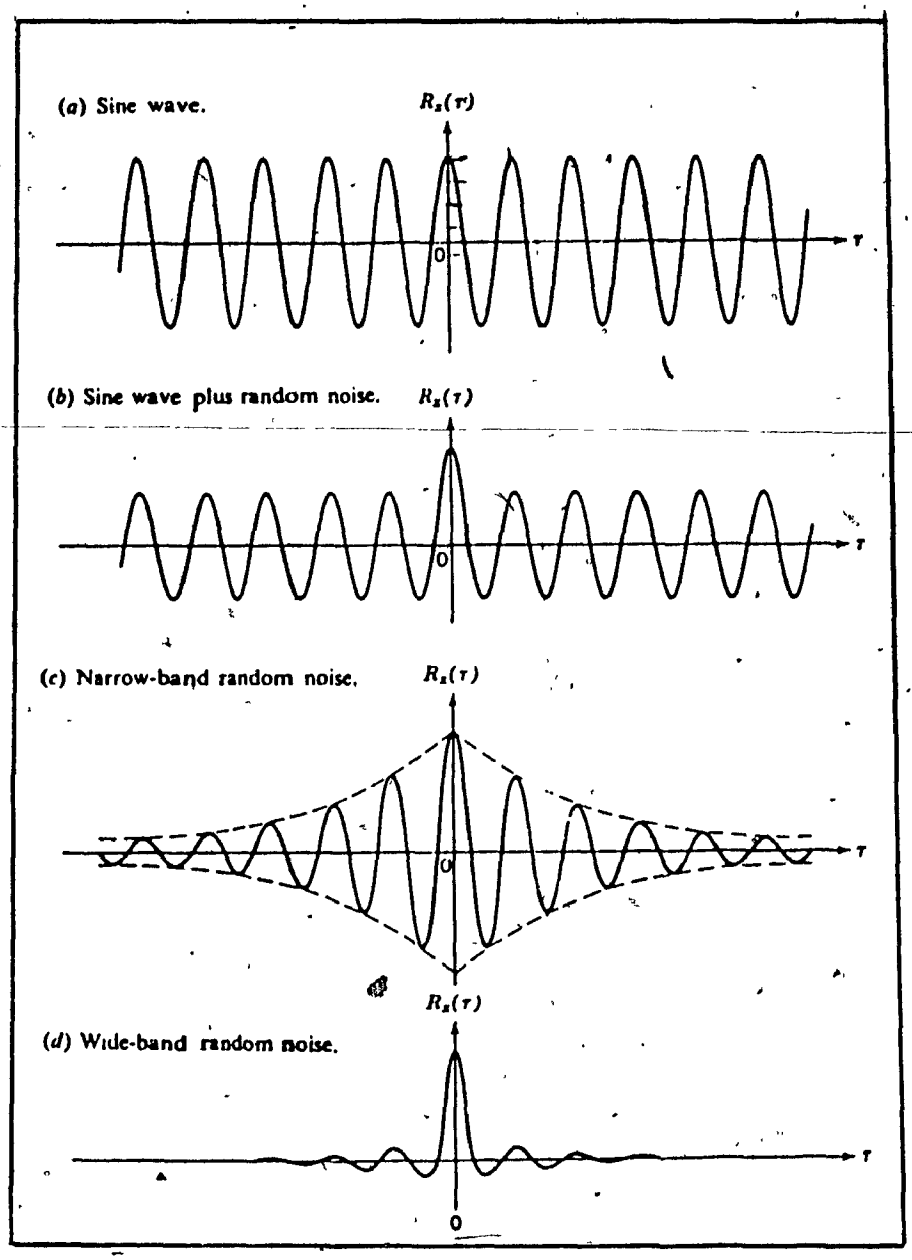

Figure 6.11 Typical autocorrelation plots. [16]

6.11 Results of Pilot Hole Drilling Tests

Further analysis of the measured signals is performed so as to bring out the effect of pilot holes on drilling forces, and in doing so, evaluate the validity of the pilot hole sizing criterion presented in chapter 4.

The Root Mean Square (RMS) spectrum is the distribution of the RMS values of the signals in the frequency domain. Individual values at particular dominant frequencies in the spectra are directly indicative of the magnitudes of the dominant components in the force signals. Therefore, the RMS spectra of the torque, thrust and radial forces are computed, and the magnitudes of the dominant peaks in them are used as the yardstick of their comparison.

6.11.1 RMS Values of Torque and Thrust Fluctuations

Figures 6.12 and 6.13 are typical RMS spectral plots of torque and thrust forces in 1/2-inch drilling. As shown, the spectra consist of a clearly dominant peak at a frequency of 12 Hz, relative to which, the remainder of the spectra is of negligible magnitude. The spectra of all the signals were seen to be very similar to these samples, differing only in the magnitude of the dominant peak.

Figures 6.14 and 6.15 present two typical spectral plots of torque and thrust in 3/8-inch drilling. As shown, a very similar characteristic with identical peaks at 12 Hz were observed. This prompted the suspicion that

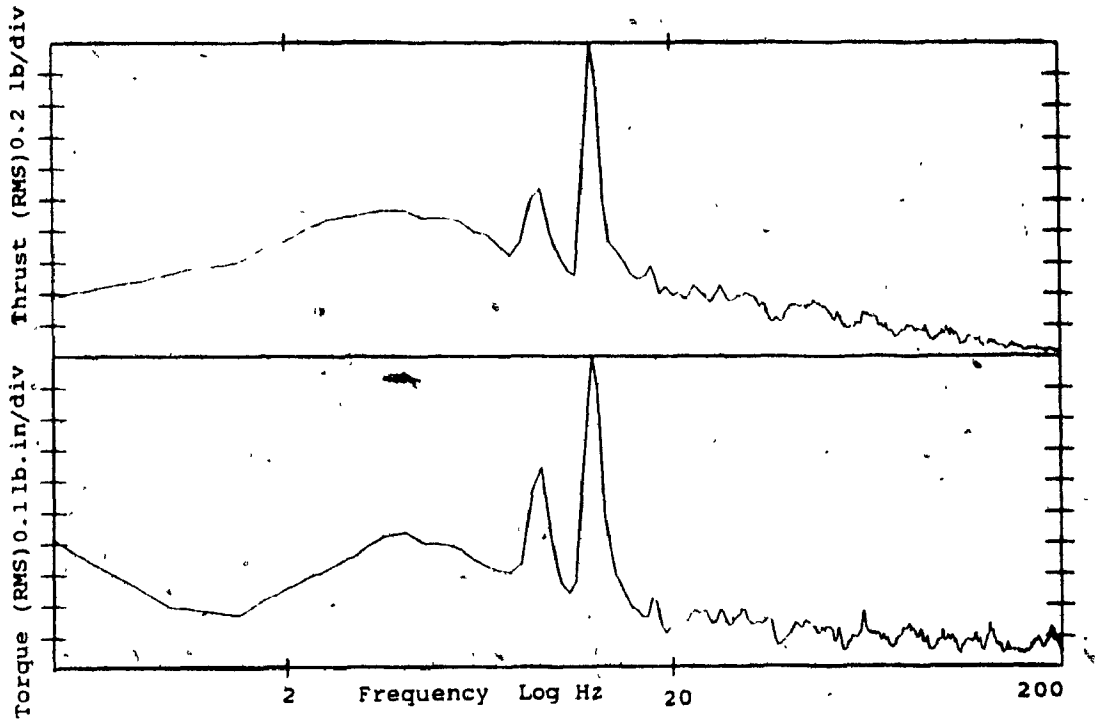

Figure 6.12 RMS spectra of torque and thrust : Expt. H7.

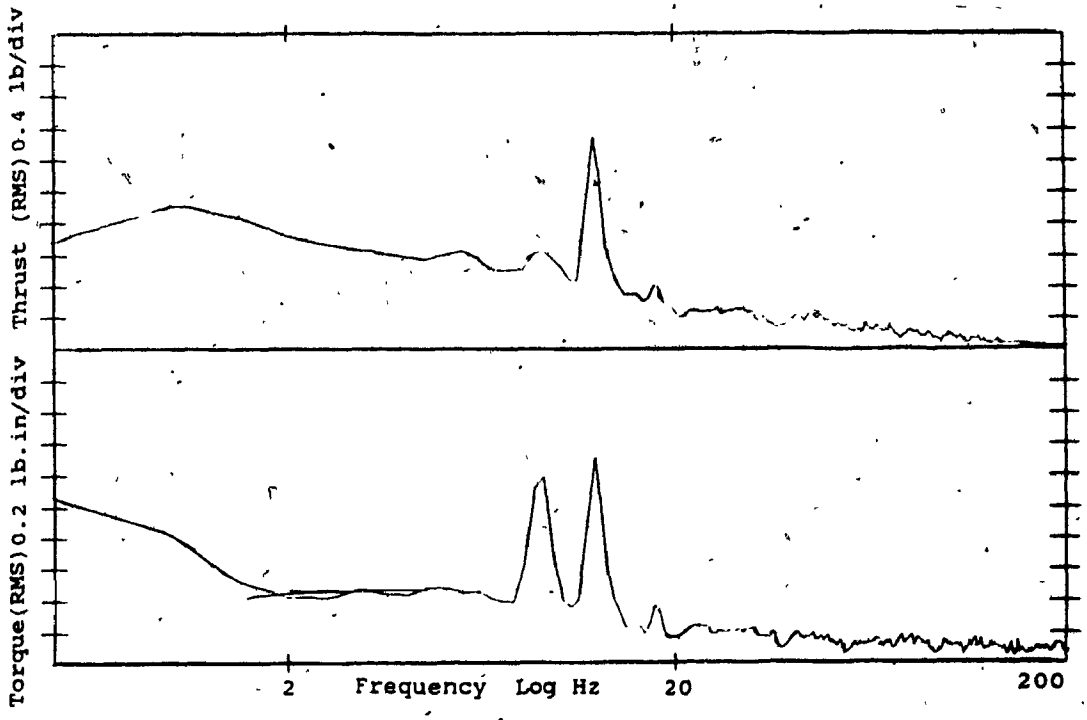

Figure 6.13 RMS spectra of torque and thrust : Expt. H9.

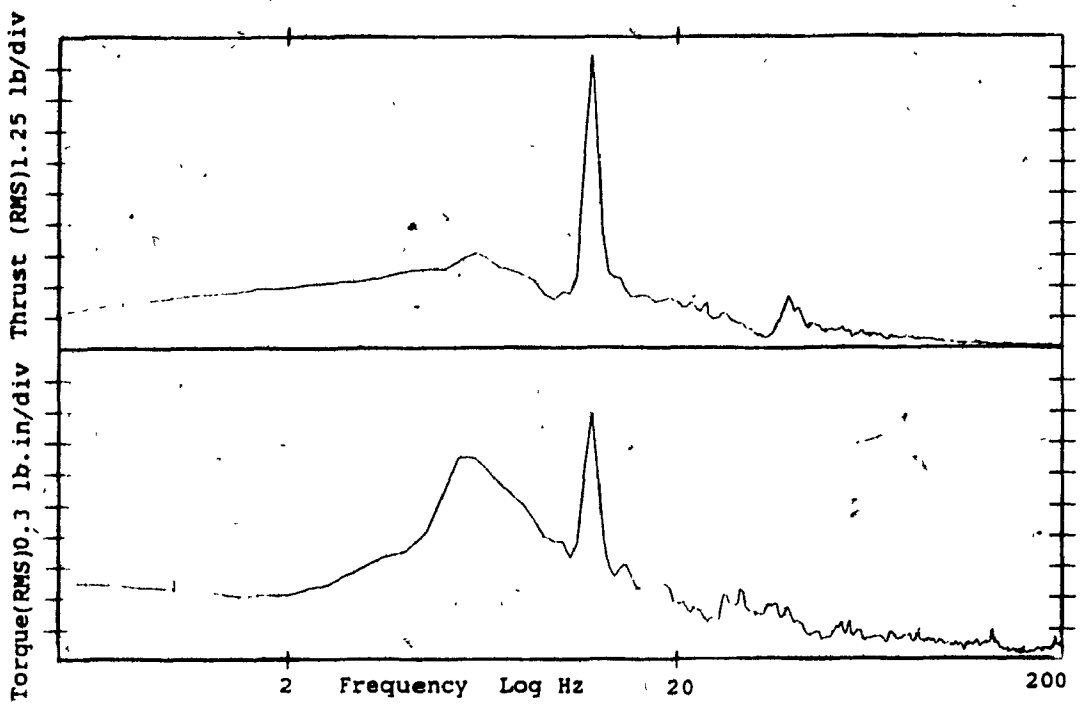

Figure 6.14 RMS spectra of torque and thrust : Expt. T2.

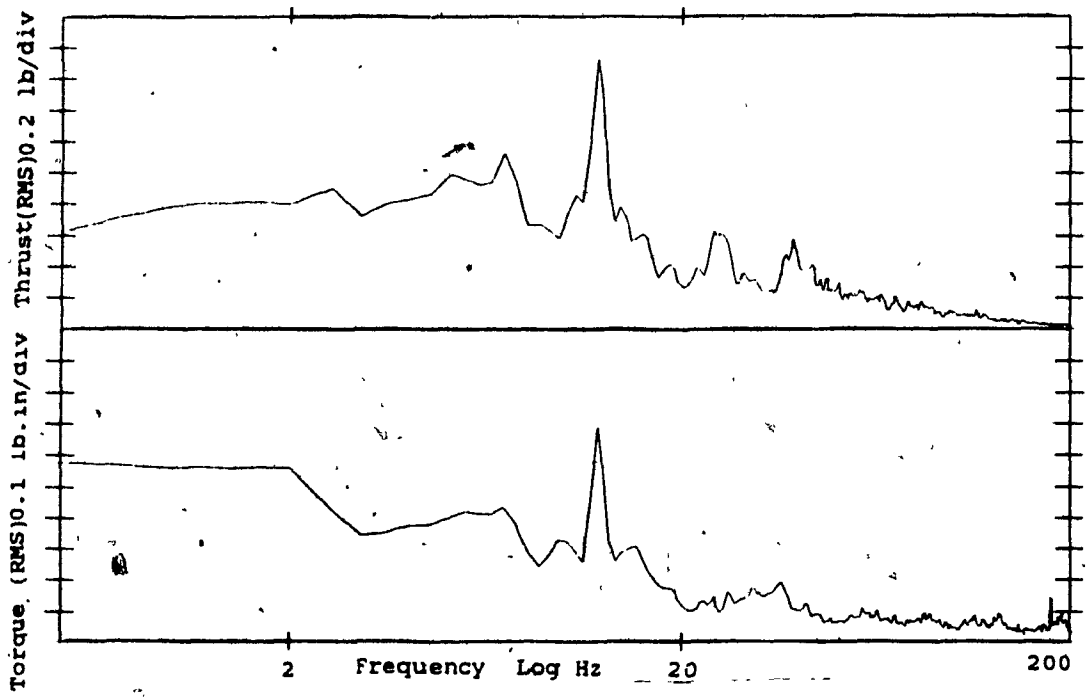

Figure 6.15 RMS spectra of torque and thrust : Expt. T5.

the peak at 12 Hz may be due to the radial drilling machine.

Therefore, a free-vibration test was performed to study the lateral (axial direction of the drill) vibrations of the machine arm. Figure 6.16 is a plot of the vibration amplitude against frequency, and it is clear that the arm vibration has a dominant natural frequency at exactly 12 Hz. Therefore, it is concluded that the peaks at 12 Hz in the torque and thrust spectra are due to the machine vibration.

The magnitudes of the peaks at 12 Hz can yet be considered as being indicative of the stability of the cutting process. Therefore these magnitudes are used to study the effect of pilot holes on the torque and thrust forces.

Table 6.7 lists the torque and thrust fluctuation magnitudes of all experiments. The results are grouped according to the feed value, and the following observations are notable :

Half-inch, low feed experiments ; Drilling with a pilot hole of diameter ϕ_1 ('wrong size'), causes the RMS value of thrust fluctuations to double as compared to the corresponding experiment without a pilot hole. The torque fluctuations increase by a factor of 4. Interestingly, for the same experiment with a pilot hole of diameter ϕ_2 (the 'right size'), the RMS values of torque and thrust are significantly lower than those of full-hole drilling.

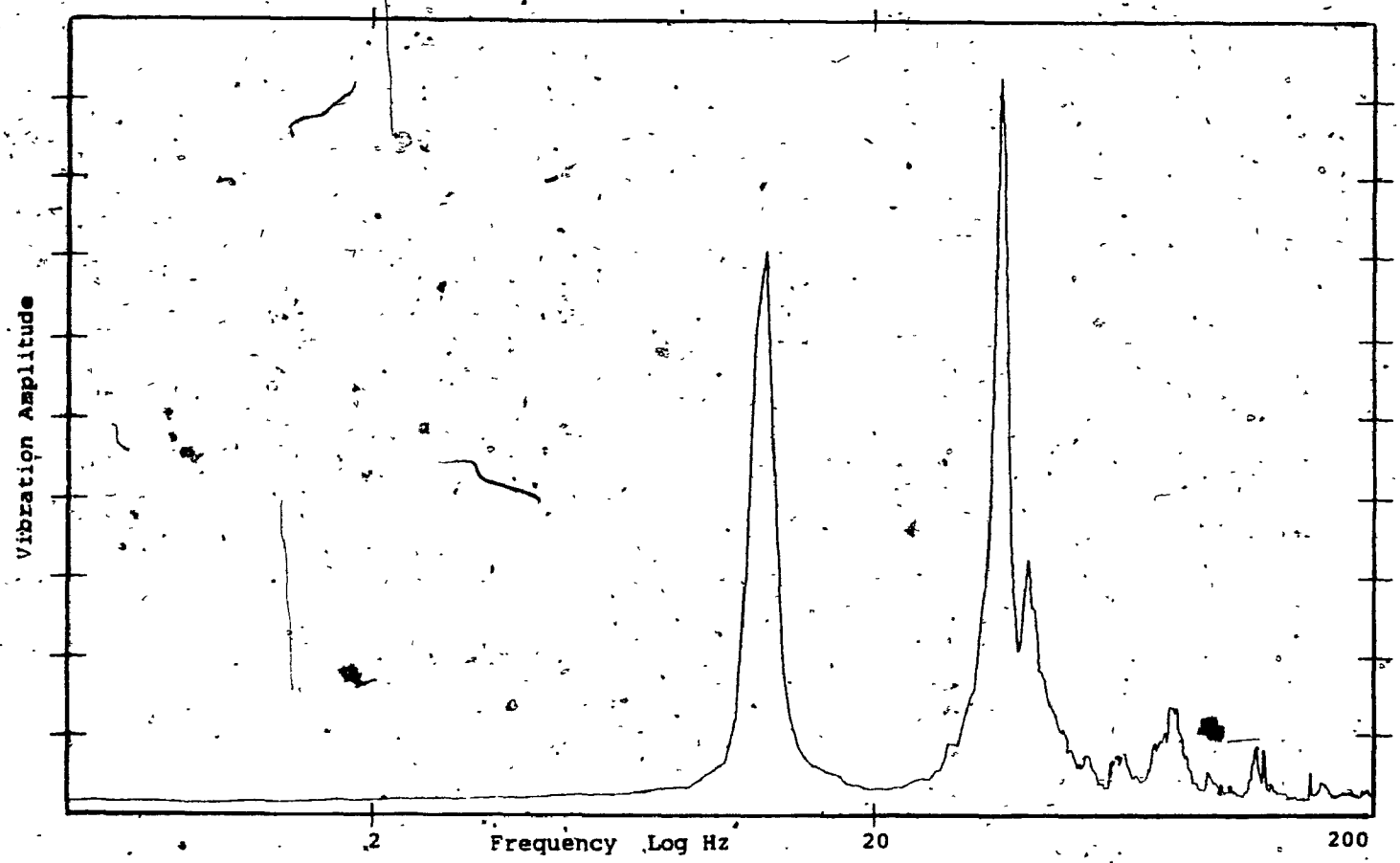

Figure 6.16 Free-vibration response of drill arm.

Table 6.7 RMS values of torque and thrust in the frequency domain.

EXPT. CODE	RMS VALUES OF FLUCTUATIONS AT 12 Hz	
	THRUST	TORQUE
High feed		
H1, $\phi_{ph} = 0$	5.0	2.0
H4, $\phi_{ph} = \phi_1$	26.0	11.0
H7, $\phi_{ph} = \phi_2$	4.0	2.0
Low feed		
H2, $\phi_{ph} = 0$	5.0	1.0
H5, $\phi_{ph} = \phi_1$	11.0	4.0
H8, $\phi_{ph} = \phi_2$	1.0	Negligible
2-step		
H3, $\phi_{ph} = 0$	7.0	3.0
H6, $\phi_{ph} = \phi_1$	25.0	10.0
H9, $\phi_{ph} = \phi_2$	4.0	2.0
T1, $\phi_{ph} = 0$	6.5	1.0
T4, $\phi_{ph} = \phi_1$	2.0	1.0
T2, $\phi_{ph} = 0$	12.0	2.6
T5, $\phi_{ph} = \phi_1$	2.0	0.8
T3, $\phi_{ph} = 0$	10.0	2.5
T6, $\phi_{ph} = \phi_1$	2.0	1.0

Half-inch, high feed and 2-step feed experiments; The above effect of pilot hole size is again observed, on a more drastic scale. Drilling with the 'wrong size' pilot hole causes the thrust fluctuations to increase five-fold. Correspondingly, the torque fluctuations increase by three to five times the values of the full-hole drilling case. Again, drilling with the 'right size' pilot hole results in significantly lower fluctuations.

3/8-inch experiments ; For all values of feed, trends similar to that of 1/2-inch drilling are observed. The RMS values of thrust fluctuations are drastically reduced when drilling with the 'right size' pilot hole, as compared to full-hole drilling. Those of torque reduce slightly or remain the same.

6.11.2 RMS Values of Radial Forces

The radial force in drilling is a single resultant force vector fixed in magnitude (nominal) and in its radial direction with respect to the cutting edges. However, since it rotates with the drill, the radial force axes of the dynamometer 'see' the force as a sinusoidally varying signal of frequency equal to the angular velocity of the drill. Therefore, in the present experiments, the frequency of radial forces in 1/2-inch drilling is 9 Hz (540 RPM) and that in 3/8-inch drilling is 12 Hz (720 RPM).

The RMS values of radial forces of all experiments are tabulated

Table 6.8 RMS values of radial forces in the frequency domain.

EXPT. CODE	RMS value of radial forces lbs
High feed	
H1, $\phi_{ph} = 0$	1.8 at 9.0 Hz
H4, $\phi_{ph} = \phi_1$	2.3 at 9.0 Hz
H7, $\phi_{ph} = \phi_2$	1.8 at 9.0 Hz
Low feed	
H2, $\phi_{ph} = 0$	4.0 at 9.0 Hz
H5, $\phi_{ph} = \phi_1$	2.8 at 9.0 Hz
H8, $\phi_{ph} = \phi_2$	1.8 at 9.0 Hz
2-step	
H3, $\phi_{ph} = 0$	1.0 at 9.0 Hz
H6, $\phi_{ph} = \phi_1$	3.3 at 9.0 Hz
H9, $\phi_{ph} = \phi_2$	2.3 at 9.0 Hz
T1, $\phi_{ph} = 0$	1.2 at 12.0 Hz
T4, $\phi_{ph} = \phi_1$	1.0 at 12.0 Hz
T2, $\phi_{ph} = 0$	2.5 at 12.0 Hz
T5, $\phi_{ph} = \phi_1$	1.0 at 12.0 Hz
T3, $\phi_{ph} = 0$	2.5 at 12.0 Hz
T6, $\phi_{ph} = \phi_1$	1.0 at 12.0 Hz

below in table 6.8. In general, drilling (1/2-inch) with the 'wrong size' pilot hole results in increased radial forces as compared to full-hole drilling. The same experiment repeated with 'right sized' pilot hole results in radial forces which are less than, or in the worst case, equal in magnitude to those of full-hole drilling.

6.11.3 Implications on Hole Quality

It is seen from the results discussed above, that the size of the pilot hole has a clear effect on the stability of the drilling process. When drilling with the 'right size' pilot hole, a drastic reduction is observed in the magnitudes of the fluctuating components of torque, thrust and the radial forces, compared to the same experiment with the 'wrong size' pilot hole. As shown by Kahng and Ham [20] such a reduction in force fluctuations (especially that of radial forces) and improved stability, implies that the quality of the machined hole, may be correspondingly better in terms of macro-geometrical errors. Since the radial forces have a direct effect on the hole-roundness, the changes in hole quality are evaluated based on the measurements of roundness error of the holes.

6.11.4 Roundness Error Measurements

The roundness error (RE) measurements on the radial profile of the machined hole are obtained using a Talyrond instrument (figure 6.17). The instrument essentially consists of a sensitive stylus probe mounted on

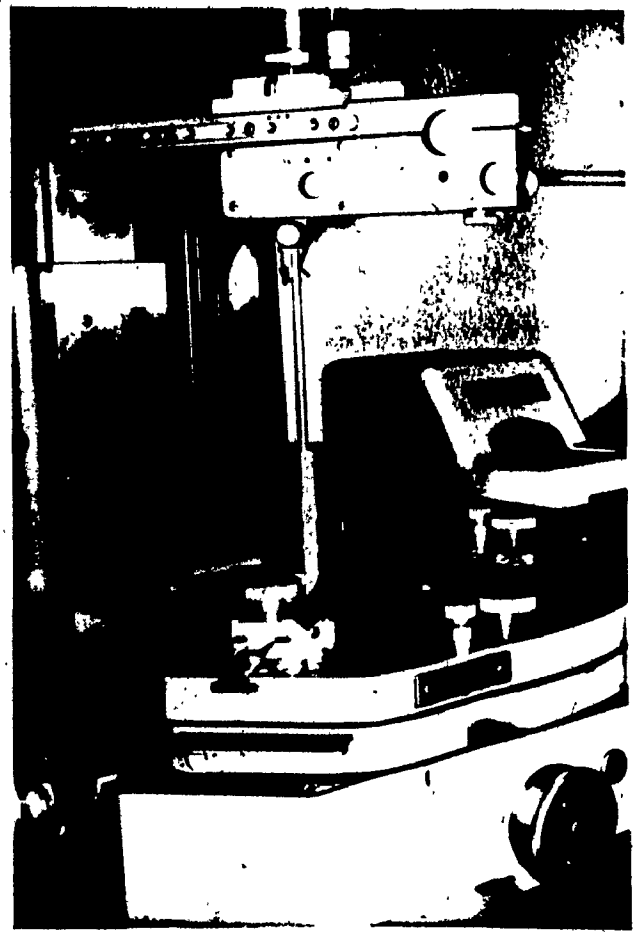

Figure 6.17 Set-up for roundness error measurement.

a rotating spindle. When the machined hole is properly centered with respect to this spindle, the stylus senses the deviations in the profile, about a 'mean' circle. The fluctuation signals are electrically amplified and hard copy traces are obtained. The measurements are carried out at three depths (starting from the hole mouth) of each workpiece, and the results are discussed below.

Figure 6.18 and part of figure 6.19 present the typical RE graphs for the set of 1/2-inch drilling experiments conducted at high feed (H1, H4 and H7). The following observations can be made regarding these graphs:

i) Comparing the profiles at the hole mouth, drilling without a pilot hole results in a generally round hole with a small amount of RE (H1T1, top). The same experiment repeated with the pilot hole of the 'wrong size', results in a badly distorted, multi-cornered hole with a large RE (H4T2, top). However, choosing the 'right size' pilot hole results in a final hole of drastically improved quality (H7-S, top).

ii) A comparison of the RE measurements at an intermediate depth reveals that the size of the pilot hole nor their absence causes any difference in the quality (RE) of the hole profile.

iii) Measurements at a further depth begin to exhibit multi-cornered profiles again, with slightly higher roundness errors (figure 6.19).

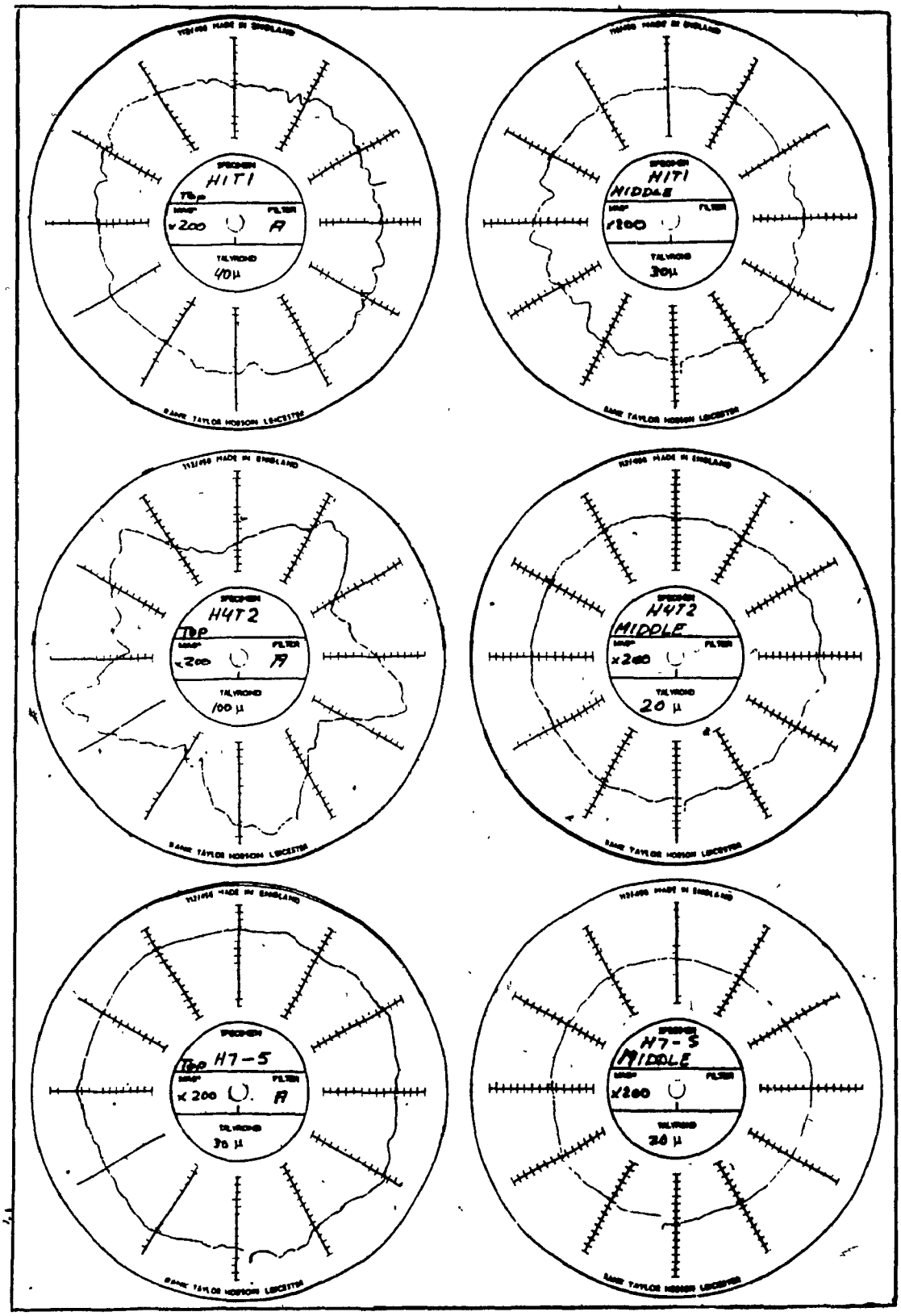

Figure 6.18 Roundness plots : Top and middle measurements.

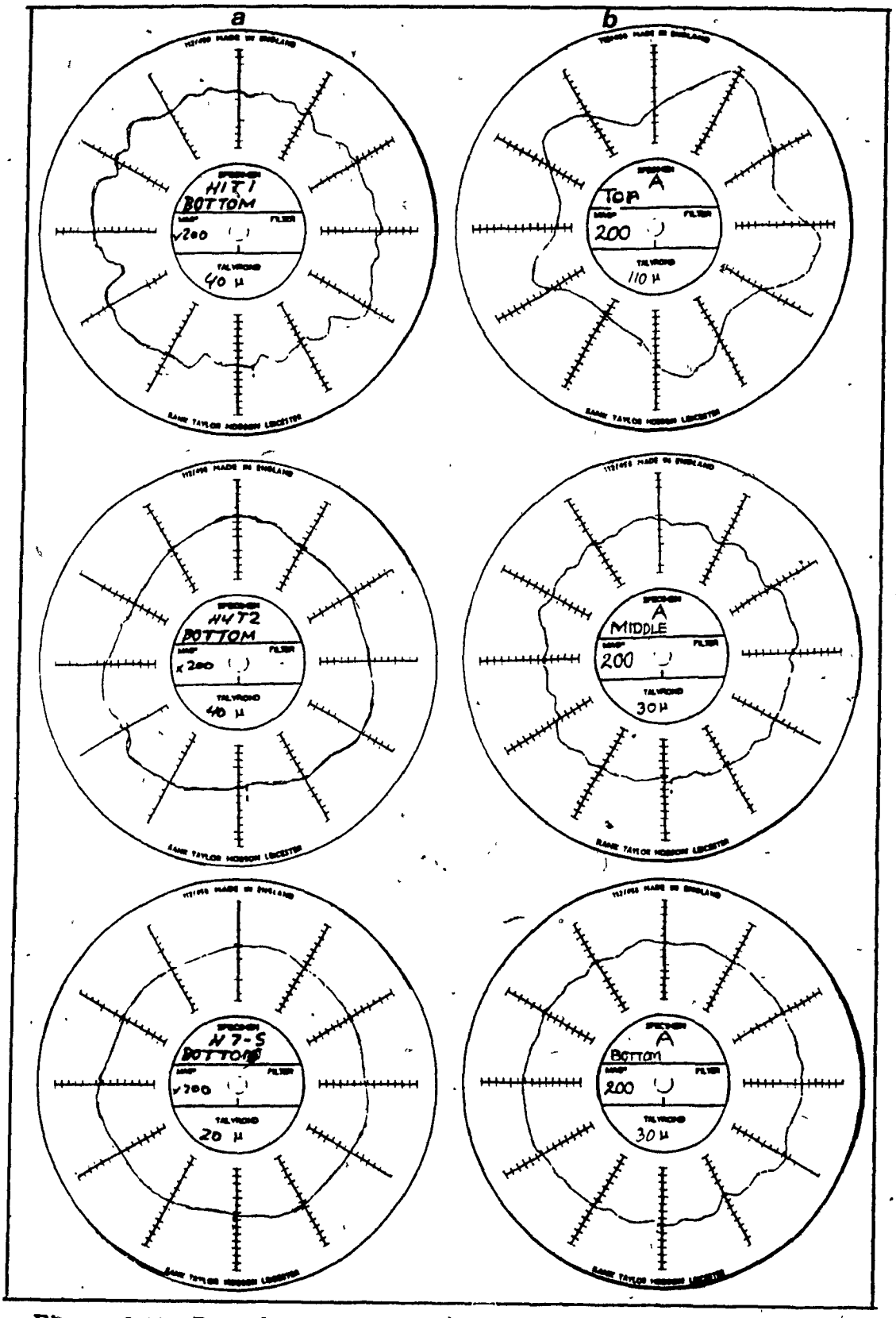

Figure 6.19 Roundness plots : a) Bottom level measurements and (b) specimens of repeat-experiments.

In order to confirm that the poor quality of holes obtained in H4-type experiments above is not an exception, a re-run was conducted. That is, the H4-type experiment was repeated, this time with a pilot hole of diameter equal to the web-thickness of the drill. The typical roundness plots obtained are shown in figure 6.19 (specimen: 'A'), and it is seen that the deterioration of the hole-quality near the hole mouth is even more pronounced in this test.

Figure 6.20 presents the typical plots of RE obtained on holes drilled with 3/8-inch drill. From the measurements, similar results are observed on the effect of pilot holes. Holes drilled with the 'right size' pilot hole exhibit quality that is equal to or better than from full-hole drilling. Table 6.9 lists the RE magnitudes obtained of all the experiments. The following discusses the RE values in other experiments :

i) When holes are drilled with low feed, the size or presence of pilot holes is of no consequence to the roundness of the machined holes. As in high feed case, the hole-quality improves (slightly, in this case) as the drill penetrates deeper.

ii) In holes drilled with a 2-step feed method, interesting results are observed. Although the actual drilling was carried out at high feed, good quality of profile is obtained near the top of the hole. This is owing to the fact that the commencement of drilling at the hole mouth was done at a very low feed. Therefore, by this method the

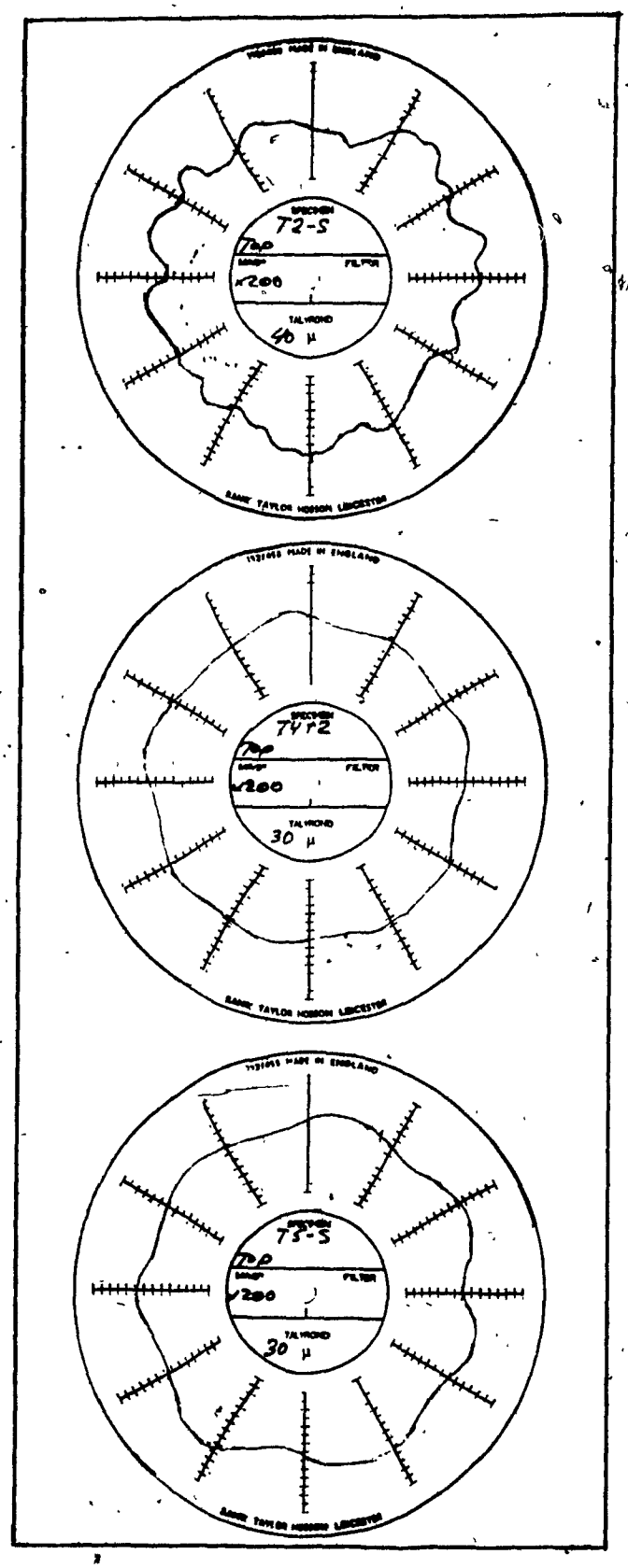

Figure 6.20 Roundness plots : 3/8-inch drilling.

Table 6.9 Roundness errors measured.

EXPT CODE	ROUNDNESS ERROR, μm		
	TOP	MIDDLE	BOTTOM
H1	40	30	30
H4	80	30	40
H7	30	30	20
H2	40	20	30
H5	40	20	20
H8	40	20	20
H3	50	30	30
H6	20	10	20
H9	30	20	20
T1	30	40	30
T4	30	20	10
T2	40	40	40
T5	40	20	20
T3	40	40	40
T6	30	20	30

final-hole quality is unaffected by the size of the pilot hole that is pre-drilled.

6.11.5 Validity of the Pilot Hole Sizing Criterion

From the analysis of the forces and the hole-quality measurements discussed above, it is clear that the pilot hole size has a significant influence on the quality of the final hole. When low feed or a 2-step feed method is used, the size of the pilot hole does not affect the quality of the final drilled hole appreciably.

However, when a medium to high value of feed is used, indiscriminate sizing of pilot holes is highly detrimental to the final hole quality. Any pilot hole smaller than the 'critical' diameter (as determined in chapter 4) results in polygonal holes with large roundness errors. Whereas, proper sizing of the same, drastically improves hole quality.

This clearly validates the pilot hole sizing criterion established in chapter 4. Therefore when drilling with pilot holes at moderate to high feed values, use of the above criterion is recommended in sizing the pilot holes.

6.12 Torque-Thrust Coupled Vibrations

In several high-feed experiments conducted with pilot holes of the 'wrong' size, the torque and thrust signals show distinct, low-frequency

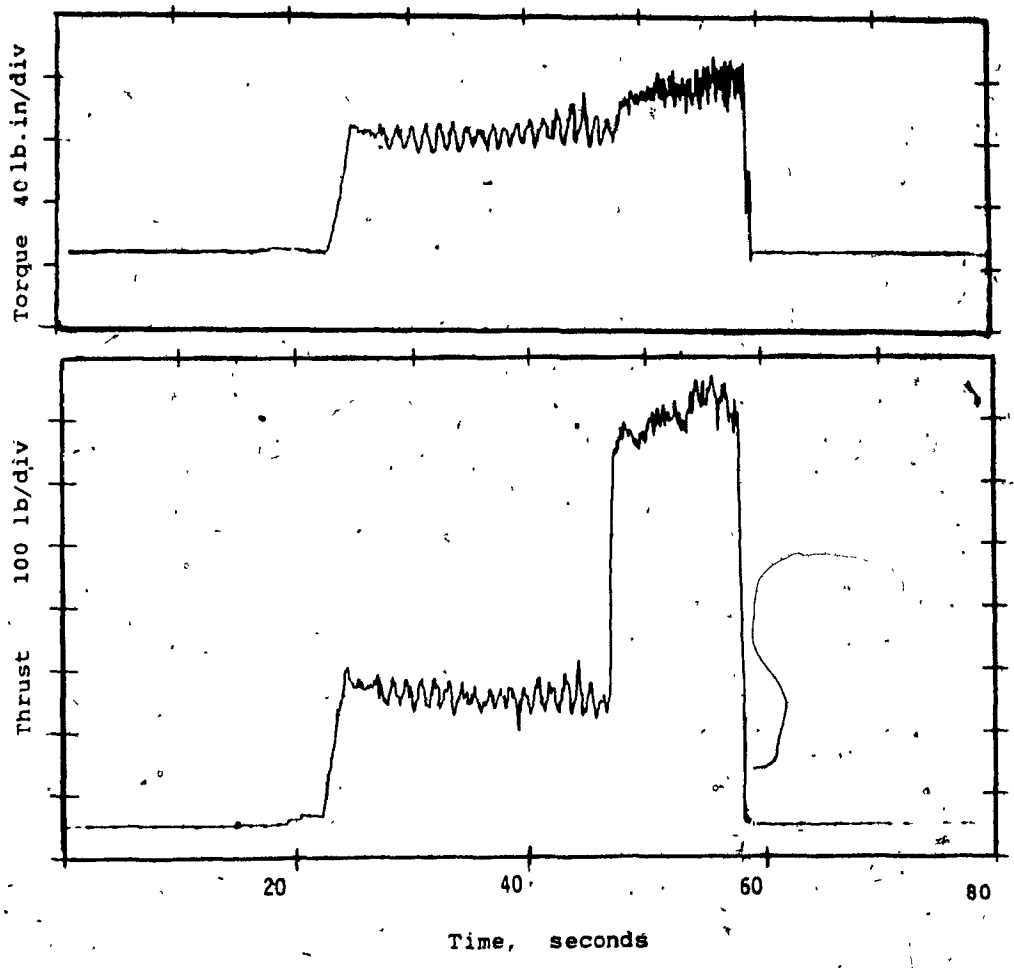

Figure 6.21 Record of torque and thrust signals : Experiment H4-S.

fluctuations. Figure 6.21 presents a typical plot of the measured signal, and it is seen that the fluctuations are of a significant magnitude (20-25 percent of static values).

Since the torque and thrust fluctuations are exactly in-phase, it is proposed that their origin is the coupled torsional-axial 'parametric' vibrations of the type discussed in section 3.8. The following is proposed as the mechanism behind this phenomenon.

When drilling commences in the presence of a pilot hole, the sharp cutting lips immediately 'dig-in' into the material causing a sudden pulse of forces, which sets up torsional vibrations. Due to the coupling effect, the drill expands and contracts correspondingly as the drill unwinds and winds in torsional vibration. This results in fluctuations in the instantaneous value of feed which again cause force pulses and sustains the vibrations.

The above mechanism explains the fact that the 'parametric' vibration phenomena occurs only in the case of pilot hole drilling. Because, in full-hole drilling disturbances in torque will not cause axial expansion of the drill due to the high axial restraint provided by the cutting forces at the web. In this way, the web acts like a 'damper' against vibrations, as concluded by Fujii, et al.[17].

6.13 Conclusions

The results of the drilling experiments are analyzed and discussed. The analysis has two main aspects namely, the static components analysis and dynamic components analysis.

The averaged values of static torque and thrust forces show that an increase of feed causes a drastic increase in their values. The feed method has the peculiar effect during full hole drilling in that, the average torque and thrust values in the case two-step feed are about 10 percent higher than in the experiment at high feed. Comparing the force measurements, it is shown that approximately 80 percent of thrust and 45 percent of torque are generated by the web and the negative rake angle region of the cutting lips.

The separation equations derived in chapter 3 are used to isolate the true cutting torque and thrust forces from the measured values and thus the measurement errors are estimated for the full-hole drilling tests. For half-inch diameter drilling, the induced thrust or 'thrust error' constitutes approximately 22 percent of the measured value and the 'torque error' forms about 15 percent. With a 3/8-inch drill the thrust error increases to 32 percent and the torque error decreases to 8 percent. A comparison based on these true cutting forces show identical effects of the change in feed and feed-method, as when compared on the basis of the measured values.

When force signals in full-hole drilling are observed (each process in its entirety) a gradual increase is observed in the static torque and thrust magnitudes. The reasoning for this is chip-accumulation and clogging along the flutes, since the holes were drilled continuously, without withdrawal of the drill.

A similar observation of the static force signals in pilot hole drilling reveals an opposite trend. Here, the torque and thrust magnitudes show a gradually decreasing trend. The following is proposed as the mechanism behind this 'decay' phenomenon : As in full hole drilling, torque and thrust forces are induced due to the coupling effect. However, in pilot hole drilling the absence of cutting at the web drastically reduces forces and thus the torsional and axial restraint on the drill. The reduced restraints are ineffective in containing the induced strains, and thus the drill begins to expand axially and wind torsionally. Simultaneously, the induced torque and thrust reaction forces corresponding to these strains, reduce. The process occurs gradually due to the viscous damper-type role played by the metal cutting process. As a result, measured torque and thrust gradually 'decay' until the induced strains are exhausted, at which time, their magnitudes reach a minimum.

It is implied in the above explanation that the magnitudes of decay correspond to the induced forces. Thus the results of chapter 3 are employed to verify if the induced forces (decay) are predictable. It is

noted that due to change in restraint conditions, the values of induced-force coefficients (K_1 and K_2) determined under full restraint conditions, are not valid for pilot hole drilling conditions. Therefore the direct-force coupling equations (3.7 and 3.8) are employed to estimate the induced forces, assuming that the final minima attained after the decay process are the true cutting torque and thrust values. The values of K_1 and K_2 are recomputed from the pilot hole drilling force measurements. From this, highly consistent predictions are obtained (particularly torque), which agree well with the experimentally measured torque and thrust decay magnitudes.

The mechanism proposed for the decay phenomenon is seen to be the most plausible one due to the consistency of the decay phenomenon and the fact that their magnitudes are predictable by employing the concepts of torque-thrust coupling. More importantly, the force inducement hypothesis is verified by inference. That is, substantial torque and thrust forces are indeed induced during full-hole drilling, and it would be erroneous to attribute all of the measured forces to metal-cutting.

A preliminary analysis of the fluctuating components of torque and thrust forces confirms the conclusions of past researchers that they are narrow-band random processes. Further analysis also reconfirms that torque and thrust fluctuations of full-hole drilling have gaussian probability distributions. Standard deviation values are determined, and their values

remain unchanged with respect to changes in feed. The torque and thrust fluctuations of pilot hole drilling are observed to be highly non-gaussian.

The pilot hole sizing criterion established in chapter 4, is evaluated based on the RMS spectral analysis of torque, thrust and radial force signals. For half-inch drilling at low-feed, a 'wrong size' pilot hole causes the RMS values of dynamic thrust to double as compared to the same experiment without a pilot hole. Correspondingly the dynamic torque increases by a factor of four. When the same experiments are done with a 'right size' pilot hole,the RMS values of fluctuations decrease significantly. Under high feed, the above effect of pilot hole size is observed on a more drastic scale. 'Wrong size' pilot holes cause the torque and thrust fluctuations to increase five-fold, whereas the 'right size' pilot hole causes significantly smaller values. The same effects are observed when drilling with the smaller drill also.

RMS values of radial forces also exhibit the same trend with regard to pilot hole sizing. The reduction in forces and improved stability while drilling with the 'right size' pilot hole implies that the hole quality may also be correspondingly better. Therefore, roundness error (RE) measurements are carried out on the drilled samples. A comparison of the profiles clearly shows that the sizing of pilot holes does have a drastic effect on hole quality. Under a moderate to high feed rate, drilling holes with a pilot hole of diameter equal to the web thickness, results in a

clear deterioration of hole quality (near hole mouth), with multi-cornered profiles and high RE values. On the other hand drilling with the 'right size' of pilot hole (as determined in chapter 4), drastically improves hole quality. Under low feed or high feed with a 2-step feed method, the pilot hole size has little or no impact on hole quality. Thus the pilot hole sizing criterion proposed is clearly validated for moderate/high feed drilling.

In several pilot hole drilling experiments, the static torque and thrust signals show low frequency fluctuations of significant amplitude (20 to 25 percent of static values). The two fluctuations are exactly in-phase with each other. Therefore it is suggested that the origin of these fluctuations is the simultaneous, coupled, torsional-axial 'parametric' vibration phenomenon of the type observed by past a researcher. According to the mechanism proposed for the same, the vibrations begin with a torsional disturbance as the sharp cutting lips 'dig-in' into the material at the commencement of drilling. The torsional unwinding thus caused also produces axial expansion due to the coupling effect. This increases the instantaneous feed, which in turn causes force pulses and sustains the vibrations.

The following chapter summarizes the major aspects of this investigation and presents recommendations for further research into these aspects.

CHAPTER 7

CONCLUSIONS AND RECOMMENDATIONS FOR FURTHER RESEARCH

7.1 Conclusions

7.1.1 Torque-Thrust Coupling Effect

The torque-thrust coupling effect in twist drills is a highly prominent phenomenon. Contrary to the perception of past researchers, the implications of the phenomenon are more significant than a mere interaction between the torsional and axial strains.

The set of direct and cross-coupling stiffnesses defined aptly describe the static deformation behaviour of the drill. Helix angle has a significant influence on the coupling effect. The coupling interaction (as measured by K_{tf} and K_{ft}) has a distinct maximum around a helix angle of 28 degrees. This variation of the coupling interaction becomes more drastic as drill diameter increases. Amongst drills of a given helix angle, the interaction increases parabolically with diameter.

Torsional stiffness shows a similar variation, with a maximum again around a helix angle of 28 degrees. It is clearly revealed that the coupling interaction produces a torsional stiffening effect when tested under axial restraint. The higher the coupling interaction, the higher will be the

torsional stiffness. Thus, drills with the 'optimal' helix angle of 28 degrees show the highest torsional stiffness.

7.1.2 Effect of Coupling on Drilling Forces and Drill Behaviour

Under torsional and axial restraint, a twist in the direction of cutting torque induces a thrust force in the drill, and a compressive thrust induces a torque in the drill. Thrust inducement increases with a decrease in drill diameter.

The torsional and axial restraint conditions during drilling are identical to static test conditions. Thus, significant torque and thrust forces are induced during drilling also, which add up with the cutting forces. Therefore, it is erroneous to attribute all of the measured torque and thrust to metal cutting. The separation equations derived on the basis of the induced force coefficients, enable the isolation of the true cutting components from the measured torque and thrust. Estimates based on the experimental measurements of this and a past investigation, show that the induced forces (when drilling with 3/8-inch and 1/2-inch drills) constitute about 20 to 30 percent of the measured thrust, and 10 to 15 percent of the measured torque values.

The decaying trend observed in the torque and thrust signals of pilot hole drilling is actually the gradual 'release' of the induced forces during drilling. The decay magnitudes are accurately estimated by employing the

induced-force coefficients for the drills. By inference, the hypothesis of force inducement (and thus, measurement errors) during drilling, is verified.

The coupling effect and the inducement of forces due to it, have important implications to drill design and the drilling process. Among the static aspects affected are the torsional stiffness and buckling tendencies of the drill. Dynamically, the torsional, axial and lateral vibration characteristics are affected by the coupling effect.

7.1.3 The Pilot Hole Sizing Criterion

The size of the pilot hole has a definite influence on the quality of the final hole. The severe, extrusion-type cutting in the negative rake region of the cutting lips, produces drift forces which cause roundness errors in pilot hole drilling.

The proposed criterion for sizing pilot holes eliminates cutting in all of the negative-rake regions. The diameter at which the normal rake angle reaches zero on the lips, is defined as the 'critical diameter' of pilot hole.

A clear improvement in hole-roundness is observed from the drilling experiments, using the above criterion. When drilling at moderate to high feed, pilot holes sized by the proposed criterion, result in highly accurate holes with low roundness errors. Drilling with pilot holes is known to improve the straightness of the final hole. Thus, holes of high

straightness and roundness can be obtained by employing the proposed sizing criterion.

The results of this investigation, particularly that of the torque-thrust coupling effect, pose many new questions and implications on the static and dynamic behaviour of the drill. However, it is beyond the scope of the present investigation to probe those aspects. Therefore, they are suggested as topics for future investigations.

7.2 Recommendations for Further Research

The following aspects warrant further study in view of the findings of this investigation :

7.2.1 On the Coupling Effect

1. A more precise determination of the 'optimal' helix angle that maximizes the coupling interaction and the torsional stiffness. This may be accomplished by experimenting with a larger choice of helix angles.

2. Study of the coupling behaviour of drills with a constant web-thickness throughout the flute length. Such drills would be highly efficient in terms of chip removal.

3. An investigation to clarify the effect of web-thickness on the coupling interaction - May be accomplished by repeating the experimentation of

chapter 2, with drills of various web-thickness values. As a result, it may be possible to design a torsionally stiff and strong drill, yet with a thin web.

4. A thorough analytical/experimental study of the effect of cross-section profile design on the coupling interactions - This may enable the optimization of the flute area versus drill strength.

5. Development of a detailed analytical static-deformation model of the drill including flute profile characteristics and helix angle. Such a model would enable a parametric study and optimization of the coupling phenomenon and its implications.

7.2.2 On the Effects of Coupling Interaction

1. Development of a complete torsional, axial and lateral vibrations model of the drill - Such a model would require analytical and experimental investigation of the natural vibration behaviour, and the influence of coupling on the same.

2. A study of the parametric instability and coupled torsional-axial vibrations observed in the present study. This follows the development of the vibration model suggested above.

3. An experimental study of the drill 'relaxation' during cutting, and the torque-thrust decay phenomenon. This has implications to the

dynamic behaviour of the drill.

4. A re-evaluation of the various analytical force-prediction models, based on the 'true' cutting torque and thrust force measurements.

REFERENCES

1. Gautschi, G.H., 'Cutting Forces in Machining and their Routine Measurement with Multi-component Piezo-Electric Force Transducers', Advances in MTDR, 1971, p.113.

2. Sen, G.C. and A. Bhattacharya, Principles of Metal Cutting, New Central Book Agency, 1969.

3. KISTLER Piezo Instrumentation, General Catalog K 2.004.

4. KISTLER Piezo Instrumentation, X-Y-Z Compensator Operating and Service manual, 0.021.

5. Chahil, G.S., 'Measurement and Stochastic Modeling of Torque and Thrust in Twist Drilling Operation', Master's Dissertation, Concordia University, 1976.

6. Hatschek, R.L., 'Metal Cutting : Today's Techniques for Engineers and Shop Personnel', American Machinist, Mc Graw-Hill, 1979.

7. 'Drill Section', Metal Cutting Tool Handbook, Metal Cutting Tool Institute, 1949.

8. De Beer, C., 'The Web Thickness of Twist Drills', Annals of CIRP, 18, 1970, p.81.

9. Lorenz, G., 'Helix Angle and Drill Performance', Annals of CIRP, 28 (1), 1979, p.83.

10. Spur, G. and J.R. Masuha, 'Drilling with Twist Drills of Different Cross Section Profiles', Annals of CIRP, 30 (1), 1981, p.31.

11. Donaldson, C., G.H. Lecain and V.C. Goold, Tool Design, Mc Graw Hill, 1973.

12. Rosen, A., 'Theoretical and Experimental Investigation of the Non-linear Torsion and Extension of Initially Twisted Bars', Trans. of the ASME : Journal of Applied Mechanics, 50, June 1983, p.321.

13. Lee, Sang Jo, 'The Influence of Drill Characteristics and Entry Mechanisms on Drill Performance', P.hd Dissertation, University of Wisconsin, Madison, 1986.

14. Galloway, G.S., 'Some Experiments on the Influence of Various Factors on Drill Performance', Trans. of the ASME, February 1957, p.191.

15. Shaw, M.C. and C.J. Oxford, 'On the Drilling of Metals : 2 - The Torque and Thrust in Drilling', Trans. of the ASME, 79, January 1957, p.139.

16. Bendat, J.S. and A.G. Piersol, Measurement and Analysis of Random Data, John Wiley and sons, 1966.

17. Fujii, H., E. Marui and S. Ema. 'Whirling Vibration in Drilling, Part 1 : Cause of Vibration and Role of Chisel Edge', Trans. of the ASME - Journal Engineering for Industry, 108, August 1986, p.157.

18. Armarego, E.J.A. and R.H. Brown, The Machining of Metals, Prentice Hall, 1969.

19. Oxford, C.J., 'On the Drilling of Metals - 1 : Basic Mechanics of the Process', Trans. of the ASME, 77, 1955, p.103.

20. Kahng, C.H. and I. Ham, 'A Study on Sequential Quality Improvement in Hole-Making Processes', Annals of the CIRP, 24 (1), 1975, p.27.

21. Narasimha, K., M.O.M. Osman, S. Chandrashekhar and J. Frazao, 'An Investigation into the Influence of Helix Angle on the Torque-Thrust Coupling Effect in Twist Drills', The International Journal of Advanced Manufacturing Technology, 2 (4), 1987, p.91.

22. Sakuma. K., H. Kiyota and H. Morita, 'Positional Accuracy of Hole in Drilling', Bulletin of the JSME, 26 (214), 1983, p.659.

23. Pal, A.K., A. Bhattacharya and G.C. Sen, 'Investigation of the Torque in Drilling Ductile Materials', International Journal of Machine Tool Design and Research, 4, 1965, p.205.

24. Williams, R.A., 'A Study of the Drilling Process', Trans. of the ASME - Journal of Engineering for Industry, 96, 1974, p.1207.

25. Wiriyacosol, S. and E.J.A. Armarego, 'Thrust and Torque Prediction in Drilling from a Cutting Mechanics Approach', Annals of the CIRP, 28 (1), 1979, p.87.

26. Watson, A.R., 'Drilling Model for Cutting Lip and Chisel Edge and Comparison of Experimental and Predicted Results - Parts I, II, III and IV', International Journal of Machine Tool Design and Research, 25 (4), 1985, p.347.